

TESI DI DOTTORATO

UNIVERSITÀ DEGLI STUDI DI NAPOLI “FEDERICO II”

DIPARTIMENTO DI INGEGNERIA BIOMEDICA,
ELETTRONICA E DELLE TELECOMUNICAZIONI

DOTTORATO DI RICERCA IN
INGEGNERIA ELETTRONICA E DELLE TELECOMUNICAZIONI

WIDELY LINEAR FILTERING
IN MODERN MIMO TRANSCEIVERS

MADDALENA LIPARDI

Il Coordinatore del Corso di Dottorato
Ch.mo Prof. Niccolò RINALDI

Il Tutore
Ch.mo Prof. Davide MATTERA

A. A. 2008–2009

“Quelli che s’innamoran di pratica senza scienza
son come ’l nocchier ch’entra in navilio senza timone o bussola,
che mai ha certezza dove si vada.”

Leonardo da Vinci, Codex G, Bibliothèque de l’Institut de France, Paris.

Acknowledgments

First, I want to express my sincere gratitude to my Supervisor, Prof. Davide Mattera, as he has been a valuable guide, professional and above all human, during the time I spent as a PhD student.

I would also like to thank Prof. Luigi Paura who was the first person I referred to when I decided to work in the scientific research.

I am very grateful to Fabio Sterle for his assistance almost up to the end of my PhD course, to Tilde Fusco for her friendship and to Jurek Nowakowski for some precious words of encouragement.

I have to thank my family if today I can obtain the Degree of *Philosophiae Doctor*. Thanks to my parents, Elena and Gennaro, for their devotion, support and trust and to my brothers, Pierluigi and Enzo, for their affection.

At last but not least, I want to thank my boyfriend, Eduardo, for his boundless love. We met during the PhD course and from then on he has made my life extraordinary.

Maddalena Lipardi

Contents

Introduction	xi
1 MIMO model	1
1.1 Multiple-input multiple-output channel model	2
1.2 Time-dispersive FIR MIMO channel	5
1.3 MIMO communications	7
1.4 MIMO receiver architectures	10
1.4.1 ML receiver	11
1.4.2 MMSE FIR equalizer	12
1.4.3 ZF FIR equalizer	14
1.4.4 Decision-feedback FIR equalizers	15
1.5 Transceiver architectures	18
2 Widely linear equalization	23
2.1 Widely linear mean square estimation with complex data	24
2.2 MMSE equalization in presence of transmitter and receiver IQ imbalance	26
2.2.1 System model	27
2.2.2 MMSE receiver for joint Tx-IQ and Rx-IQ imbalance compensation	29
2.2.3 Numerical results	31
2.3 Constellation design in widely linear transceivers	35
2.3.1 System model	37
2.3.2 Feedforward-based MMSE equalizer	38
2.3.3 Constellation design	40
2.3.4 Numerical results	50

3	Equalization for OFDM-OQAM systems	59
3.1	OFDM-OQAM MIMO model	61
3.1.1	Noise correlation matrix	66
3.2	Multiple antenna OFDM-OQAM MIMO model	67
3.2.1	Ad hoc equalizers	68
3.3	Synthesis of the MMSE WL-DF MIMO equalizer with minimum storage requirements	69
3.3.1	Problem setting	70
3.3.2	Scenario 1	76
3.3.3	Unsorted Scenario 2	76
3.3.4	Sorted Scenario 2	78
3.3.5	Scenario 3	84
3.3.6	The conjugate gradient method for solving the linear system	86
3.3.7	Specializing the iterative solution method to the given system of equations	88
3.3.8	Implementation complexity and numerical results	92
	Conclusion	99
	A	101
A.1	Proof of Lemma 3.3	101
	Bibliography	105

List of Figures

1.1	Analogic low-pass equivalent MIMO channel model.	3
1.2	Block diagram of the LTI time-dispersive MIMO channel of order ν	7
1.3	Multiantenna system.	8
1.4	Block diagram of a linear receiver.	13
1.5	The decision feedback equalizer structure.	16
1.6	The decision feedback equalizer in absence of error propagation.	17
1.7	The transceiver architecture.	19
1.8	Linear transceiver architecture.	19
2.1	MSE Loss of the MMSE L equalizer versus the Tx-IQ imbalance.	33
2.2	MSE Loss of the MMSE WL equalizer versus the Tx-IQ imbalance.	33
2.3	MSE Loss of the MMSE L equalizer versus the Rx-IQ imbalance.	34
2.4	SERs of the MMSE WL equalizer and the L one versus the SNR, for 16-QAM transmissions.	34
2.5	System model.	35
2.6	Transceiver structure.	42
2.7	Optimum constellations for $K = 4$ and $K = 8$: (a) QPSK, (b) Rhombic QPSK, (c) 4-PAM, (d) Foschini&All 8-QAM, (e) "1-7" 8-QAM, (f) 8-PAM, (g) Rectangular 8-QAM, (h) Non-circular 8-QAM, (i) Non-uniform 8-QAM.	49
2.8	Constellation optimization for $K = 4$ over fixed channel ($\rho = 0.9$); for each point, the letter specifies the constellation (of those in Fig. 2.7) typically obtained.	52
2.9	Constellation optimization for $K = 8$ over fixed channel ($\rho = 0.9$); for each point, the letter specifies the constellation (of those in Fig. 2.7) typically obtained.	53

2.10	Constellation optimization for $K = 8$ over fixed channel ($\rho = 0.6$); for each point, the letter specifies the constellation (of those in Fig. 2.7) typically obtained.	53
2.11	SERs of the considered architectures versus SNR.	55
2.12	Loss in dB of the PAM-based, QAM-based and <i>two-choice</i> -based architectures with respect to the OPT-based one for several target SER.	56
3.1	OFDM-OQAM system model.	62
3.2	Subchannel energy according to the ITU Vehicular-A channel model ($M = 64$).	66
3.3	Multiple antenna scenario scheme.	67
3.4	DF MIMO equalizer scheme.	71
3.5	Error probability versus SNR with the number of iterations varying.	95
3.6	Error probability versus the number of iterations for each input symbol to a specific channel.	95
3.7	Error probability versus the number of iterations for each input symbol to another specific channel.	96
3.8	Error probability versus the number of iterations averaged over the input symbols and the channels.	96
3.9	Symbol error probability in two different scenarios: per-subcarrier equalization and ad hoc one.	97

Introduction

Handling the still increasing amount of digital traffic is today a large and important research area. As it is well known, the information capacity of the conventional single-input single-output (SISO) systems grows in a logarithmic fashion with the signal-to-noise ratio. Since the signal-to-noise ratio is related to the transmitted power and the ambient noise, one way to answer the demand of high bit-rate services is to increase the transmitted power. Unfortunately, in the modern multi-user environments, the ambient noise is due to other users transmitting within the same frequency bands. It follows from this that the increase in the transmit power does not guarantee a capacity gain because it implies a proportional increase in the overall disturbance. Moreover, higher power level implies the cost of a nonlinearity in the power amplifier. For some years, the single-input multiple-output (SIMO) systems, as well as the multiple-input single-output (MISO) ones, have represented a possible solution in attempting to increase the signal-to-noise ratio, and consequently the capacity of the SISO systems. The multiple output (input) character of such communication systems is usually related to the adoption of receive (transmit) diversity techniques. For instance, the use of multi element array at the receiver (transmitter) and one element at the transmitter (receiver), has been extensively studied. Unfortunately, the capacity achieved by the SIMO systems increases very slowly with the number of system outputs, whereas the capacity achieved by the MISO ones rapidly reaches saturation as the number of input increases. The natural conjunction between SIMO and MISO systems leads to the more attractive multiple-input multiple-output (MIMO) systems. Foschini and Telatar showed that a huge capacity gain can be achieved over the SISO, SIMO, and MISO systems: more specifically, the capacity of a MIMO system can grow, in principle, linearly with the minimum over the number of inputs and outputs. For this reason, over the last decade, there has been a growth of research activity in the area of MIMO systems.

We have used the MIMO system model to describe the multi-carrier sys-

tem orthogonal frequency division multiplexing with offset quadrature amplitude modulation (OFDM-OQAM). Such system is considered a promise of the mobile communications because it overcomes the drawbacks of the widely adopted OFDM system, first among all the spectral efficiency. We have focused on the equalization of such systems in a multiple antenna scenario and we have chosen to employ the decision feedback (DF) MIMO equalizer, in its widely linear (WL) version in order to exploit the statistical redundancy exhibited by the system input sequence. In the class of symbol-by-symbol equalizers, the DF equalizer plays an important role since it performs almost as well as the optimum equalizer, although it requires a computational complexity only slightly higher than that of the linear equalizer. The WL filtering, extensively used in this thesis, generalizes the conventional linear filtering by jointly processing both the real part and the imaginary one of the input signal, or, equivalently, both the signal itself and its complex conjugate version; the WL filtering outperforms the linear one in presence of the so called *rotationally variant* signals, i.e., those signals which exhibit a nonnull correlation with their complex conjugate version. We have made use of the tool of the WL filtering in two other scenarios, i.e., both in order to compensate the transmitter and the receiver in-phase and quadrature (IQ) imbalance and in order to optimize the transmitted constellation on the basis of the state of channel (assumed known at the receiver) when at the receiver side there is a minimum mean square error (MMSE) equalizer.

The outline of the thesis is the following:

Chapter 1 presents the general framework. The MIMO system model is introduced and the basic properties of MIMO receivers as well as MIMO transceivers are described.

Chapter 2 presents two application scenarios of the WL filtering within MMSE equalizers. The former concerns the IQ imbalance compensation, of the transmitter and the receiver; the latter deals with the design of the constellation to be transmitted over a channel whose state is known at the receiver.

Chapter 3 presents OFDM-OQAM systems. After having modelled such system with a MIMO channel, they are equalized by a WL-DF MIMO equalizer which, according to the channel characteristics, can operate *selectively*

achieving so a good trade-off between performance and complexity.

Chapter 1

MIMO model

The increasing requirements on data rate and quality of service for wireless communications systems call for new techniques to improve spectrum efficiency as well as link reliability. In this context, much attention has been focused on multiple-input multiple-output (MIMO) communication channel models for various reasons, such as, for instance:

- a) the increasing exploitation of multiple antennas both at the transmitter and at the receiver side to introduce spatial redundancy as well as to utilize the recent space-time coding techniques;
- b) the widespread use of multiplexing and multiple access techniques which require to resort to a MIMO channel model, since it can describe the mutual interferences among the different symbol streams. More specifically, resorting to a MIMO model is mandatory in modern communication systems that utilize code-division multiple-access (CDMA) techniques such as direct sequence (DS) CDMA, multi carrier (MC) CDMA and orthogonal frequency division multiplexing (OFDM).

In this chapter, we derive the bandpass equivalent linear-time-invariant (LTI) finite-impulse-response (FIR) MIMO channel model, whose equalization represents the main subject of the thesis. The versatility of the adopted model is demonstrated by showing that a FIR MIMO model arises in many communication systems such as multiple antenna systems, OFDM systems, etc.

Then, both basic MIMO receiver and transceiver architectures are introduced to provide the general frameworks utilized in the next chapters. More specifically, when the MIMO channel transfer function is known at only the

receiver side, the linear and the decision-feedback equalizers are considered rather than the optimum (in the Maximum Likelihood Sense) due to their lower computational complexity. If the channel state information is available at both ends of the link, the transmitter and the receiver structures can be jointly designed to improve the system performance.

1.1 Multiple-input multiple-output channel model

The block diagram of the equivalent low-pass continuous-time linear¹ MIMO channel with N_i input signals and N_o output signals is depicted in Fig. 1.1. At the transmitter side, $s_k^{(\ell)}$ denotes the k th complex-valued symbol to be transmitted on the ℓ th channel input; T_s the symbol period and $\psi_T(t)$ the time-invariant unit-energy impulse response of the transmit filters ([1] and references therein). The continuous-time linear MIMO channel is characterized by the $N_o N_i$ impulse responses $g^{(\ell,k)}(t, \tau)$ with $\ell = 1, \dots, N_o$ and $k = 1, \dots, N_i$; each of them, i.e., given (ℓ, k) , describes the linear time-variant (LTV) subchannel connecting the ℓ th MIMO channel output with the k th MIMO channel input (let us remind that $g^{(\ell,k)}(t, \tau)$ represents the response of the subchannel at the time t to a Dirac impulse applied at the time $t - \tau$). At the receiver side, $v^{(\ell)}(t)$ represents some additive noise at the ℓ th output and $\psi_R(t)$ the time-invariant unit-energy impulse response of the receive filters. The ℓ th MIMO channel output $y^{(\ell)}(t)$ is sampled with a sampling period $T_c \triangleq \frac{T_s}{q}$, with $q \in \mathbb{N}$.

According to such model, the input-output relationship of the MIMO channel can be written as follows:

$$y^{(\ell)}(t) = \sum_{n=-\infty}^{\infty} \sum_{i=1}^{N_i} s_n^{(i)} h^{(\ell,i)}(t, t - nT_s) + n^{(\ell)}(t) \quad \ell = 1, \dots, N_o \quad (1.1)$$

where

$$h^{(\ell,k)}(t, \tau) \triangleq \psi_T(\tau) * g^{(\ell,k)}(t, \tau) * \psi_R(\tau) \quad (1.2)$$

$$n^{(\ell)}(t) \triangleq v^{(\ell)}(t) * \psi_R(t) \quad (1.3)$$

with $*$ denoting the continuous-time convolution operator. In the following, we will refer to $h^{(\ell,k)}(t, \tau)$ as the impulse response of the subchannel (ℓ, k)

¹The modeling of the channel as a linear system agrees with the observed behavior of a large number of communication channels.

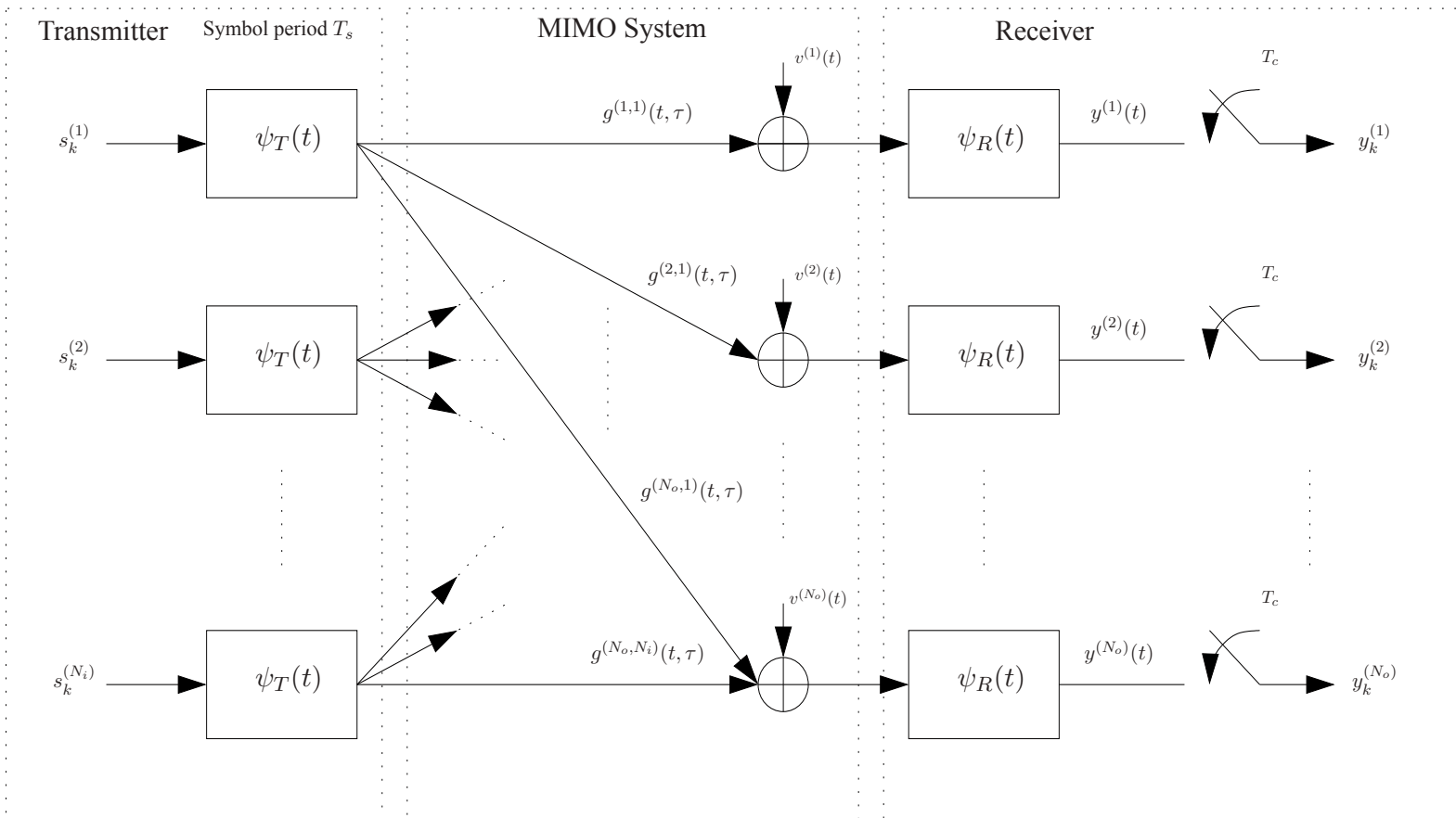


Figure 1.1: Analog low-pass equivalent MIMO channel model.

and to the $N_o \times N_i$ matrix

$$\mathbf{H}(t, \tau) \triangleq \begin{bmatrix} h^{(1,1)}(t, \tau) & h^{(1,2)}(t, \tau) & \dots & h^{(1,N_i)}(t, \tau) \\ h^{(2,1)}(t, \tau) & h^{(2,2)}(t, \tau) & \dots & h^{(2,N_i)}(t, \tau) \\ \vdots & \vdots & \ddots & \vdots \\ h^{(N_o,1)}(t, \tau) & h^{(N_o,2)}(t, \tau) & \dots & h^{(N_o,N_i)}(t, \tau) \end{bmatrix} \quad (1.4)$$

as the MIMO channel matrix, whereas the column vector $[h^{(1,i)}(t, \tau) \ h^{(2,i)}(t, \tau) \ \dots \ h^{(N_o,i)}(t, \tau)]^T$ is usually referred to as the signature induced by the i th input across the channel outputs. In the current literature, the special cases ($N_i = 1, N_o > 1$) and ($N_i > 1, N_o = 1$) are referred to as single-input multiple-output (SIMO) system and multiple-input single-output (MISO) system, respectively; if $N_i = N_o = 1$, then the MIMO system will degenerate into the conventional single-input single-output (SISO) system.

The sampled version $y_k^{(\ell)}$ with $\ell = 1, \dots, N_o$ of the MIMO channel output $y^{(\ell)}(t)$ is such that

$$\begin{aligned} y_k^{(\ell)} &= y^{(\ell)}(kT_c) \\ &= \sum_{n=-\infty}^{\infty} \sum_{i=1}^{N_i} s_n^{(i)} h^{(\ell,i)}(kT_c, kT_c - qnT_c) + n_k^{(\ell)} \end{aligned} \quad (1.5)$$

where $n_k^{(\ell)} \triangleq n^{(\ell)}(kT_c)$ denotes the sampled version of the noise signal $n^{(\ell)}(t)$. The discrete-time model in (1.5) is written as a function of two data rates, $1/T_s$ and $1/T_c$. A suitable model, expressed as a function of one data rate, can be provided by introducing the symbol sequence $x_k^{(\ell)}$ as follows:

$$x_k^{(\ell)} \triangleq \begin{cases} s_{k/q}^{(\ell)} & \text{if } \frac{k}{q} \text{ is integer} \\ 0 & \text{otherwise} \end{cases} \quad (1.6)$$

It is the oversampled (or expanded) version by q of $s_k^{(\ell)}$, i.e., it is obtained by inserting $q - 1$ zeros between any two consecutive samples of the signal. According to (1.6), the input-output relationship in (1.5) becomes

$$y_k^{(\ell)} = \sum_{n=-\infty}^{\infty} \sum_{i=1}^{N_i} x_{k-n}^{(i)} h_{k,n}^{(\ell,i)} + n_k^{(\ell)} \quad \ell = 1, \dots, N_o \quad (1.7)$$

where $h_{k,n}^{(\ell,i)} \triangleq h^{(\ell,i)}(kT_c, nT_c)$. The equation (1.7) provides the T_c -space sampled discrete-time MIMO channel model; with no loss of generality, in this thesis we will assume $T_c = T_s$ unless specified.

1.2 Time-dispersive FIR MIMO channel

In modern communication systems, especially for mobile applications, the increasing demand of high bit-rate transmissions and the need to use stationary channel models drive to the adoption of a very short symbol period, which therefore will be usually less than the coherence time of the radio channel. On the other hand, as the bandwidth of the transmitted signals is usually greater than the coherence bandwidth of the channel, it will prove frequency selective or, equivalently, time-dispersive.

Consequently, the MIMO channel input-output relationship in (1.1) and the corresponding T_c -space sampled version in (1.7) can be rewritten, respectively, as follows:

$$y^{(\ell)}(t) = \sum_{n=-\infty}^{\infty} \sum_{i=1}^{N_i} s_n^{(i)} h^{(\ell,i)}(t - nT_s) + n^{(\ell)}(t) \quad (1.8)$$

$$y_k^{(\ell)} = \sum_{n=-\infty}^{\infty} \sum_{i=1}^{N_i} x_{k-n}^{(i)} h_n^{(\ell,i)} + n_k^{(\ell)} \quad (1.9)$$

where $h_n^{(\ell,i)} \triangleq h_{0,n}^{(\ell,i)} = h^{(\ell,i)}(0, nT_c)$.

It is clear that the total number of T_c -space discrete-time channel coefficients $h_n^{(\ell,i)}$ is determined by the maximum delay spread of the physical fading channels $g^{(\ell,i)}(t, \tau)$ and the time durations of the transmit and receive filters, which are usually infinite in theory to maintain limited frequency bandwidth. Therefore, $h_n^{(\ell,i)}$ is a time-invariant filter with infinite impulse response (IIR). However, in practice, the time domain tails of the transmit and receive filters are designed to fall off rapidly, and it is reasonable to assume a finite range for the values of n over which the amplitudes of the channel coefficients $h_n^{(\ell,i)}$ are essentially nonzero. Thus, by eliminating the coefficients which do not affect significantly (owing to their small power) the channel output, the channel impulse response $h_n^{(\ell,i)}$ can be truncated to a finite impulse response (FIR). For such reason, without loss of generality, we will assume:

$$\begin{aligned} h_n^{(\ell,i)} &\neq 0 && \text{if } n = 0, \dots, \nu^{(\ell,i)} \\ h_n^{(\ell,i)} &= 0 && \text{otherwise} \end{aligned}$$

with $\nu^{(\ell,i)}$ denoting the memory of the subchannel (ℓ, i) . Hence, the input-output relationship of the MIMO channel in the discrete time domain can be

written as follows:

$$y_k^{(\ell)} = \sum_{n=0}^{\nu^{(\ell,i)}} \sum_{i=1}^{N_i} x_{k-n}^{(i)} h_n^{(\ell,i)} + n_k^{(\ell)} \quad 1 \leq \ell \leq N_o \quad (1.10)$$

By grouping the received samples at the k th instant from all the N_o channel outputs into the $N_o \times 1$ column vector

$$\mathbf{y}_k \triangleq \begin{bmatrix} y_k^{(1)} & y_k^{(2)} & \dots & y_k^{(N_o)} \end{bmatrix}^T \quad (1.11)$$

one can relate \mathbf{y}_k to the corresponding input and noise column vectors

$$\mathbf{x}_k \triangleq \begin{bmatrix} x_k^{(1)} & x_k^{(2)} & \dots & x_k^{(N_i)} \end{bmatrix}^T \quad (1.12)$$

$$\mathbf{n}_k \triangleq \begin{bmatrix} n_k^{(1)} & n_k^{(2)} & \dots & n_k^{(N_o)} \end{bmatrix}^T \quad (1.13)$$

as follows:

$$\begin{aligned} \mathbf{y}_k &= \sum_{n=0}^{\nu} \mathbf{H}_n \mathbf{x}_{k-n} + \mathbf{n}_k \\ &= \mathbf{H}_k \star \mathbf{x}_k + \mathbf{n}_k \end{aligned} \quad (1.14)$$

where \mathbf{H}_n is the $N_o \times N_i$ matrix whose (ℓ, i) -entry is $h_n^{(\ell,i)}$, ν is the maximum length of the $N_o N_i$ channel impulse responses, i.e., $\nu = \max_{(\ell,i)} \nu^{(\ell,i)}$, and \star denotes the discrete-time convolution operator. The block diagram of the obtained MIMO channel model is depicted in Fig. 1.2, where z^{-1} denotes the unit-delay block (i.e., the system which responds to the input \mathbf{x}_k with the output \mathbf{x}_{k-1}).

The time-dispersive MIMO channel model in (1.14), as it will be shown in next section, arises in many applications, such as multi-antenna systems, spread-spectrum multiuser communications, multi-carrier systems. Nevertheless, although it well describes the linear distortion introduced by the radio channel, it does not take into account other impairments such as the nonlinear distortion introduced by the A/D converters, and/or the phase and time jitter due to imperfect synchronization between the transmit oscillators and the receive ones. Since the linear distortion represents the most important cause of performance degradation in communication systems, we will refer to such model to design the receiver or jointly the transmitter and the receiver in order to reduce the effect of the frequency selectivity of the communication channels.

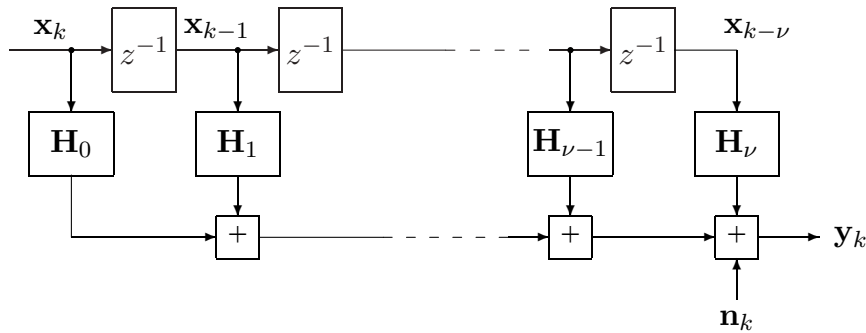


Figure 1.2: Block diagram of the LTI time-dispersive MIMO channel of order ν .

1.3 MIMO communications

The model in (1.14) describes the input-output relationship of an abstract system with several inputs and/or outputs; in fact, its derivation has been carried out with no assumption regarding the specific application scenario. In the literature, the MIMO communication systems are usually identified with the ones that employ multiple antennas both at the transmitter side and the receiver one. However, we point out that, although it is not always explicit, a “virtual” MIMO model frequently arises in many communication systems. For example, in many applications, a more exact description of the detection scenario requires to take into account the presence of several signals that, together with the transmitted one, affect the channel output: according to the conventional SISO schemes, the effects of such signals are modeled as additive noise. Otherwise, a MIMO model whose inputs include the undesired signals can be adopted to improve the system performances, provided that some a priori information about such undesired signals is available. It is clear that this model is not an actual MIMO one since the MIMO character is generated by an ad hoc representation of the transmitted signals. In the following, we report just two examples of MIMO systems, multiple antenna systems and OFDM systems.

Multiple antenna systems

Multiple antenna systems (see Fig. 1.3) have drawn a considerable attention in the last years for their capability to reject interference and to reduce the effect of fading and noise. The earliest way of antenna systems for increasing the performance was antenna diversity, which mitigated the effect of fading. More recently, smart antenna systems, which attempt to actively mitigate the chan-

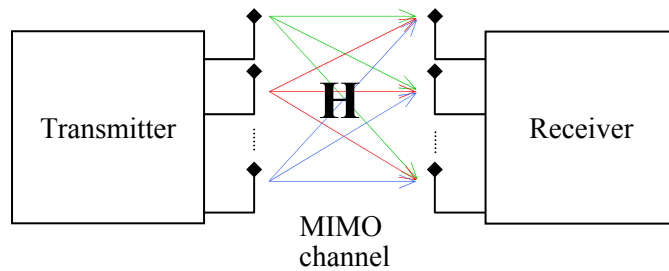


Figure 1.3: Multiantenna system.

nel impairments, have been developed [2]. The communication systems that employ multiple antennas at the transmitter and at the receiver are popularly known as MIMO systems. Their structure naturally leads to a MIMO system model where the signals transmitted by the transmit antennas represent the channel inputs, while the ones received by the receive antennas represent the channel outputs. In [1] it is derived the MIMO channel impulse response for a multiple antenna system described by the physical scattering model known in literature as *one-ring* model [3]. Such model is appropriate in the fixed communication context, where the transmitter is elevated and seldom obstructed. Under some assumptions (the reciprocal communication bandwidth is much smaller than delay spread, the number of scatterers is sufficiently large, etc.), one gets that the channel coefficients $h_n^{(\ell,i)}$ can be modelled as Gaussian random variables.

OFDM systems

Orthogonal frequency division multiplexing (OFDM) is a digital multi-carrier transmission technique that distributes the digitally encoded symbols over several parallel carriers in order to reduce the symbol rate and to achieve robustness against long echoes in a multipath radio channel. Unlike conventional frequency division multiplexing, the spectra of the OFDM carriers partially overlap. Nevertheless, they will exhibit orthogonality on a symbol interval if they are spaced in frequency exactly of the reciprocal of the symbol interval. Such a requirement can be fulfilled by using the discrete Fourier transform and by introducing a guard interval equal or greater than the delay spread of the channel. In this section, we provide a description of the OFDM communication systems in terms of MIMO systems.

In an OFDM system, N input symbols (say, OFDM word) are transferred

by the serial-to-parallel converter (S/P) to the OFDM modulator. Then, each symbol is modulated by the corresponding subcarrier, it is sampled and D/A converted. The discrete-time OFDM signal, implemented by an inverse discrete Fourier transform (IDFT), can be expressed as follows:

$$x_{kN+p} = \frac{1}{N} \sum_{m=0}^{N-1} s_{kN+m} e^{j \frac{2\pi pm}{N}} \quad 0 \leq p < N \quad -\infty \leq k \leq \infty \quad (1.15)$$

where s_{kN+m} ($m = 0, \dots, N-1$) denotes the OFDM word to be transmitted, x_{kN+p} represents the $(kN+p)$ th output sample of the IFFT block. After pulse shaping and parallel-to-serial (P/S) conversion, the signal is transmitted over a SISO time-variant multipath fading channel that consists of L propagation paths with complex-valued channel gains $h_{k,\ell}$ (the apex $(1, 1)$ is omitted for brevity). At receiver side, after matched filtering and removing the cyclic prefix, the received signal can be written as

$$y_{kN+p} = \sum_{\ell=0}^{L-1} h_{kN+p,\ell} x_{kN+p-\ell} + n_{kN+p} \quad (1.16)$$

where n_{kN+p} denotes the additive noise samples. After S/P conversion of the received samples, the demodulated signal $Y_k^{(p)}$ is obtained by taking the discrete Fourier transform (DFT) of the vector $[y_{kN} \ \dots \ y_{kN+N-1}]^T$, i.e.:

$$\begin{aligned} Y_k^{(p)} &= \frac{1}{N} \sum_{i=0}^{N-1} \sum_{\ell=0}^{L-1} \sum_{m=0}^{N-1} s_{kN+m} h_{kN+i,\ell} e^{j \frac{2\pi(i-\ell)m}{N}} e^{-j \frac{2\pi pi}{N}} + \underbrace{\sum_{i=0}^{N-1} n_{kN+i} e^{-j \frac{2\pi pi}{N}}}_{\triangleq N_k^{(p)}} \\ &= \sum_{\ell=0}^{L-1} \sum_{m=0}^{N-1} s_{kN+m} \underbrace{\frac{1}{N} \sum_{i=0}^{N-1} h_{kN+i,\ell} e^{-j \frac{2\pi(p-m)i}{N}} e^{-j \frac{2\pi \ell m}{N}}}_{\triangleq H_k^{(p-m,\ell)}} + N_k^{(p)} \\ &= \sum_{\ell=0}^{L-1} \sum_{m=0}^{N-1} H_k^{(p-m,\ell)} s_{kN+m} e^{-j \frac{2\pi \ell m}{N}} + N_k^{(p)} \end{aligned} \quad (1.17)$$

The input-output relationship (1.17) can be rewritten in a matrix form as follows:

$$\mathbf{Y}_k = \mathbf{C}_k \mathbf{s}_k + \mathbf{N}_k \quad (1.18)$$

with

$$\mathbf{s}_k \triangleq \begin{bmatrix} s_{kN} \\ s_{kN+1} \\ \vdots \\ s_{kN+(N-1)} \end{bmatrix} \quad \mathbf{Y}_k \triangleq \begin{bmatrix} Y_k^{(0)} \\ Y_k^{(1)} \\ \vdots \\ Y_k^{(N-1)} \end{bmatrix} \quad \mathbf{N}_k \triangleq \begin{bmatrix} N_k^{(0)} \\ N_k^{(1)} \\ \vdots \\ N_k^{(N-1)} \end{bmatrix} \quad (1.19)$$

and where the (m, i) -entry of the $N \times N$ matrix \mathbf{C}_k is defined as

$$C_k^{(m,i)} \triangleq H_k^{(0,m-i)} + H_k^{(1,m-i)} e^{-j\frac{2\pi i}{N}} + \dots + H_k^{(L-1,m-i)} e^{-j\frac{2\pi(L-1)i}{N}} \quad (1.20)$$

From this it follows that the OFDM system is equivalent to a LTV non-dispersive MIMO system with impulse response \mathbf{C}_k .

If the channel impulse response remains constant over the word interval, one will have $H_k^{(p-m,\ell)} = 0$ for $p \neq m$, implying that \mathbf{C}_k degenerates into a diagonal matrix, and there exists no intercarrier interference (ICI). In such a case, the received samples $Y_k^{(p)}$ are affected by only the multiplicative distortion, which can be easily compensated for by a one-tap frequency-domain equalizer: in other words, the OFDM effectively converts a frequency selective fading channel into a set of N flat fading channels. On the other hand, the variations of the channel impulse response during the word interval, as well as the existence of a frequency offset², destroy the orthogonality among the OFDM subcarriers leading to a non-diagonal matrix \mathbf{C}_k , which accounts for the presence of ICI.

Recently, multiple antenna solutions and OFDM modulation have been combined to obtain the MIMO-OFDM systems [4]. Also in this case, it is possible to show that the overall system equation can be represented by a MIMO model.

1.4 MIMO receiver architectures

In this section, we provide a overview of the main receiving architectures for MIMO channels, which allow to achieve a *multiplexing gain* [1]. Let us first introduce the working framework. At the transmitter side, the data stream to be transmitted is demultiplexed into N_i streams $x_k^{(\ell)}$ ($\ell = 1, \dots, N_i$) which, after coding and modulation, are simultaneously sent over many antennas with

²Frequency offset in communication systems is caused by the mismatches between the oscillators at the transmitter and at the receiver, by Doppler shifts, etc.

symbol period equal to T_s . At the receiver side, N_o antennas are employed to recover as many superpositions of the transmitted signals. The received signals $y^{(\ell)}(t)$ are T_s -space sampled³ and then, are processed to separate the different N_i transmitted sequences $x_k^{(\ell)}$, which are finally remultiplexed to recover the original data stream. The separation step can be performed according to different (optimization) criteria and, clearly, it determines the computational complexity of the receiver: in practical scenarios, the aim to be pursued is represented by the achievement of an acceptable compromise between performance and computational complexity. For such a reason, the maximum likelihood (ML) receiver, that yields the best performance in terms of error rate at the expense of computational complexity, is often replaced by suboptimal equalizers that exhibit a sustainable complexity.

In the following, we introduce some of the main receiver architectures for MIMO systems:

- ML receiver
- minimum mean square error (MMSE) linear receiver
- zero-forcing (ZF) linear receiver
- decision-feedback (DF) based receiver.

The MMSE receiver structures and the DF-based ones are only introduced here, but they will constitute the main subject of the next chapters.

1.4.1 ML receiver

Let us consider a time non-dispersive LTI MIMO channel with N_i inputs and N_o outputs. The input-output relationship corresponding to the ℓ th output can be specialized as follows:

$$y_k^{(\ell)} = \sum_{i=1}^{N_i} x_k^{(i)} h^{(\ell,i)} + n_k^{(\ell)} \quad \ell = 1, \dots, N_o \quad (1.21)$$

where $h^{(\ell,i)} \triangleq h_k^{(\ell,i)} (\forall k)$, and where $x_k^{(i)}$ is drawn from the alphabet \mathcal{A} . We aim at recovering the transmitted symbol $x_k^{(\ell)}$ from the observation $y_k^{(\ell)}$ in the case where the channel impulse response is known at the receiver. By denoting with $f_n(\cdot)$ the probability density function of the additive noise $n_k^{(\ell)}$,

³We have assumed $T_c = T_s$ in (1.5).

the likelihood function of the observation, conditioned by the symbols $x_k^{(i)}$ ($i = 1, \dots, N_i$) is equal to

$$\mathcal{L}(y_k^{(\ell)} / \mathbf{x}_k) = f_n \left(y_k^{(\ell)} - \sum_{i=1}^{N_i} x_k^{(i)} h^{(\ell, i)} \right) \quad (1.22)$$

The ML symbol decision is given simply by the argument that maximizes $\mathcal{L}(y_k^{(\ell)} / \mathbf{x}_k)$ over the symbol alphabet

$$\hat{x}_k^{(\ell)} = \operatorname{argmax}_{\mathbf{x} \in \mathcal{A}^{N_i}} \left(\mathcal{L}(y_k^{(\ell)} / \mathbf{x}_k = \mathbf{x}) \right) \quad (1.23)$$

Thus, the ML detection requires an exhaustive search over a total of \mathcal{A}^{N_i} vector symbols, rendering the decoding complexity exponential in the number of channel inputs.

In the more general case of time-dispersive LTI MIMO channel, we should consider the likelihood function of the observation conditioned by the frame of symbols $x_k^{(i)}, x_{k-1}^{(i)}, \dots, x_{k-\nu}^{(i)}$ ($\forall i$). Thus, the exponential complexity of the ML receiver increases simultaneously with the number of inputs and with the channel memory, making its implementation costly for MIMO detection on severe ISI channels, especially as the input signal constellation size increases to improve spectral efficiency.

1.4.2 MMSE FIR equalizer

Let us consider the time-dispersive LTI MIMO channel model in (1.14). For a block of N_f received symbols, rewrite the system equation in the following matrix form:

$$\begin{bmatrix} \mathbf{y}_k \\ \mathbf{y}_{k-1} \\ \vdots \\ \mathbf{y}_{k-(N_f-1)} \end{bmatrix} = \begin{bmatrix} \mathbf{H}_0 & \mathbf{H}_1 & \dots & \mathbf{H}_\nu & \mathbf{0} & \dots & \mathbf{0} \\ \mathbf{0} & \mathbf{H}_0 & \mathbf{H}_1 & \dots & \mathbf{H}_\nu & \dots & \mathbf{0} \\ \vdots & & \ddots & & \ddots & & \vdots \\ \mathbf{0} & \dots & \mathbf{0} & \mathbf{H}_0 & \mathbf{H}_1 & \dots & \mathbf{H}_\nu \end{bmatrix} \begin{bmatrix} \mathbf{x}_k \\ \mathbf{x}_{k-1} \\ \vdots \\ \mathbf{x}_{k-(N_f-1)-\nu} \end{bmatrix} + \begin{bmatrix} \mathbf{n}_k \\ \mathbf{n}_{k-1} \\ \vdots \\ \mathbf{n}_{k-(N_f-1)} \end{bmatrix} \quad (1.24)$$

or, more compactly,

$$\mathbf{y} = \mathbf{H}\mathbf{x} + \mathbf{n} \quad (1.25)$$

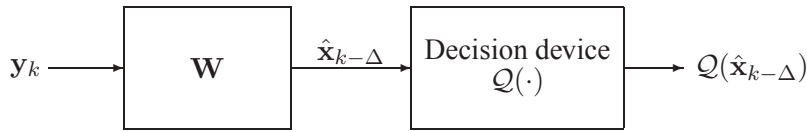


Figure 1.4: Block diagram of a linear receiver.

The vector \mathbf{y} is processed by a linear FIR equalizer to provide an estimate of the transmitted symbol vector; such an estimate is then quantized by the decision device $\mathcal{Q}(\cdot)$ to produce the symbol constellation (see Fig. 1.4). The output of the equalizer is equal to

$$\begin{aligned}\hat{\mathbf{x}}_k &= \sum_{\ell=0}^{N_f-1} \mathbf{W}_\ell \mathbf{y}_{k-\ell} \\ &= \underbrace{\begin{bmatrix} \mathbf{W}_0^H & \mathbf{W}_1^H & \dots & \mathbf{W}_{N_f-1}^H \end{bmatrix}}_{\triangleq \mathbf{W}} \mathbf{y}\end{aligned}\quad (1.26)$$

where \mathbf{W}_ℓ denotes the complex-valued matrix taps of size $N_o \times N_i$. The equalizer output $\hat{\mathbf{x}}_k$ is the estimate of the transmitted symbol vector $\mathbf{x}_{k-\Delta}$, with Δ denoting a processing delay. The value of Δ is related to the capability of the equalizer in performing causal and anticausal processing: the case $\Delta = 0$ corresponds to a strictly causal filtering, while the case $\Delta = N_f + \nu - 1$ corresponds to a strictly anticausal filtering.

The MMSE equalizer \mathbf{W} minimizes the trace of the error correlation matrix⁴

$$\begin{aligned}\mathbf{R}_e &\triangleq E [(\hat{\mathbf{x}}_k - \mathbf{x}_k)(\hat{\mathbf{x}}_k - \mathbf{x}_k)^H] \\ &\triangleq E [\mathbf{e}_k \mathbf{e}_k^H]\end{aligned}\quad (1.27)$$

By resorting to the orthogonality principle, and accounting for the independence of \mathbf{x} from \mathbf{n} , the optimum \mathbf{W} can be written as follows:

$$\mathbf{W}_{\text{MMSE}} = \mathbf{R}_y^{-1} \mathbf{H} \mathbf{R}_x \mathbf{e}_{\Delta+1}\quad (1.28)$$

⁴Let us note that it would be advisable to design the equalizer to adjust the properties of $\mathcal{Q}(\hat{\mathbf{x}}_k)$, instead of $\hat{\mathbf{x}}_k$, for instance to minimize the error rate. However, controlling the properties of $\mathcal{Q}(\hat{\mathbf{x}}_k)$ is much more difficult than controlling the properties of $\hat{\mathbf{x}}_k$.

where

$$\begin{aligned}
\mathbf{R}_x &\triangleq E[\mathbf{x}\mathbf{x}^H] \\
\mathbf{R}_n &\triangleq E[\mathbf{n}\mathbf{n}^H] \\
\mathbf{R}_y &\triangleq \mathbf{H}\mathbf{R}_x\mathbf{H} + \mathbf{R}_n \\
\mathbf{e}_{\Delta+1} &\triangleq \begin{bmatrix} \mathbf{0}_{N_i \times N_i \Delta} & \mathbf{I}_{N_i} & \mathbf{0}_{N_i \times N_i(N_f + \nu - \Delta - 1)} \end{bmatrix}^T
\end{aligned} \tag{1.29}$$

or, in other words, \mathbf{W}_{MMSE} is the conventional Wiener filter that processes the observation vector \mathbf{y} in order to estimate the desired vector $\mathbf{x}_{k-\Delta}$. Let us emphasize the importance of optimizing the delay Δ , which greatly affects the trace of \mathbf{R}_e : unfortunately, the optimization over Δ can be usually carried out only by an exhaustive procedure. Moreover, for the sake of completeness, we point out that, in the MIMO environment, different delays Δ_ℓ ($\ell = 1, \dots, N_i$) can be chosen for each one of the symbols $x_{k-\Delta_\ell}^{(\ell)}$ to be estimated. However, since the optimization over Δ_ℓ is carried out by an exhaustive procedure, the computational complexity can be unsustainable.

Unfortunately, some channels will still be difficult to be equalized by utilizing only a linear filter. In fact, when the channel exhibits zeros close to the unit circle, the equalizer would need poles outside the unit circle becoming unstable and, at the same time, amplifying received noise, which leads to frequent decision errors.

In the following of the thesis, we will refer to the widely linear version of such equalizer rather than to the linear one [5].

1.4.3 ZF FIR equalizer

Let us rewrite the input-output relationship of the LTI time-dispersive MIMO channel in (1.14) as follows:

$$y_k^{(\ell)} = h_0^{(\ell, \ell)} x_k^{(\ell)} + \underbrace{\sum_{i \neq \ell} x_k^{(i)} h_0^{(\ell, i)}}_{\text{co-channel interference}} + \underbrace{\sum_{n=1}^{\nu^{(\ell, i)}} x_{k-n}^{(i)} h_n^{(\ell, i)}}_{\text{ISI}} + n_k^{(\ell)} \tag{1.30}$$

where the second term at the right-hand-side accounts for the effects of the remaining $N_i - 1$ inputs over the ℓ th output at the time instant k , while the third term accounts for the ISI. The ZF FIR equalizer is the linear filter which processes the observation vectors $\mathbf{y}_k, \mathbf{y}_{k-1}, \dots, \mathbf{y}_{k-(N_f-1)}$ to minimize the (co-channel interference + ISI) power measured at the output of the equalizer.

To this aim, consider the system model (1.25) and assume that $x_k^{(1)}$ is the symbol to be estimated⁵ on the basis of the observation \mathbf{y} , which is rewritten in the following equivalent form:

$$\mathbf{y} = \mathbf{H}(:, 1)x_k^{(1)} + \underbrace{\mathbf{H}_{(-1)}\mathbf{x}_{(-1)}}_{\triangleq \mathbf{z}} + \mathbf{n} \quad (1.31)$$

where $\mathbf{H}(:, k)$ denotes the k th column of \mathbf{H} , $\mathbf{H}_{(-1)}$ is given by \mathbf{H} deprived of its first column, and $\mathbf{x}_{(-1)}$ is given by \mathbf{x} deprived of its first row; the vector \mathbf{z} accounts for both the co-channel interference and the ISI. According to (1.26), the first column of the ZF matrix filter \mathbf{W}_{ZF} , i.e., the vector filter that provides the estimate $\hat{x}_k^{(1)}$ of $x_k^{(1)}$ by processing \mathbf{y} , is obtained by solving the following optimization problem:

$$\mathbf{W}_{\text{ZF}}(:, 1) = \underset{\mathbf{w}}{\operatorname{argmin}} |\mathbf{w}^H \mathbf{z}|^2 \quad \text{subject to: } \mathbf{w}^H \mathbf{H}(:, 1) = \beta^2 \quad (1.32)$$

with $\beta \in \mathbb{R}$. As known, the optimum filter is derived by exploiting the Lagrange multiplier method and is given by:

$$\mathbf{W}_{\text{ZF}}(:, 1) = \frac{\beta^2}{\mathbf{H}(:, 1)^H \mathbf{R}_z^{-1} \mathbf{H}(:, 1)} \mathbf{R}_z^{-1} \mathbf{H}(:, 1) \quad (1.33)$$

where $\mathbf{R}_z \triangleq E[\mathbf{z}\mathbf{z}^H]$. The same reasonings apply to $\mathbf{W}_{\text{ZF}}(:, \ell)$ ($\ell = 1, \dots, N_i$). For ill-conditioned \mathbf{H} , it is known that the ZF equalizer suffers from the noise enhancement; on the other hand, it is equivalent to the MMSE equalizer in presence of low noise level.

1.4.4 Decision-feedback FIR equalizers

In the class of the non-linear equalizers, the DF FIR equalizer constitutes an attractive compromise between complexity and performance. It can perform almost as well as the ML detector, but it requires a computational complexity only slightly higher than the linear equalizer. Its structure is depicted in Fig. 1.5. The received signal \mathbf{y}_k is the input of a linear feedforward FIR filter, whose output is denoted with \mathbf{z}_k . The estimate $\hat{x}_{k-\Delta}^{(\ell)}$ of the symbol $x_{k-\Delta}^{(\ell)}$ is obtained by subtracting from \mathbf{z}_k the output of a linear feedback FIR filter, which processes the past decisions provided by the decision device on the basis of the estimated symbols. In such a way, the output of the feedforward filter

⁵For the sake of clarity, we consider the case $\Delta = 0$.

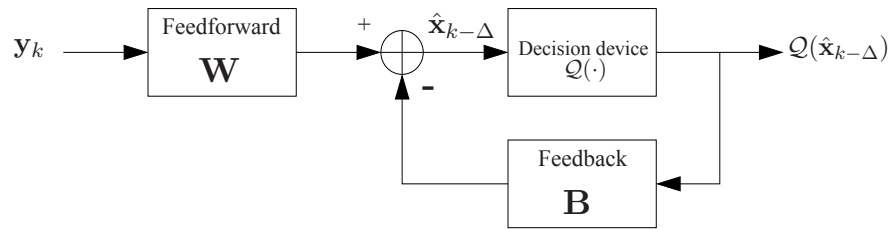


Figure 1.5: The decision feedback equalizer structure.

can be deprived of the co-channel interference and ISI due to previously transmitted symbols. As long as the decisions are correct, the equalizer provides a good estimate of the transmitted sequences.

Differently from the conventional SISO environment, three MIMO DF equalizer structures can be defined:

Scenario 1 The DF equalizer provides the estimate of $x_{k-\Delta}^{(\ell)}$ ($\ell = 1, \dots, N_i$) by resorting to the past decisions $Q(\hat{x}_{k-\Delta-n}^{(\ell)})$ with $n > 0$ and $\forall \ell$. Such an equalizer represents the MIMO DF counterpart of the conventional SISO DF equalizer.

Scenario 2 Assume that the channel inputs are ordered so that lower indexed components of \mathbf{x}_k are detected first; then, the DF equalizer utilizes, together with past decisions, the current decisions $Q(\hat{x}_{k-\Delta}^{(1)})$, $Q(\hat{x}_{k-\Delta}^{(2)})$, \dots , $Q(\hat{x}_{k-\Delta}^{(\ell-1)})$ to estimate the symbol $x_{k-\Delta}^{(\ell)}$. In other words, the decisions are taken sequentially starting with the lower indexed components.

Scenario 3 When all the current decisions $Q(\hat{x}_{k-\Delta}^{(1)})$, $Q(\hat{x}_{k-\Delta}^{(2)})$, \dots , $Q(\hat{x}_{k-\Delta}^{(N_i)})$ are available from a previous detection stage, then they can be processed together with past decisions to provide the estimate of the symbol of interest $x_{k-\Delta}^{(\ell)}$. Such a detection scenario deals with the multistage detection [6].

Accounting for the system model (1.25), the output of the DF FIR equalizer

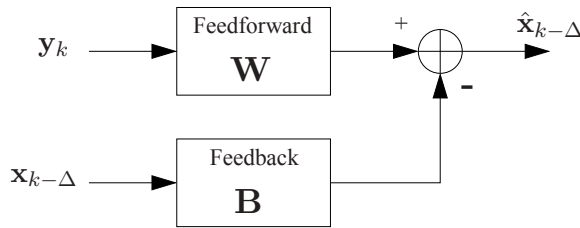


Figure 1.6: The decision feedback equalizer in absence of error propagation.

can be written as follows:

$$\hat{\mathbf{x}}_{k-\Delta} = \underbrace{\begin{bmatrix} \mathbf{W}_0^H & \mathbf{W}_1^H & \dots & \mathbf{W}_{N_f-1}^H \end{bmatrix}}_{\triangleq \mathbf{W}^H} \mathbf{y} - \underbrace{\begin{bmatrix} \mathbf{B}_0^H - \mathbf{I}_{N_i} & \mathbf{B}_1^H & \dots & \mathbf{B}_{N_b}^H \end{bmatrix}}_{\triangleq \mathbf{B}^H - \begin{bmatrix} \mathbf{I}_{N_i} & \mathbf{0}_{N_i \times N_i N_b} \end{bmatrix}} \cdot \begin{bmatrix} Q(\hat{\mathbf{x}}_{k-\Delta}) \\ Q(\hat{\mathbf{x}}_{k-\Delta-1}) \\ \vdots \\ Q(\hat{\mathbf{x}}_{k-\Delta-N_b}) \end{bmatrix} \quad (1.34)$$

where N_b is the number of the $N_i \times N_i$ matrix taps \mathbf{B}_ℓ constituting the feedback filter \mathbf{B} . The three different equalizer structures previously discussed can be mathematically described by some constraints on the matrix tap \mathbf{B}_0 . Specifically, one has that the constraint $\mathbf{B}_0 = \mathbf{I}_{N_i}$ holds in Scenario 1, whereas, in Scenario 2, the matrix \mathbf{B}_0^H is constrained to be monic⁶ lower triangular. Finally, in Scenario 3, \mathbf{B}_0^H is constrained to be monic.

The feedforward filter \mathbf{W} and the feedback one \mathbf{B} in (1.34) can be designed according to any chosen optimization criterion. Let us note that any optimization procedure should take into account the non-linearity of the decision device. However, also for simple decision mechanism, the derivation of a closed form for the optimum equalizer is impossible to obtain. For such a reason, in this thesis we adopt the common assumption that the decisions which affect the current estimate, are correct, i.e., $Q(\hat{x}_k^{(\ell)}) = x_k^{(\ell)}$. According to such an assumption, the feedback filter can be treated as a feedforward filter which processes a delayed version of the transmitted symbols, as depicted in Fig. 1.6. However, it is clear that, in a realistic environment, the error propagation can not be ignored and the performance loss due to the feeding-back of incorrect decisions has to be measured.

⁶A square matrix with diagonal elements all equal to 1.

As previously discussed about the linear equalization, in all the three detection scenarios the delay Δ has to be optimized, especially for short feedforward filters. Moreover, different delays Δ_ℓ ($\ell = 1, \dots, N_i$) for each one of the symbols to be estimated can be chosen. However, apart from the computational complexity in optimizing such parameters, allowing different processing delays does not make available all the past decisions in Scenario 1, and all the current ones in Scenario 2 and Scenario 3, leading so to a more complicated mathematical formulation for the DF-based equalization.

The MMSE DF equalization will be considered in details in Chapter 3. Moreover, we will refer to the widely linear version of such equalizer [7], which provides better performance than that got by the conventional linear DF equalizer.

1.5 Transceiver architectures

Let us consider the MIMO communication system model depicted in Fig. 1.7. At the transmitter side, the information bit streams are mapped to generate the information symbol streams. Hence, such streams are processed by a precoder and transmitted over the MIMO channel. At the receiver side, the channel outputs are processed by the decoder which provides an estimate of the precoder inputs. Finally, the symbol de-mapper allows one to recover the (estimated) information bit streams. When the channel state information (CSI) is available at both ends of the link, the precoder and the decoder can be jointly designed, according to the chosen optimization criterion, to improve the system performance.

In Fig. 1.8 we have depicted a transceiver structure employing a linear filter as precoder and decoder. For simplicity, we assume the time non-dispersive channel model

$$\mathbf{y}_k = \mathbf{H}\mathbf{x}_k + \mathbf{n}_k \quad (1.35)$$

affected by additive spatially and temporally white noise with correlation matrix $\mathbf{R}_n = \mathbf{I}_{N_o}$. The symbol vector to be transmitted is denoted with $\mathbf{s}_k \triangleq [s_k^{(1)}, s_k^{(2)}, \dots, s_k^{(B)}]^T$ with $s_k^{(\ell)}$ drawn from the constellation \mathcal{A}_ℓ ($\ell = 1, \dots, B$). Moreover, we assume $E[\mathbf{s}_k \mathbf{s}_{k-n}^T] = \mathbf{I}_B \delta_{k-n}$. The precoder $\mathbf{F} \in \mathbb{C}^{N_i \times B}$ processes \mathbf{s}_k and provides the channel input vector $\mathbf{x}_k \triangleq \mathbf{F}\mathbf{s}_k$ of size N_i . At the receiver side, the equalizer provides the estimate $\hat{\mathbf{s}}_k$ of \mathbf{s}_k by processing the received vector \mathbf{y}_k . The overall system equation is given by:

$$\hat{\mathbf{s}}_k = \mathbf{G}\mathbf{H}\mathbf{F}\mathbf{s}_k + \mathbf{G}\mathbf{n}_k \quad (1.36)$$

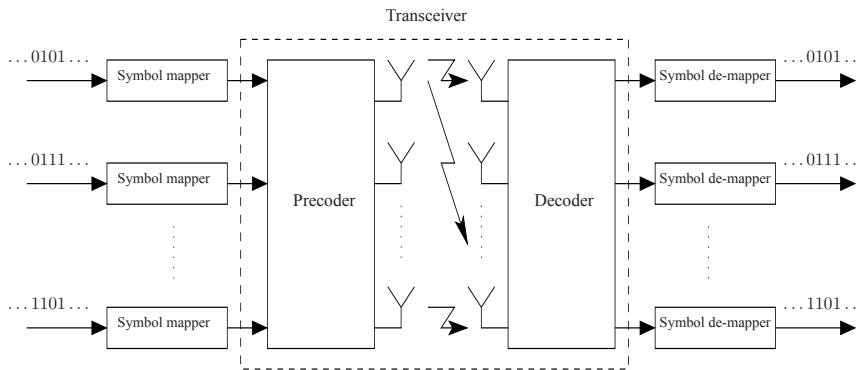


Figure 1.7: The transceiver architecture.

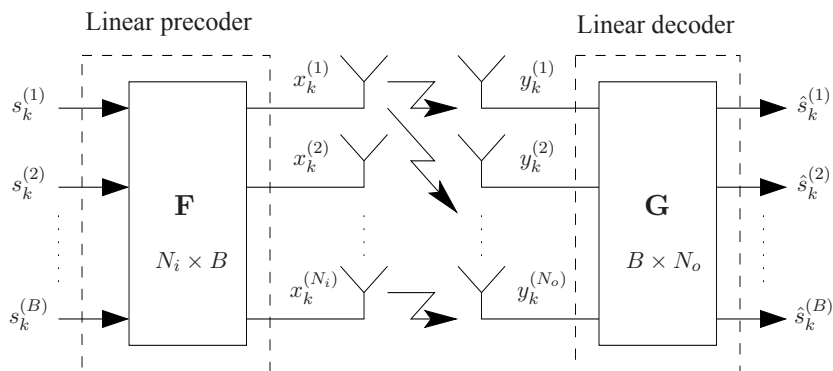


Figure 1.8: Linear transceiver architecture.

The transceiver can be optimized according to the MMSE criterion as well as the ZF criterion. In addition, the transmitter and the receiver can be jointly designed to maximize the mutual information between precoder input and decoder output, say $\mathcal{I}(\mathbf{s}_k, \hat{\mathbf{s}}_k)$: in such a case, it has been shown in [8] that the precoder maximizing the mutual information is unique, whereas the optimum decoder is nonunique and the available degrees of freedom can be utilized to synthesize the receiver according any other optimization criterion.

It can be shown that (see [9, 8]), according to any optimization criterion, the optimum matrices \mathbf{F} and \mathbf{G} are given by

$$\begin{aligned} \mathbf{F}^{(opt)} &= \mathbf{V}\Phi \\ \mathbf{G}^{(opt)} &= \mathbf{\Gamma}\mathbf{\Lambda}^{-1}\mathbf{V}^H\mathbf{H}^H \end{aligned} \quad (1.37)$$

where \mathbf{V} and $\mathbf{\Lambda}$ are the eigenvector and the eigenvalue matrices, respectively, of $\mathbf{H}^H \mathbf{H}$ being \mathbf{H} the channel matrix, and where $\mathbf{\Phi}$ and $\mathbf{\Gamma}$ represent a diagonal matrix with positive entries and an invertible matrix, respectively, that depend on the chosen optimization criterion.

Let now $\mathbf{\Gamma}$ be a diagonal matrix. It is straightforward to verify that, in such a special case, the overall MIMO system is described by the diagonal matrix $\mathbf{\Phi}\mathbf{\Gamma}$ and, hence, the transmission over the MIMO channel \mathbf{H} is equivalent to $\text{rank}(\mathbf{H})$ transmissions over $\text{rank}(\mathbf{H})$ parallel non-dispersive subchannels characterized by a transmit gain ϕ_i , corresponding to the i th diagonal element of $\mathbf{\Phi}$, and a receive gain γ_i , corresponding to the i th diagonal element of $\mathbf{\Gamma}$. It can be shown that such a model arises when $\mathcal{I}(\mathbf{s}_k, \hat{\mathbf{s}}_k)$ has to be maximized, as well as when we adopt the MMSE criterion or the ZF one [1].

Before concluding this section, it is important to underline two interesting issues recently discussed in [10] about MIMO communication systems:

- According to the transceiver defined in (1.37), let us evaluate the correlation matrix of the estimation error measured at the output of the decoder:

$$\mathbf{R}_e \triangleq E [(\hat{\mathbf{s}}_k - \mathbf{s}_k)(\hat{\mathbf{s}}_k - \mathbf{s}_k)^H] \quad (1.38)$$

$$= \mathbf{\Gamma} (\mathbf{\Phi}^2 + \mathbf{\Lambda}^{-1}) \mathbf{\Gamma}^H - \mathbf{\Phi}\mathbf{\Gamma}^H + \mathbf{\Gamma}\mathbf{\Phi} + \mathbf{I}_B \quad (1.39)$$

The choice of a diagonal $\mathbf{\Gamma}$ allows one to obtain uncorrelated estimates of \mathbf{s}_k and, hence, uncorrelated estimation errors. This represents an important advantage provided by such a transceiver structure since the decision device can separately detect the transmitted symbols, requiring so a lower computational complexity⁷.

- It can be simply verified that, given a diagonal $\mathbf{\Gamma}$, the mutual information $\mathcal{I}(\mathbf{s}_k, \hat{\mathbf{s}}_k)$ is equal to:

$$\mathcal{I}(\mathbf{s}_k, \hat{\mathbf{s}}_k) = \sum_{i=1}^{\text{rank}(\mathbf{H}_k)} \log(1 + \lambda_i \phi_i^2) \quad (1.40)$$

i.e., it is equal to the sum of the capacities of $\text{rank}(\mathbf{H})$ SISO non-dispersive channels. However, note that, due to the different values of the eigenvalues λ_ℓ , one has that:

⁷When \mathbf{R}_e is not diagonal, the correlation among the different estimates contains useful information to be exploited by the subsequent decoding; hence, the optimum decoding procedure becomes more complicated.

1. since different symbol rates are achieved over each subchannel, different symbol alphabets can be utilized at the transmitter: specifically, dense constellations can be transmitted over subchannels corresponding to large λ_ℓ , while thin constellations has to be utilized over subchannels corresponding to small λ_ℓ . Hence, more complicated symbol mapper/de-mapper devices are in general required to achieve the capacity.
2. Different error rates are achieved over each subchannel. Such an undesirable behavior can be overcome by exploiting non linear processing techniques which allow us to design the transceiver in a more flexible manner. For instance, in [11], the precoder is designed to maximize $\mathcal{I}(\mathbf{s}_k, \hat{\mathbf{s}}_k)$, whereas a DF-based decoder, designed according to the MMSE criterion, is employed⁸: it can be shown that such a transceiver structure allows one to reach the same error rate over all the subchannel. An alternative, but expensive, solution is to utilize a large number of receiving antennas, i.e., $N_o \gg N_i$.

In [13], it is considered the joint design of the transmitter and the receiver, according to MMSE criterion, for MIMO channels by employing WL filters.

⁸Analogously, in [12], the authors synthesize the decoder according to the ZF criterion.

Chapter 2

Widely linear equalization

Complex random vectors and processes are a convenient tool to describe statistical fluctuation phenomena, including waves. They are thus used in fields as diverse as optics, quantum mechanics, electro-magnetics, and communications. Although technically a complex vector could always be replaced by a pair of real vectors, much of the beauty and simplicity of the description would be lost. Oftentimes, it is subliminally assumed that the theory of complex random vectors is no different than that of real ones, as long as the definition of the covariance matrix of a random vector \mathbf{x} is changed from $E[\mathbf{x}\mathbf{x}^T]$ in the real case to $E[\mathbf{x}\mathbf{x}^H]$, using the conjugate transpose H . Most of the time, this assumption is justified. However, it can happen that \mathbf{x} and its conjugate \mathbf{x}^* are correlated. Then, the covariance matrix $E[\mathbf{x}\mathbf{x}^H]$ no longer completely describes the second-order behavior of \mathbf{x} and another quantity, which is also known as the *complementary covariance* or *pseudo-covariance* $E[\mathbf{x}\mathbf{x}^T]$, has to be taken into account. In the following, we will assume that the statistical expectations of the involved random signals are null, hence we will deal with the correlation and *pseudo-correlation* matrices; this assumption simplifies the mathematical processing with no loss of generality.

Vectors which have a vanishing pseudo-covariance are called *proper* or *circularly symmetric*; the others *improper* or *rotationally variant* [14, 15, 16, 17, 18, 19]. In the next sections, we will present two results which have been obtained by taking full advantage of second-order information of rotationally variant signals by means of widely linear (WL) filtering in the mean square estimation. The former result regards the joint transmitter and receiver in-phase and quadrature (IQ) imbalance compensation by means of a minimum mean square error (MMSE) WL equalizer; with a limited increase in the computa-

tional complexity of the equalization stage, one gets considerable gains both in terms of MMSE and symbol error rate (SER) in comparison with a conventional MMSE linear equalizer. The latter result concerns the problem of the constellation optimization in presence of a WL MMSE equalizer; a scheme which performs a WL transformation, dependent on the channel state, of the transmitted symbols has been proposed in order to optimize the receiver performance in terms of SER. Optimum and suboptimum procedures have been considered and their performance analysis has shown that also the simplest suboptimum procedure provides significant improvements over a fixed-constellation scheme. The main tool used in both cases to exploit the statistical redundancy of the improper signals, i.e., the WL mean square estimation, is described in a preliminary section.

Notation

The following notation is adopted throughout the chapter: the superscripts $*$, T and H denote the complex-conjugate, transpose and hermitian operators, respectively; j the imaginary unit; $E[\cdot]$ the statistical expectation; δ_k the Kronecker delta; \mathbf{I}_N the identity matrix of size N ; \mathbf{e}_k the vector having 1 as the $(k + 1)$ th entry and 0 elsewhere; $\mathbf{0}$ the vector/matrix with all zero entries (the size is omitted for brevity); $\Re\{\cdot\}$ and $\Im\{\cdot\}$ the real part and the imaginary one of their arguments, respectively; a_i the i th entry of the vector \mathbf{a} ; a_{ik} the (i, k) entry of the matrix \mathbf{A} ; \mathbf{a}_k the k th column of \mathbf{A} ; $\|\cdot\|_p$ the p -norm with $\|\mathbf{a}\|_{-\infty} \triangleq \min_i |a_i|$; $H(z) \triangleq \sum_{k=-\infty}^{+\infty} h_k z^{-k}$ the z -transform of h_k .

2.1 Widely linear mean square estimation with complex data

Mean square estimation is one of the most fundamental techniques of statistical signal processing. The problem can be stated as follows: let \mathbf{d} be a M -dimensional zero-mean random vector to be estimated (estimandum) in terms of an observation which is a N -dimensional zero-mean random vector $\mathbf{r} \in \mathbb{C}^N$. In (linear mean square estimation) LMSE, the problem is to find an estimation written as

$$\hat{\mathbf{d}} = \mathbf{W}^H \mathbf{r} \quad (2.1)$$

where \mathbf{W} is a $N \times M$ complex-valued matrix. Let $\mathbf{e} \triangleq \mathbf{d} - \hat{\mathbf{d}}$ be the error vector whose correlation matrix is denoted with $\mathbf{R}_{ee} = E[\mathbf{e}\mathbf{e}^H]$. The linear

filter which minimizes the mean square error (MSE), hence, the $\text{trace}\{\mathbf{R}_{ee}\}$, is called Wiener filter; it is equal to

$$\mathbf{W}^{(opt)} = \mathbf{R}_{rr}^{-1} \mathbf{R}_{rd} \quad (2.2)$$

where $\mathbf{R}_{rr} \triangleq E[\mathbf{r}\mathbf{r}^H]$ and $\mathbf{R}_{rd} \triangleq E[\mathbf{r}\mathbf{d}^H]$. From this, the error correlation matrix follows

$$\mathbf{R}_{ee}^L = \mathbf{R}_{dd} - \mathbf{R}_{rd}^H \mathbf{R}_{rr}^{-1} \mathbf{R}_{rd} \quad (2.3)$$

with $\mathbf{R}_{dd} \triangleq E[\mathbf{d}\mathbf{d}^H]$.

Let us consider now the problem of widely linear mean square estimation (WLMSE) which consists of finding the matrices \mathbf{F} and \mathbf{G} in such a way that

$$\hat{\mathbf{d}} = \mathbf{F}^H \mathbf{r} + \mathbf{G}^H \mathbf{r}^* \quad (2.4)$$

gives the MMSE, hence, the minimum of the $\text{trace}\{\mathbf{R}_{ee}\}$ according to (2.4) [16]. It is clear that $\hat{\mathbf{d}}$ is no more a linear function of \mathbf{r} as in (2.1). However, the moment of order k of $\hat{\mathbf{d}}$ is completely defined from the moments of order k of \mathbf{r} and \mathbf{r}^* , which characterizes a form of linearity. This is why (2.4) is called a *wide sense linear* filter or system. The optimum filters are

$$\mathbf{F}^{(opt)} = [\mathbf{R}_{rr} - \mathbf{R}_{rr^*} \mathbf{R}_{rr^*}^{-1} \mathbf{R}_{rr^*}]^{-1} \cdot [\mathbf{R}_{rd} - \mathbf{R}_{rr^*} \mathbf{R}_{rr^*}^{-1} \mathbf{R}_{rd^*}] \quad (2.5)$$

$$\mathbf{G}^{(opt)} = [\mathbf{R}_{rr} - \mathbf{R}_{rr^*} \mathbf{R}_{rr^*}^{-1} \mathbf{R}_{rr^*}]^{-*} \cdot [\mathbf{R}_{rd^*} - \mathbf{R}_{rr^*} \mathbf{R}_{rr^*}^{-1} \mathbf{R}_{rd}]^* \quad (2.6)$$

where $\mathbf{R}_{rr^*} \triangleq E[\mathbf{r}\mathbf{r}^T]$ is also called *pseudo-correlation* matrix and $\mathbf{R}_{rd^*} \triangleq E[\mathbf{r}\mathbf{d}^T]$; we assume that the involved inverse matrices exist, too. The error correlation matrix follows

$$\mathbf{R}_{ee}^{WL} = \mathbf{R}_{dd} - \left(\mathbf{F}^{(opt)H} \mathbf{R}_{rd} + \mathbf{G}^{(opt)H} \mathbf{R}_{rd^*} \right) \quad (2.7)$$

The advantage of the WLMSE procedure over the strictly linear one is characterized by the matrix $\Delta_{ee} \triangleq \mathbf{R}_{ee}^L - \mathbf{R}_{ee}^{WL}$, which can be expressed as

$$\Delta_{ee} = [\mathbf{R}_{rd^*} \mathbf{R}_{rr^*} \mathbf{R}_{rr^*}^{-1} \mathbf{R}_{rd}]^H [\mathbf{R}_{rr} - \mathbf{R}_{rr^*} \mathbf{R}_{rr^*}^{-1} \mathbf{R}_{rr^*}]^{-1} \cdot [\mathbf{R}_{rd^*} \mathbf{R}_{rr^*} \mathbf{R}_{rr^*}^{-1} \mathbf{R}_{rd}] \quad (2.8)$$

As the matrix $[\mathbf{R}_{rr} - \mathbf{R}_{rr^*} \mathbf{R}_{rr^*}^{-1} \mathbf{R}_{rr^*}]$ is positive definite, the LMSE cannot outperform the WL one.

Let us note that, if \mathbf{r} is circularly symmetric, i.e., $\mathbf{R}_{rr^*} = \mathbf{0}$ and, moreover, \mathbf{r} and \mathbf{d} are cross-circularly symmetric, i.e., $\mathbf{R}_{rd^*} = \mathbf{0}$, then $\mathbf{F}^{(opt)} = \mathbf{W}^{(opt)}$

and $\mathbf{G}^{(opt)} = \mathbf{0}$, hence $\Delta_{ee} = \mathbf{0}$: this means that the WL MMSE estimator will degenerate into the linear one, providing so the same performance. A special case is represented by the estimation of a real-valued random vector \mathbf{d} : $\mathbf{d} = \Re\{\mathbf{d}\}$ from a complex-valued observation vector. Being $\mathbf{R}_{rd} = \mathbf{R}_{rd^*}$, one has (see (2.5)-(2.6))

$$\mathbf{F} = \mathbf{G}^* \Rightarrow \hat{\mathbf{d}} = 2\Re\{\mathbf{F}^H \mathbf{r}\} \quad (2.9)$$

Therefore, the WL filtering leads to a real-valued estimation unlike the linear filtering which provides a complex-valued estimation of a real-valued estimandum. Finally, if data were real, i.e., $\mathbf{r} = \Re\{\mathbf{r}\}$, the WLMSE would degenerate into the linear one: in fact, it would be redundant to process jointly \mathbf{r} and \mathbf{r}^* .

To conclude, one can state that, if the observation vector and/or the one to be estimated are rotationally variant, i.e., their pseudo-correlation matrices are nonnull, then the employment of a linear filter can not be an optimum choice in an MMSE estimation because it doesn't exploit the statistical redundancy exhibited by the signals which the WL filtering provides for.

2.2 MMSE equalization in presence of transmitter and receiver IQ imbalance

In the last years, the mass production of the modern communication systems has favoured the wide spread of low-cost fabrication technologies (e.g., the CMOS technology) giving rise to some unpredictable imperfections associated with the transmitting and receiving architectures. Since such imperfections can greatly affect the system performances, proper countermeasures have to be adopted. In this context, it is well known [20] that the analog stage which performs the frequency conversion suffers from the imbalance between the two periodic signals in the in-phase (I) and quadrature (Q) branches of the converter: $|c_1^I| \neq |c_1^Q|$ and/or $\arg\{c_1^I\} \neq \arg\{c_1^Q\} + 90^\circ$, where we have denoted with c_1^I and c_1^Q the first Fourier coefficient of the periodic signal employed in the I and Q branches, respectively.

The receiver design in presence of both transmitter IQ (Tx-IQ) imbalance, i.e., the one at the up-conversion stage, and receiver IQ (Rx-IQ) imbalance, i.e., the one at the down-conversion stage, has been already addressed [21] with reference to an orthogonal frequency division multiplexing (OFDM) system. However, at the best of our knowledge, this problem has not yet been addressed with reference to a single-carrier scheme operating over a single-input single-output linear time-dispersive channel. For such a reason, in the

paper [22], we address the design of the MMSE feedforward-based finite impulse response (FIR) equalizer in the presence of both Tx-IQ and Rx-IQ imbalance. We first note that the IQ impairments render the received signal rotationally variant (i.e., its pseudo-correlation is nonnull). Then, we resort to the WL equalizer [16, 5], i.e., the one which processes both the received signal and its conjugate version, to estimate the transmitted signal. In fact, it is well known that the WL filtering allows one to improve the performances of the conventional linear (L) equalizer by exploiting the statistical redundancy exhibited by the signal to be processed. However, while the Rx-IQ imbalance can be completely compensated by resorting [21, 23, 24] to a time non-dispersive WL equalizer, we show that the Tx-IQ imbalance can not be compensated at the receiver side, with the exception of the very special case where the channel is non-dispersive and the noise is absent. Finally, the performance loss due to the IQ impairments are evaluated in terms of MMSE and symbol error rate, for both the WL MMSE equalizer and L one.

2.2.1 System model

In this section, we introduce the SISO linear time-invariant and time-dispersive noisy channel affected by both the Tx-IQ and the Rx-IQ imbalance.

Let us denote with s_k the zero-mean unit-power circularly symmetric wide-sense-stationary (WSS) sequence to be transmitted. By accounting for the Tx-IQ imbalance, one has that the channel input is given by

$$x_k = \frac{1}{\sqrt{|\mu_{Tx}|^2 + |\nu_{Tx}|^2}} \cdot (\mu_{Tx}s_k + \nu_{Tx}s_k^*) \quad (2.10)$$

where

$$\mu_{Tx} \triangleq \cos(\theta_{Tx}/2) + j\alpha_{Tx} \sin(\theta_{Tx}/2) \quad (2.11)$$

$$\nu_{Tx} \triangleq \alpha_{Tx} \cos(\theta_{Tx}/2) - j \sin(\theta_{Tx}/2) \quad (2.12)$$

with α_{Tx} and θ_{Tx} denoting the up-converter amplitude and the phase imbalance, respectively. From (2.10)-(2.12) one has that

$$\mathbb{E}[x_k x_{k-\ell}^*] = \delta_\ell \quad (2.13)$$

$$\mathbb{E}[x_k x_{k-\ell}] = \frac{2\mu_{Tx}\nu_{Tx}}{|\mu_{Tx}|^2 + |\nu_{Tx}|^2} \cdot \delta_\ell \quad (2.14)$$

i.e., the channel input exhibits a nonnull pseudo-correlation and, hence, it is rotationally variant. By assuming that the down-converter at the receiver side

is affected by the amplitude imbalance α_{Tx} and the phase one θ_{Tx} , the received signal can be written as follows:

$$z_k = \mu_{Rx} y_k + \nu_{Rx} y_k^* \quad (2.15)$$

where

$$y_k = \sum_{\ell=0}^L h_{\ell} x_{k-\ell} + n_k \quad (2.16)$$

denotes the output of the linear time-dispersive channel with FIR $h_{\ell}(\ell = 0, \dots, L)$, n_k the WSS additive noise assumed circularly symmetric and independent of the useful signal, and μ_{Rx} and ν_{Rx} are defined accordingly to (2.11) and (2.12). Let us note that, in our model, the Tx-IQ and the Rx-IQ imbalances are defined according to each other, with the exception of the transmit-power normalization at the transmitter side. Such a choice follows from the fact that the while the Rx-IQ imbalance affects both the useful signal and the noise (letting the signal-to-noise unchanged), the Tx-IQ imbalance affects the only useful signal and, without the proper normalization, can increase the signal-to-noise ratio measured at the receiver side.

With reference to a block of N_f received samples, the overall system equation can be expressed in matrix notation as follows:

$$\mathbf{z}_k \triangleq \begin{bmatrix} z_k \\ z_{k-1} \\ \vdots \\ z_{k-(N_f-1)} \end{bmatrix} = \mu_{Rx} \mathbf{y}_k + \nu_{Rx} \mathbf{y}_k^* \quad (2.17)$$

where

$$\begin{aligned} \mathbf{y}_k &\triangleq \begin{bmatrix} h_0 & h_1 & \dots & h_L & 0 & \dots & 0 \\ 0 & h_0 & h_1 & \dots & h_L & 0 & \dots \\ \vdots & & \ddots & & \ddots & & \vdots \\ 0 & 0 & 0 & h_0 & h_1 & \dots & h_L \end{bmatrix} \mathbf{x}_k + \mathbf{n}_k \\ &= \mathbf{H} \mathbf{x}_k + \mathbf{n}_k \end{aligned} \quad (2.18)$$

$\mathbf{x}_k \triangleq [x_k \ x_{k-1} \ \dots \ x_{k-N_f+L-1}]^T$ with entries given by (2.10), and $\mathbf{n}_k \in \mathbb{C}^{N_f \times 1}$ defined according to \mathbf{z}_k .

It is easy verified that the correlation and the pseudo-correlation matrices $\mathbf{R}_{zz} \triangleq \mathbb{E}[\mathbf{z}_k \mathbf{z}_k^H]$ and $\mathbf{R}_{zz^*} \triangleq \mathbb{E}[\mathbf{z}_k \mathbf{z}_k^T]$, respectively, are given by:

$$\mathbf{R}_{zz} = |\mu_{Rx}|^2 \mathbf{R}_{yy} + 2\Re\{\mu_{Rx} \nu_{Rx}^* \mathbf{R}_{yy^*}\} + |\nu_{Rx}|^2 \mathbf{R}_{yy}^* \quad (2.19)$$

$$\mathbf{R}_{zz^*} = \mu_{Rx}^2 \mathbf{R}_{yy^*} + 2\mu_{Rx} \nu_{Rx} \Re\{\mathbf{R}_{yy}\} + \nu_{Rx}^2 \mathbf{R}_{yy}^* \quad (2.20)$$

where $\mathbf{R}_{yy} \triangleq \mathbb{E}[\mathbf{y}_k \mathbf{y}_k^H]$ and $\mathbf{R}_{yy^*} \triangleq \mathbb{E}[\mathbf{y}_k \mathbf{y}_k^T]$ are equal to

$$\mathbf{R}_{yy} = \mathbf{H}\mathbf{H}^H + \mathbf{R}_n \quad (2.21)$$

$$\mathbf{R}_{yy^*} = \frac{2\mu_{Tx}v_{Tx}}{|\mu_{Tx}|^2 + |v_{Tx}|^2} \mathbf{H}\mathbf{H}^T \quad (2.22)$$

and \mathbf{R}_n is the noise correlation matrix. From (2.19)-(2.22), it follows that the received signal is rotationally variant when the Tx-IQ or/and Rx-IQ imbalance is/are present.

2.2.2 MMSE receiver for joint Tx-IQ and Rx-IQ imbalance compensation

In this section, the joint compensation of the Tx-IQ and Rx-IQ imbalances is addressed by resorting to an MMSE feedforward-based FIR equalizer. More specifically, we derive the widely linear equalizer structure in the presence of Tx-IQ and Rx-IQ imbalance and its performances.

The WL MMSE equalizer is constituted by two FIR filters $\mathbf{w} \triangleq [w_0 \ w_1 \ \dots \ w_{N_f-1}]^T$ and $\mathbf{g} \triangleq [g_0 \ g_1 \ \dots \ g_{N_f-1}]^T$ that process the down-converter output z_k and its conjugate version z_k^* , respectively. The optimum filters $\mathbf{w}^{(opt)}$ and $\mathbf{g}^{(opt)}$ minimizing the mean square error $\mathbb{E}[|s_{k-\Delta} - \mathbf{w}^H \mathbf{z}_k - \mathbf{g}^H \mathbf{z}_k^*|^2]$ are given by [25, 5]:

$$\begin{bmatrix} \mathbf{w}^{(opt)} \\ \mathbf{g}^{(opt)} \end{bmatrix} = \begin{bmatrix} \mathbf{R}_{zz} & \mathbf{R}_{zz^*} \\ \mathbf{R}_{zz^*}^* & \mathbf{R}_{zz}^* \end{bmatrix}^{-1} \begin{bmatrix} \mathbf{p}_{zs} \\ \mathbf{p}_{zs^*}^* \end{bmatrix} \quad (2.23)$$

where $\mathbf{p}_{zs} \triangleq \mathbb{E}[\mathbf{z}s_{k-\Delta}^*]$, $\mathbf{p}_{zs^*} \triangleq \mathbb{E}[\mathbf{z}s_{k-\Delta}]$, and with the integer Δ denoting the decision delay to be chosen according to the MMSE criterion. From (2.23), by utilizing the matrix inversion lemma and after some matrix manipulations, it can be shown that the equalizer is constituted by the cascade of the zero-memory WL filter which completely compensates the Rx-IQ imbalance [23, 26, 24], and the WL MMSE equalizer that provides the estimate of $s_{k-\Delta}$ by processing the \mathbf{y}_k ; more specifically, one has:

$$\begin{bmatrix} \mathbf{w}^{(opt)} \\ \mathbf{g}^{(opt)} \end{bmatrix} = \begin{bmatrix} \mu_{Rx}^* \mathbf{I} & v_{Rx} \mathbf{I} \\ v_{Rx}^* \mathbf{I} & \mu_{Rx} \mathbf{I} \end{bmatrix}^{-1} \begin{bmatrix} \mathbf{w}_0^{(opt)} \\ \mathbf{g}_0^{(opt)} \end{bmatrix} \quad (2.24)$$

where

$$\begin{aligned} \mathbf{w}_0^{(opt)} \triangleq & \frac{1}{\sqrt{|\mu_{Tx}|^2 + |v_{Tx}|^2}} [\mathbf{R}_{yy} - \mathbf{R}_{yy^*} \mathbf{R}_{yy}^{-*} \mathbf{R}_{yy^*}^*]^{-1} \\ & \times [\mu_{Tx} \mathbf{H} - v_{Tx}^* \mathbf{R}_{yy^*} \mathbf{R}_{yy}^{-*} \mathbf{H}^*] \mathbf{e}_\Delta \end{aligned} \quad (2.25)$$

$$\mathbf{g}_0^{(opt)} \triangleq \frac{1}{\sqrt{|\mu_{Tx}|^2 + |\nu_{Tx}|^2}} [\mathbf{R}_{yy} - \mathbf{R}_{yy}^* \mathbf{R}_{yy}^{-*} \mathbf{R}_{yy}^*]^{-*} \quad (2.26)$$

$$\times [\nu_{Tx} \mathbf{H} - \nu_{Tx}^* \mathbf{R}_{yy}^* \mathbf{R}_{yy}^{-*} \mathbf{H}^*]^{-*} \mathbf{e}_\Delta$$

are the two filters which process \mathbf{y}_k and \mathbf{y}_k^* , respectively, or, equivalently, are the WL MMSE equalizer filters in the absence of Rx-IQ imbalance. It is straightforwardly verified that *a)* in the absence of both Tx-IQ and Rx-IQ imbalances, the MMSE equalizer is the linear MMSE equalizer, i.e., the WL MMSE equalizer degenerates into the linear one; *b)* in the presence of only Rx-IQ imbalance, the MMSE equalizer is WL, but the equalization is achieved by means of the WL zero-memory compensator followed by a linear filter, i.e., $g_0^{(opt)} = \mathbf{0}$; *c)* in the presence of only Tx-IQ imbalance, the MMSE equalizer is WL.

The MMSE achieved by the WL receiver, say $\varepsilon_{WL}(\mu_{Tx}, \nu_{Tx})$, does not depend on the Rx-IQ imbalance level and is equal to

$$\varepsilon_{WL}(\mu_{Tx}, \nu_{Tx}) = 1 - \mathbf{e}_\Delta^H \mathbf{H}^H \mathbf{Q}^{-1} \mathbf{H} \mathbf{e}_\Delta + \frac{4 |\mu_{Tx}|^2 |\nu_{Tx}|^2}{|\mu_{Tx}|^2 + |\nu_{Tx}|^2}$$

$$\cdot \Re \{ \mathbf{e}_\Delta^H \mathbf{H}^H \mathbf{Q}^{-1} \mathbf{H} \mathbf{H}^T \mathbf{R}_{yy}^{-*} \mathbf{H}^* \mathbf{e}_\Delta \} \quad (2.27)$$

with $\mathbf{Q} \triangleq \mathbf{R}_{yy} - \mathbf{R}_{yy}^* \mathbf{R}_{yy}^{-*} \mathbf{R}_{yy}^*$. Let us point out that the Tx-IQ imbalance, in general, can not be compensated for the following reasons: *i)* the useful signal and the noise suffer from different IQ impairments; *ii)* the presence of the time-dispersive channel. In fact, rewrite, up to the factor $(|\mu_{Tx}|^2 + |\nu_{Tx}|^2)^{-1/2}$, the input-output relation (2.18) as follows¹:

$$\begin{bmatrix} \mathbf{y}_k \\ \mathbf{y}_k^* \end{bmatrix} = \begin{bmatrix} \mathbf{H} & \mathbf{0} \\ \mathbf{0} & \mathbf{H}^* \end{bmatrix} \begin{bmatrix} \mu_{Tx} \mathbf{I}_{N_f+L} & \nu_{Tx} \mathbf{I}_{N_f+L} \\ \nu_{Tx}^* \mathbf{I}_{N_f+L} & \mu_{Tx}^* \mathbf{I}_{N_f+L} \end{bmatrix} \begin{bmatrix} \mathbf{s}_k \\ \mathbf{s}_k^* \end{bmatrix} + \begin{bmatrix} \mathbf{n}_k \\ \mathbf{n}_k^* \end{bmatrix} \quad (2.28)$$

It is straightforwardly verified that unless the channel is non-dispersive, i.e., \mathbf{H} is invertible (or, equivalently, diagonal with entries h_0), and the noise is absent, the Tx-IQ imbalance can not be completely compensated at the receiver side. It follows that unless the Tx-IQ imbalance is compensated at the transmitter side (by resorting to the WL zero-memory compensator), its effects can not be removed at the receiver side.

Linear MMSE equalizer

Our focus on the WL-filtering based equalizer has been motivated by non-circularity properties of the received signal z_k . In order to assess the perfor-

¹Assume that the Rx-IQ imbalance has been compensated.

mance advantages provided by the WL MMSE equalizer in the presence of both Tx-IQ and Rx-IQ imbalances, let us derive the conventional linear (L) MMSE equalizer, which does not exploits the statistical redundancy exhibited by z_k . By accounting for (2.18)-(2.22), one has that the optimum linear equalizer is given by

$$\mathbf{f}_L^{(opt)} = \mathbf{R}_{zz}^{-1} (\mu_{Rx} \mu_{Tx} \mathbf{H} \mathbf{e}_\Delta + \nu_{Rx} \nu_{Tx}^* \mathbf{H} \mathbf{e}_\Delta) \frac{1}{\sqrt{|\mu_{Tx}|^2 + |\nu_{Tx}|^2}} \quad (2.29)$$

and the corresponding MMSE is equal to

$$\begin{aligned} \varepsilon_L(\mu_{Tx}, \nu_{Tx}, \mu_{Rx}, \nu_{Rx}) &= 1 - \frac{1}{|\mu_{Tx}|^2 + |\nu_{Tx}|^2} \\ &\cdot (|\mu_{Tx}|^2 |\mu_{Rx}|^2 \mathbf{e}_\Delta^H \mathbf{R}_{zz}^{-1} \mathbf{H} \mathbf{e}_\Delta + |\nu_{Tx}|^2 |\nu_{Rx}|^2 \mathbf{e}_\Delta^T \mathbf{R}_{zz}^{-1} \mathbf{H}^* \mathbf{e}_\Delta \\ &+ 2\Re\{\mu_{Tx} \nu_{Tx} \mu_{Rx} \nu_{Tx}^* \mathbf{e}_\Delta^H \mathbf{H}^T \mathbf{R}_{zz}^{-1} \mathbf{H} \mathbf{e}_\Delta\}) \end{aligned} \quad (2.30)$$

i.e., it depends on both the Tx-IQ and Rx-IQ imbalances. Since the Rx-IQ imbalance can be compensated at the receiver side, let us consider the special case where the only Tx-IQ imbalance is present. It can be easily verified that also when the channel is non-dispersive and the noise is absent, the L MMSE receiver can not compensate the Tx-IQ imbalance, in fact, $\varepsilon_L(\mu_{Tx}, \nu_{Tx}, 1, 0) = 1 - \frac{|\mu_{Tx}|^2}{|\mu_{Tx}|^2 + |\nu_{Tx}|^2}$, which is null only for $\mu_{Tx} = 1$ and $\nu_{Tx} = 0$.

2.2.3 Numerical results

Our numerical results are aimed at evaluating the performance degradations exhibited by the L MMSE equalizer and the WL one in the presence of the Tx-IQ and Rx-IQ imbalance. More specifically, in the first set of experiments, the performances have been evaluated in terms of the MMSE loss defined as

$$\text{MSE Loss} = \frac{\varepsilon(\mu_{Tx}, \nu_{Tx}, \mu_{Rx}, \nu_{Rx})}{\varepsilon(1, 0, 1, 0)} \quad (2.31)$$

where $\varepsilon(1, 0, 1, 0)$ is the MMSE in absence of IQ impairments² and $\varepsilon(\mu_{Tx}, \nu_{Tx}, \mu_{Rx}, \nu_{Rx})$ is the MMSE achieved by the L MMSE equalizer (given by (2.30)) or by the WL one (given by (2.27)). Afterwards, the performance are evaluated in terms of the symbol error rate (SER) at the output of the decision device.

²Note that, according to the assumption considered here, $\varepsilon(1, 0, 1, 0) = \varepsilon_{WL}(1, 0, 1, 0) = \varepsilon_L(1, 0, 1, 0)$.

The performances have been averaged over 100 independent trials. In each trial, the channel taps h_k ($k = 0, \dots, L$), with $L = 3$, are randomly generated according to a complex-valued circularly symmetric zero-mean white Gaussian process with variance $1/L$ (i.e., $E[(\Re\{h_k\})^2] = E[(\Im\{h_k\})^2] = \frac{1}{2L}$ and $E[\Re\{h_k\}\Im\{h_k\}] = 0$) and are uncorrelated with each other. The noise is modeled as a complex-valued white WSS Gaussian process with zero-mean and variance σ_n^2 ; accordingly, we define the signal-to-noise ratio as $\text{SNR} = 1/\sigma_n^2$. Finally, we assume that the FIR equalizers have $N_f = 20$ taps and the optimum delay Δ is chosen to optimize the performances. In Fig. 2.1 and 2.2, the MMSE loss (in dB) of the L MMSE equalizer and of the WL one, respectively, are plotted versus the amplitude and phase imbalances³ α_{Tx} and θ_{Tx} for $\text{SNR} = 25\text{dB}$. Although the performances of both the equalizers decrease when the Tx-IQ imbalance is present, the L MMSE is much more sensitive than the WL one to the IQ impairments. Since the WL equalizer completely compensates the Rx-IQ imbalance, in Fig. 2.3, only the performance loss of the L MMSE equalizer is plotted versus the amplitude and phase imbalances α_{Rx} and θ_{Rx} . By comparing Fig. 2.1 and Fig. 2.3, it follows that the Tx-IQ imbalance and the Rx-IQ one determine, in practice, the same performance loss in terms of MMSE.

Finally, we compare the considered equalizers in terms of SER when the transmitted symbols are drawn from the 16-QAM alphabet, the Rx-IQ imbalance is absent, $\alpha_{Tx} = 0.2$ and $\theta_{Tx} = \pi/18$. In Fig. 2.4, the SERs achieved by the L MMSE equalizer and the WL one are plotted together with the SER of the optimum equalizer in absence of IQ impairments. The results show that the adoption of the WL equalizer structure allows one to greatly reduce the SER loss in the presence of Tx-IQ imbalance.

Conclusion

In the paper [22], we have addressed the design of the MMSE equalizer in the presence of both Tx-IQ and Rx-IQ imbalance. More specifically, since the IQ impairments render the received signal rotationally variant, a widely-linear equalizer has been employed. The MMSE equalizer structure has been derived by assuming the perfect knowledge of the channel impulse response, the noise statistics, and the imbalance parameters. It has been shown that, unlike the Rx-IQ imbalance, the Tx-IQ imbalance can not be completely compensated at the receiver side due to the channel in-between and the noise presence. The

³The amplitude and the phase imbalance are sampled with a step size of 0.05.

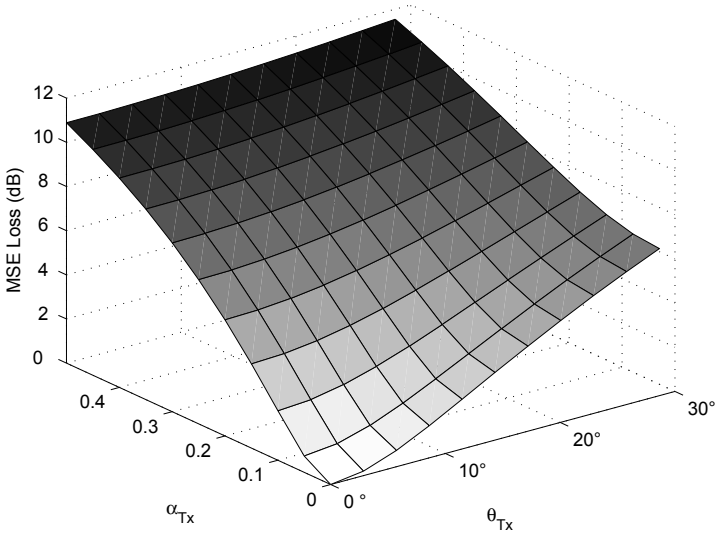


Figure 2.1: MSE Loss of the MMSE L equalizer versus the Tx-IQ imbalance.

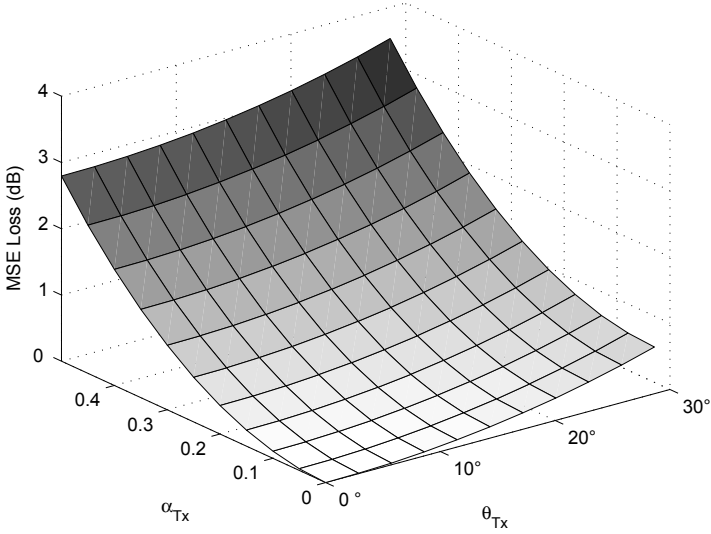


Figure 2.2: MSE Loss of the MMSE WL equalizer versus the Tx-IQ imbalance.

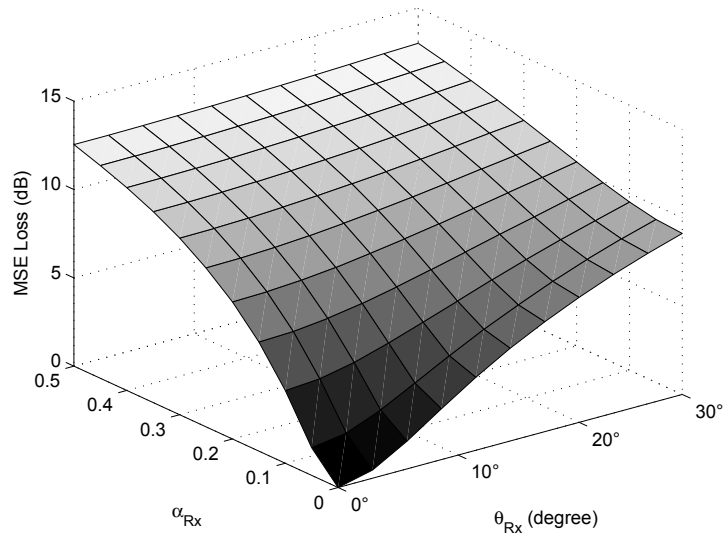


Figure 2.3: MSE Loss of the MMSE L equalizer versus the Rx-IQ imbalance.

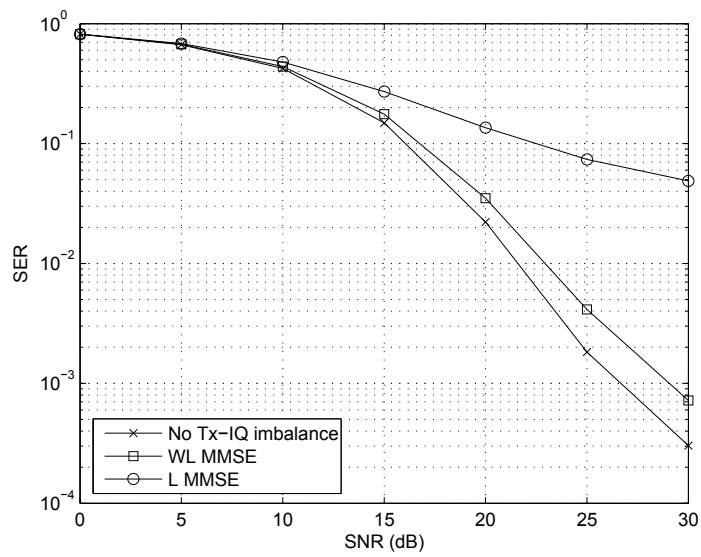


Figure 2.4: SERs of the MMSE WL equalizer and the L one versus the SNR, for 16-QAM transmissions.

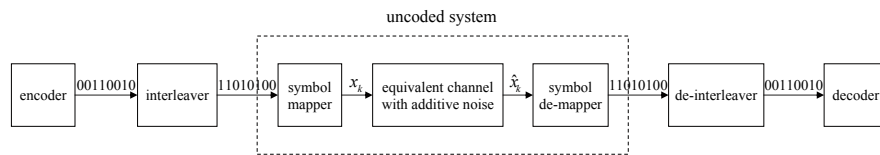


Figure 2.5: System model.

performances of the widely-linear MMSE equalizer have been compared with those of the linear MMSE equalizer in terms of MMSE loss and SER. The results of the simulations have shown that the adoption of the widely-linear receiver allows one to limit the performance losses due to the IQ impairments.

2.3 Constellation design in widely linear transceivers

The recent demand of high bit-rate services has tuned the attention on new transmit and receive processing techniques aimed at achieving both reliable data transmissions and high data-rate. To this aim, in early works (see, for example, [27, 28]), the optimization of the two-dimensional constellation to minimize the symbol error rate (SER) was first addressed. More precisely, consider the communication system model in Fig. 2.5. The purpose of the bit interleaver is to separate adjacent information bits in time destroying the correlation among them. Then, each block of $\log_2(K)$ bits of the interleaved sequence is mapped by the symbol-mapper into the points of the chosen signal constellation and the resulting symbol sequence x_k is transmitted over the channel affected by additive noise: the equivalent channel is the cascade of the transmit filter, the channel and the receive filter. The estimate \hat{x}_k of x_k is fed to the symbol de-mapper and then to the de-interleaver to provide the estimate of the transmitted bit sequence. In [27, 28], with reference to the transmission over a nondispersive channel affected by additive noise, the optimization of the symbol-mapper to minimize the SER at the output of the decision device has been addressed, i.e., the authors focused on the boxed section shown in Fig. 2.5, which is referred as the uncoded system part. For the sake of clarity, let us point out that the overall system performance depends on both the uncoded system part and the coded part (encoder/decoder and interleaver/de-interleaver). However, it is customary and convenient to consider such parts independently in order to simplify the design and the analysis [29].

With reference to the uncoded system, the advantage provided by the constellations with two degrees of freedom (such as quadrature amplitude

modulation (QAM)) over the ones with one degree of freedom (such as phase-shift-keying (PSK) and pulse amplitude modulation (PAM)) has been shown [27] and a proper mapping (based on a gradient-descent procedure) of the $\log_2 K$ information bits into K points of a two-dimensional constellation was proposed [28]. However, the adoption of an additive-noise nondispersive channel model allows one to consider the constellation mapping independently of the equivalent channel. On the other hand, an amount of literature (e.g., [30, 31, 32, 11, 33]) refers to the optimization of the transmitter and/or the receiver without including the choice of the constellation in the optimization procedure. In fact, most of the transmit and receive processing is optimized (according to a chosen criterion) by only exploiting the knowledge of the statistics of the information symbol sequence. The problem of the constellation choice has been addressed in [34] and in [29] with reference to the discrete multi-tone (DMT) transceiver and to multiple-input multiple-output transceiver, respectively.

The paper we have submitted for the publication on EURASIP Journal on Advances in Signal Processing [35] addresses the constellation design in an uncoded system under the assumption that the transmitter is fixed (i.e., by considering an equivalent channel representing the transmitter and the channel) and a widely linear (WL) minimum mean square error (MMSE) equalizer is employed at the receiver side [17, 16, 36, 37, 38]. The WL filtering generalizes the conventional linear filtering and allows one to achieve a performance gain by exploiting the statistical redundancy possibly exhibited by a rotationally variant transmitted (and/or received) signal. For such a reason, the adoption of the WL equalization has frequently been confined to the transmission of one-dimensional constellations (see, for example, [39, 25, 40] and references therein) since most of the two-dimensional signaling schemes are circularly symmetric. It should be noted, however, that the two-dimensional constellations (especially high-order ones) are often preferred to the one-dimensional constellations in order to maximize the minimum distance between the constellation points [27]. Since the performance of the WL MMSE equalizer is sensitive to the second-order statistics of the received signal, and more specifically to its pseudo-correlation, we address the constellation design under the assumption that the channel state information (CSI) is available and we propose a CSI-dependent symbol mapping that optimizes the performance of the WL MMSE receiver. Symbol mapping is adapted by using a feedback channel (between the receiver and the transmitter) carrying information about the optimum constellation. Moreover, suboptimum strategies are proposed in order

to reduce both the amount of information to be transmitted on the feedback channel and the computational complexity of the optimization procedure.

2.3.1 System model

Let us consider the following finite-impulse-response (FIR) baseband-equivalent noisy communication channel

$$y_k = \sum_{\ell=0}^{\nu} h_{\ell} x_{k-\ell} + n_k \quad (2.32)$$

where the transmitted symbols x_k are independent identically distributed (i.i.d.) zero-mean random variables drawn from the complex-valued constellation $\mathbf{c} \in \mathbb{C}^K$ whose (finite) order K determines the bit rate ($\log_2 K$ bits per symbol) of the uncoded system part. With no loss of generality, we assume that $\mathbb{E}[x_k x_{k-\ell}^*] = \delta_{\ell}$ and $\mathbb{E}[x_k x_{k-\ell}] = \beta \delta_{\ell}$, i.e., the transmitted available power is unit, and that x_k exhibits a possibly nonnull pseudo-correlation $\beta = \mathbb{E}[\Re\{x_k\}^2] - \mathbb{E}[\Im\{x_k\}^2] + 2j\mathbb{E}[\Re\{x_k\}\Im\{x_k\}] \in \mathbb{C}$, such that⁴ $|\beta| \leq 1$; note that the non circularity of x_k consists in the difference between the power of the in-phase component and the quadrature one and in the correlation between them. Such assumption allows one to consider both the conventional circularly symmetric constellations ($\beta = 0$), such as M -PSK and square M -QAM with $M > 2$, and the rotationally variant constellations, such as the well-known PAM ($\beta = 1$) and its rotated version (for which it exists θ such that $x_k e^{-j\theta}$ is real-valued and, consequently, $\beta = e^{j2\theta}$), non-square QAM (with $\beta = \Re(\beta) \neq 0$ since a different power is allocated to the in-phase and quadrature components). The time-invariant FIR channel impulse response h_k of memory ν is assumed to be known at the receiver side. Finally, the additive noise n_k , whose power σ_n^2 is assumed known at the receiver, is modeled as zero-mean complex-valued wide-sense stationary time-uncorrelated and independent of the useful signal.

At the receiver side, the feedforward-based equalization is performed by processing the block of N_f received samples $\mathbf{y}_k \triangleq [y_k \ y_{k-1} \ \dots \ y_{k-N_f+1}]^T$ which, in a matrix notation, can be written as

⁴If $|\beta| \leq 1$, then the correlation matrix of the 2×1 random vector $[x_k \ x_k^*]^T$ will be positive semi-definite.

follows:

$$\mathbf{y}_k = \begin{bmatrix} h_0 & h_1 & \dots & h_\nu & 0 & \dots & 0 \\ 0 & h_0 & h_1 & \dots & h_\nu & 0 & \dots \\ \vdots & & \ddots & & \ddots & & \vdots \\ 0 & \dots & 0 & h_0 & h_1 & \dots & h_\nu \end{bmatrix} \begin{bmatrix} x_k \\ x_{k-1} \\ \vdots \\ x_{k-\nu-N_f+1} \end{bmatrix} + \begin{bmatrix} n_k \\ n_{k-1} \\ \vdots \\ n_{k-N_f+1} \end{bmatrix} = \mathbf{H}\mathbf{x}_k + \mathbf{n}_k \quad (2.33)$$

According to the previous assumptions, the following correlation and pseudo-correlation matrices can be written as:

$$\mathbf{R}_{xx} \triangleq E[\mathbf{x}_k \mathbf{x}_k^H] = \mathbf{I}_{N_f+\nu} \quad \mathbf{R}_{xx^*} \triangleq E[\mathbf{x}_k \mathbf{x}_k^T] = \beta \mathbf{I}_{N_f+\nu} \quad (2.34)$$

$$\mathbf{R}_{yy} \triangleq E[\mathbf{y}_k \mathbf{y}_k^H] = \mathbf{H}\mathbf{H}^H + \sigma_n^2 \mathbf{I}_{N_f} \quad \mathbf{R}_{yy^*} \triangleq E[\mathbf{y}_k \mathbf{y}_k^T] = \beta \mathbf{H}\mathbf{H}^T + \gamma \mathbf{I}_{N_f} \quad (2.35)$$

where $\gamma \triangleq E[n_k^2]$ is the (possibly) nonnull noise pseudo-correlation (if $\gamma = 0$, then the noise is circularly symmetric).

2.3.2 Feedforward-based MMSE equalizer

Since the transmitted sequence x_k and consequently the received one y_k in (2.32) can be rotationally variant, we adopt a widely-linear receiver in order to exploit the statistical redundancy exhibited by the received signal. Note that such a choice improves the performance since the linear equalizers are a subset of the WL equalizers; their performances coincide only in the presence of circularly symmetric signals [16]. Therefore, we resort to the two FIR filters $\mathbf{w} \triangleq [w_0 \ w_1 \ \dots \ w_{N_f-1}]^T$ and $\mathbf{g} \triangleq [g_0 \ g_1 \ \dots \ g_{N_f-1}]^T$ that process the received vector \mathbf{y}_k and its complex conjugate version \mathbf{y}_k^* , respectively. The optimum filters $\mathbf{w}^{(opt)}$ and $\mathbf{g}^{(opt)}$ minimizing the mean square error $E[|x_{k-\Delta} - \mathbf{w}^H \mathbf{y}_k - \mathbf{g}^H \mathbf{y}_k^*|^2]$ are given by [25, 5]

$$\mathbf{w}^{(opt)} = [\mathbf{R}_{yy} - \mathbf{R}_{yy^*} \mathbf{R}_{yy}^{-*} \mathbf{R}_{yy^*}^*]^{-1} [\mathbf{h}_{\Delta+1} - \mathbf{R}_{yy^*} \mathbf{R}_{yy}^{-*} \mathbf{h}_{\Delta+1}^* \beta^*] \quad (2.36)$$

$$\mathbf{g}^{(opt)} = [\mathbf{R}_{yy} - \mathbf{R}_{yy^*} \mathbf{R}_{yy}^{-*} \mathbf{R}_{yy^*}^*]^{-*} [\mathbf{h}_{\Delta+1} \beta - \mathbf{R}_{yy^*} \mathbf{R}_{yy}^{-*} \mathbf{h}_{\Delta+1}^*]^* \quad (2.37)$$

where the processing delay $0 \leq \Delta \leq N_f + \nu - 1$ has to be chosen in order to optimize the performance. For notational simplicity, in (2.36)-(2.37) we have

omitted the dependence of $\mathbf{w}^{(opt)}$ and $\mathbf{g}^{(opt)}$ on β . Let us point out that when $\beta = 0$, i.e., the transmitted symbols are drawn from a circularly symmetric constellation, $\mathbf{g}^{(opt)} = \mathbf{0}$ and, therefore, the WL MMSE equalizer degenerates into the conventional linear MMSE equalizer. Another special case is represented by the scenario where a real-valued constellation is adopted: in fact, since $\beta = 1$, $\mathbf{g}^{(opt)} = \mathbf{w}^{(opt)*}$ and the WL MMSE equalizer becomes $\Re\{2\mathbf{w}^{(opt)H}\mathbf{y}_k\}$, i.e., it is implemented by extracting the in-phase component of the linear equalizer $\mathbf{w}^{(opt)}$, which does not coincide, however, with the linear MMSE equalizer.

Since the optimum equalizer and, hence, its performance depends on the pseudo-correlation β of the transmitted signal, let us analyze the dependence on β of the MMSE. To this end, denote with $e(\beta, \Delta) \triangleq x_{k-\Delta} - \mathbf{w}^{(opt)H}\mathbf{y}_k - \mathbf{g}^{(opt)H}\mathbf{y}_k^*$ the error measured at the output of the WL MMSE equalizer for given values of β and Δ . It can be easily shown that

$$\begin{aligned}\sigma_e(\beta, \Delta)^2 &\triangleq \mathbb{E}[|e(\beta, \Delta)|^2] \\ &= 1 - \mathbf{w}^{(opt)H}\mathbf{h}_{\Delta+1} - \mathbf{g}^{(opt)H}\mathbf{h}_{\Delta+1}^*\beta^*\end{aligned}\quad (2.38)$$

$$\begin{aligned}\zeta(\beta, \Delta) &\triangleq \sigma_e(0, \Delta)^2 - \sigma_e(\beta, \Delta)^2 \\ &= [\mathbf{h}_{\Delta+1}\beta - \mathbf{R}_{yy^*}\mathbf{R}_{yy}^{-*}\mathbf{h}_{\Delta+1}^*]^T [\mathbf{R}_{yy} - \mathbf{R}_{yy^*}\mathbf{R}_{yy}^{-*}\mathbf{R}_{yy^*}]^{-*} \\ &\quad [\mathbf{h}_{\Delta+1}\beta - \mathbf{R}_{yy^*}\mathbf{R}_{yy}^{-*}\mathbf{h}_{\Delta+1}^*]^* \end{aligned}\quad (2.39)$$

Since $\sigma_e(0, \Delta)^2$ is the MMSE at the outputs of both the WL MMSE equalizer and the linear MMSE equalizer in the presence of a circularly symmetric constellation, $\zeta(\beta, \Delta)$ represents the MMSE gain achieved by properly choosing the pseudo-correlation β of the transmitted constellation. When $\gamma = 0$, i.e., the noise is circularly symmetric, the (first) derivative⁵ of $\zeta(\beta, \Delta)$ with respect to $|\beta|$ can be written as

$$\begin{aligned}\frac{\partial \zeta(\beta, \Delta)}{\partial |\beta|} &= \frac{2}{|\beta|} [\mathbf{h}_{\Delta+1}\beta - \mathbf{R}_{yy^*}\mathbf{R}_{yy}^{-*}\mathbf{h}_{\Delta+1}^*]^T [\mathbf{R}_{yy} - \mathbf{R}_{yy^*}\mathbf{R}_{yy}^{-*}\mathbf{R}_{yy^*}]^{-*} \\ &\quad \times \mathbf{R}_{yy}^* [\mathbf{R}_{yy} - \mathbf{R}_{yy^*}\mathbf{R}_{yy}^{-*}\mathbf{R}_{yy^*}]^{-*} [\mathbf{h}_{\Delta+1}\beta - \mathbf{R}_{yy^*}\mathbf{R}_{yy}^{-*}\mathbf{h}_{\Delta+1}^*]^* \end{aligned}\quad (2.40)$$

Since $[\mathbf{R}_{yy} - \mathbf{R}_{yy^*}\mathbf{R}_{yy}^{-*}\mathbf{R}_{yy^*}]^{-*}$ and \mathbf{R}_{yy} are positive semidefinite, one has $\frac{\partial \zeta(\beta, \Delta)}{\partial |\beta|} \geq 0$ and, hence, increasing the degree of non-circularity of the transmitted signal improves the MMSE. For such a reason, the use of a real-valued

⁵Note that in such a scenario $\zeta(\beta, \Delta)$ depends on $|\beta|$ instead of β .

transmitted sequence together with a WL MMSE equalizer corresponds to the optimum choice as far as the MMSE is adopted as the performance measure. As a consequence, in the literature, many works on WL processing focuses of real-valued transmissions.

On the other hand, when $\gamma \neq 0$, the variations of $\zeta(\beta, \Delta)$ with respect to β depend on the specific values of the channel impulse response and the noise statistics and, consequently, a general rule for setting β appears difficult to be found. However, in order to understand the basic effects of non circular noise on the value of β minimizing the MMSE, let us consider the transmission over the non-dispersive channel $h_k = h_0\delta_k$ with $h_0 = e^{j\theta_h}$. In such a scenario, (2.39) can be rewritten as follows:

$$\zeta(\beta) = \frac{(1 + \sigma_n^2)^2|\beta|^2 - 2(1 + \sigma_n^2)(|\beta|^2 + |\beta||\gamma| \cos(\theta_{diff})) + |\beta|^2 + |\gamma|^2}{(1 + \sigma_n^2)[(1 + \sigma_n^2)^2 - |\beta|^2 - |\gamma|^2 - 2|\beta||\gamma| \cos(\theta_{diff})]} + \frac{2|\beta||\gamma| \cos(\theta_{diff})}{(1 + \sigma_n^2)[(1 + \sigma_n^2)^2 - |\beta|^2 - |\gamma|^2 - 2|\beta||\gamma| \cos(\theta_{diff})]} \quad (2.41)$$

where we omit the dependence on $\Delta = 0$ and where $\theta_{diff} \triangleq 2\theta_h + \theta_\beta - \theta_\gamma$, with θ_β and θ_γ such that $\beta \triangleq |\beta|e^{j\theta_\beta}$ and $\gamma \triangleq |\gamma|e^{j\theta_\gamma}$, respectively. We have verified by numerical computation of (2.41) that the behavior of $\zeta(\beta)$ depends on the specific value of σ_n^2 and γ and that, in general, it does not increase with $|\beta|$. As very special case, assume $n_k = n'_k e^{j\frac{\theta_\gamma}{2}}$ with n'_k real-valued and such that $E[|n'_k|^2] = \sigma_n^2$, i.e., $|\gamma| = \sigma_n^2$: the numerical analysis shows that $\zeta(\beta)$ is maximum when $|\beta| = 1$ and $\theta_{diff} = \pi$. Let us briefly discuss such result. If x_k is a rotated version with angle $\frac{\theta_\beta}{2}$ of a real-valued signal ($|\beta| = 1$), then $\zeta(\beta)$ is maximum when θ_β is chosen so that the channel output $z_k \triangleq h_0 x_k$ is equal to $z_k = |x_k|e^{j(\frac{\theta_\gamma}{2} + \frac{\pi}{2})}$: in other words, the useful signal and the noise are one-dimensional signals along orthogonal directions in the complex plane and, in practice, the transmission is not affected by noise. On the other hand, $\zeta(\beta)$ is null when $\theta_{diff} = 0$, i.e., when the useful signal $z_k = |x_k|e^{j\frac{\theta_\gamma}{2}}$ and the noise are one dimensional signals along the same directions in the complex plane.

2.3.3 Constellation design

In this section, we address the design of the K -order constellation with K fixed under the assumption that the WL MMSE equalizer is used. More precisely, the results in the previous section allow one to state that, by using a real-valued constellation ($\beta = 1$) instead of a complex-valued non-redundant ($\beta = 0$) one,

a performance gain can be achieved in terms of the MMSE at the equalizer output. On the other hand, not always an MSE gain provided by the WL equalizer leads to a SER gain [41]. In fact, for a fixed expended average energy per bit, the reduction of the minimum distance between the constellation points, due to the adoption of one-dimensional constellations rather than two-dimensional ones (for example, when we adopt the K -PAM rather than the K -QAM), leads to a potential increase in the SER. Therefore, we address the constellation design minimizing the SER at the WL MMSE equalizer output by accounting for its rotationally variant properties.

In the literature (e.g., [28, 42]), most of the constellations employed by the transmission stage are circularly symmetric ($\beta = 0$), while statistically redundant constellations are confined to the real-valued ones. Moreover, in [28], with reference to the transmission over a time non-dispersive channel ($h_k = \delta_k$) affected by circularly symmetric noise, a procedure for constellation optimization has been proposed, showing also that, for large signal-to-noise ratios (SNR), the performance of the conventional QAM maximum-likelihood (ML) receiver is invariant with respect to rhombic transformations of the complex-plane. However, it is important to point out that a rhombic transformation of a circular constellation makes it rotationally variant and, for some values of K (e.g. $K = 8$), the procedure in [28] provides a rotationally variant constellation. On the other hand, the WL equalizer is equivalent to the linear equalizer over the nondispersive channel considered in [28] and, therefore, optimizing the circularity degree of the constellation does not provide any performance advantage. On the other hand, when a time-dispersive channel is considered, the WL MMSE equalizer is sensitive to the rotationally variant properties of the transmitted signal and, therefore, we propose a transceiver structure (see Fig. 2.6) where: *i*) the transmitter can switch between the available constellations of order K ; *ii*) the WL MMSE receiver accounts for the CSI and informs the transmitter, by means of a feedback channel, about which constellation has to be adopted to minimize the SER.

Constellation optimization in the presence of Gaussian rotationally variant noise

With no loss of generality, assume that $\Delta = 0$ and rewrite the output of the FIR equalizer as follows

$$\begin{aligned} z_k(\beta) &= \mathbf{w}^{(opt)H} \mathbf{y}_k + \mathbf{g}^{(opt)H} \mathbf{y}_k^* \\ &= x_k(\beta) + e_k(\beta) \end{aligned} \quad (2.42)$$

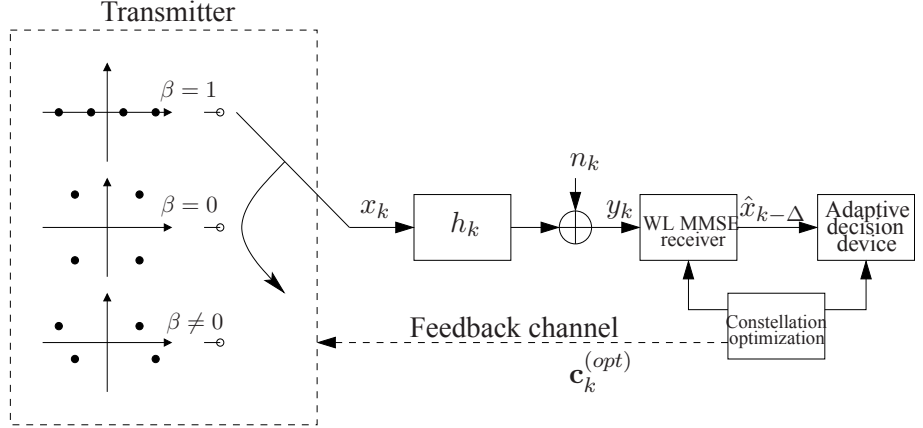


Figure 2.6: Transceiver structure.

where $x_k(\beta)$ is the transmitted symbol drawn from the complex-valued constellation $\mathbf{c} \triangleq [c_1 \ c_2 \ \dots \ c_K]^T$ with $\mathbb{E}[|x_k(\beta)|^2] = 1$ and $\mathbb{E}[x_k(\beta)^2] = \beta$, and $e_k(\beta)$ is the residual disturbance that includes the intersymbol interference and the noise terms after the WL equalizer filtering. The circularly symmetric model for the additive disturbance is inadequate since the output of a WL filter is, in general, rotationally variant. Therefore, we model $e_k(\beta)$ as rotationally variant, i.e., $\mathbb{E}[\Re\{e_k(\beta)\}^2] \triangleq \sigma_{e,R}(\beta)^2$, $\mathbb{E}[\Im\{e_k(\beta)\}^2] \triangleq \sigma_{e,I}(\beta)^2 = \sigma_e(\beta)^2 - \sigma_{e,R}(\beta)^2$, and $\mathbb{E}[\Re\{e_k(\beta)\}\Im\{e_k(\beta)\}] = \sigma_{e,RI}(\beta)$. Moreover, in order to make the constellation design analytically tractable, we approximate $e_k(\beta)$ as Gaussian. For the sake of clarity, let us note that, if symbols $x_k(\beta)$ and noise are circularly symmetric ($\beta = \gamma = 0$), then the additive disturbance $e_k(0)$ and the equalizer output $z_k(0)$ will be circularly symmetric too; on the other hand, if $x_k(\beta)$ is rotationally variant, then $z_k(\beta)$ will be rotationally variant too, but nothing can be stated about the circularity properties of $e_k(\beta)$ also when $\gamma = 0$.

The sample $z_k(\beta)$ is the input of the decision device which performs the symbol-by-symbol ML detection of the transmitted symbol. By defining the

following eigenvalue decomposition⁶:

$$\begin{bmatrix} \sigma_{e,R}(\beta)^2 & \sigma_{e,RI}(\beta) \\ \sigma_{e,RI}(\beta) & \sigma_{e,I}(\beta)^2 \end{bmatrix} \triangleq \underbrace{\begin{bmatrix} v_{11} & v_{12} \\ v_{12} & v_{22} \end{bmatrix}}_{\mathbf{V}} \underbrace{\begin{bmatrix} s_1 & 0 \\ 0 & s_2 \end{bmatrix}}_{\mathbf{S}} \underbrace{\begin{bmatrix} v_{11} & v_{12} \\ v_{12} & v_{22} \end{bmatrix}}_{\mathbf{V}^T} \quad (s_1 \geq s_2 \geq 0) \quad (2.43)$$

with \mathbf{V} being the eigenvector matrix and \mathbf{S} having on the diagonal the eigenvalues, it can be verified that the pair-wise error probability $P(c_i \rightarrow c_\ell)$ [42], i.e., the probability of transmitting c_i and deciding (at the receiver) in favor of c_ℓ when the transmission system uses only c_i and c_ℓ , is given by:

$$P(c_i \rightarrow c_\ell; \beta) = \frac{1}{2} \operatorname{erfc} \left(\frac{1}{2\sqrt{2}} \sqrt{\frac{(c_{i,R} - c_{\ell,R})^2}{\psi_R(\beta)} + \frac{(c_{i,I} - c_{\ell,I})^2}{\psi_I(\beta)} + \psi_{RI}(c_{i,R} - c_{\ell,R})(c_{i,I} - c_{\ell,I})} \right) \quad (2.44)$$

where $c_{k,R} \triangleq \Re\{c_k\}$ and $c_{k,I} \triangleq \Im\{c_k\}$, and, for $s_1 \neq 0$ and $s_2 \neq 0$,

$$\psi_R(\beta) \triangleq \left(\frac{v_{11}^2}{s_1} + \frac{v_{12}^2}{s_2} \right)^{-1} \quad (2.45)$$

$$\psi_I(\beta) \triangleq \left(\frac{v_{12}^2}{s_1} + \frac{v_{22}^2}{s_2} \right)^{-1} \quad (2.46)$$

$$\psi_{RI}(\beta) \triangleq 2 \left(\frac{v_{11}}{s_1} + \frac{v_{22}}{s_2} \right) v_{12} \quad (2.47)$$

When $s_2 = 0$, $\psi_R(\beta) \triangleq \frac{s_1}{v_{11}^2}$ and analogously for $\psi_I(\beta)$ and $\psi_{RI}(\beta)$. By utilizing (2.44), assuming that the symbols c_k are equally probable, and resorting to both the union bound and Chernoff bound techniques, the SER $P_e^{(true)}(\mathbf{c})$ is upper-bounded as follows

$$P_e^{(true)}(\mathbf{c}) \leq P_e(\mathbf{c}; \beta) \triangleq \frac{1}{K} \sum_{i=1}^K \sum_{\ell \neq i} \exp \left\{ -\frac{1}{8} \left[\frac{(c_{i,R} - c_{\ell,R})^2}{\psi_R(\beta)} + \frac{(c_{i,I} - c_{\ell,I})^2}{\psi_I(\beta)} + \psi_{RI}(c_{i,R} - c_{\ell,R})(c_{i,I} - c_{\ell,I}) \right] \right\} \quad (2.48)$$

⁶The dependence on β at the right-hand-side is omitted for simplicity.

and, therefore, the optimum constellation can be approximated with the solution $\mathbf{c}^{(opt)}$ of the following problem:

$$\begin{cases} \mathbf{c}^{(opt)} = \arg \min_{\mathbf{c} \in \mathbb{C}^K, \beta \in \mathbb{C}} P_e(\mathbf{c}; \beta) \\ \frac{1}{K} \sum_{i=1}^K |c_i|^2 = 1 \\ \frac{1}{K} \sum_{i=1}^K c_i^2 = \beta \\ |\beta| \leq 1 \end{cases} \quad (2.49)$$

Unfortunately, it is difficult to find the closed-form expression of the solution of such an optimization problem. For such a reason, we propose to find a local solution by means of numerical algorithms based on the constrained gradient method. To this aim, we can exploit the gradient of $P_e(\mathbf{c}; \beta)$ with respect to \mathbf{c} , while we resort to numerical approximation of the gradient with respect to β since it is difficult to obtain its analytical expression.

Before proceeding, let us discuss the property of the locally optimum constellation for a fixed β . The k th component of the gradient of $P_e(\mathbf{c}; \beta)$ is given by⁷:

$$\begin{aligned} \frac{\partial P_e(\mathbf{c}; \beta)}{\partial c_k} = & -\frac{1}{2K} \sum_{\ell \neq k} \exp \left\{ -\frac{1}{8} \left[\frac{(c_{k,R} - c_{\ell,R})^2}{\psi_R(\beta)} + \frac{(c_{k,I} - c_{\ell,I})^2}{\psi_I(\beta)} \right. \right. \\ & \left. \left. + \psi_{RI}(\beta)(c_{k,R} - c_{\ell,R})(c_{k,I} - c_{\ell,I}) \right] \right\} \times \left[\frac{c_{k,R} - c_{\ell,R}}{\psi_R(\beta)} + j \frac{c_{k,I} - c_{\ell,I}}{\psi_I(\beta)} \right. \\ & \left. + j \frac{\psi_{RI}(\beta)}{2} ((c_{k,R} - c_{\ell,R}) - j(c_{k,I} - c_{\ell,I})) \right] \end{aligned} \quad (2.50)$$

By zeroing the gradient of the Lagrangian

$$\begin{aligned} F(\mathbf{c}, \beta, \lambda_1, \lambda_2, \lambda_3) \triangleq & P_e(\mathbf{c}; \beta) + \lambda_1 \left(\frac{1}{K} \sum_{k=1}^K |c_k|^2 - 1 \right) \\ & + \lambda_2 \left(\frac{1}{K} \sum_{k=1}^K (c_{k,R}^2 - c_{k,I}^2) - \Re\{\beta\} \right) + \lambda_3 \left(\frac{1}{K} \sum_{k=1}^K c_{k,R} c_{k,I} - \Im\{\beta\} \right) \end{aligned} \quad (2.51)$$

⁷ $\frac{\partial f(\mathbf{c})}{\partial c_k} = \frac{\partial f(\mathbf{c})}{\partial c_{k,R}} + j \frac{\partial f(\mathbf{c})}{\partial c_{k,I}}$.

one has that the locally optimum \mathbf{c} satisfies the following equation:

$$\frac{1}{2} \sum_{\ell \neq k} \xi(k, \ell) \left[\frac{c_{k,R} - c_{\ell,R}}{\psi_R(\beta)} + j \frac{c_{k,I} - c_{\ell,I}}{\psi_I(\beta)} + j \frac{\psi_{RI}(\beta)}{2} ((c_{k,R} - c_{\ell,R}) - j(c_{k,I} - c_{\ell,I})) \right] = 2\lambda_1 c_k + 2(\lambda_2 + j\lambda_3) c_k^* \quad k = 1, \dots, K \quad (2.52)$$

with

$$\xi(k, \ell) \triangleq \exp \left\{ -\frac{1}{8} \left[\frac{(c_{k,R} - c_{\ell,R})^2}{\psi_R(\beta)} + \frac{(c_{k,I} - c_{\ell,I})^2}{\psi_I(\beta)} + \psi_{RI}(\beta)(c_{k,R} - c_{\ell,R})(c_{k,I} - c_{\ell,I}) \right] \right\} \quad (2.53)$$

The condition (2.52) generalizes the result of [28] to the case of e_k rotationally variant (i.e., $\sigma_{e,R}(\beta)^2 \neq \sigma_{e,I}(\beta)^2$ or $\sigma_{e,RI}(\beta) \neq 0$) and with a constrained pseudo-correlation. In fact, (2.52) with $\lambda_2 = \lambda_3 = 0$ (i.e., no constraint is imposed on the pseudo-correlation) requires that c_k is proportional to the weighted sum (with weights $\frac{\xi(k,\ell)}{\psi_R(\beta)}$) of $c_k - c_\ell, \forall \ell \neq k$, as found in [28]. For the sake of clarity, let us note that the procedure proposed in [28] does not allow one to exploit the potential advantage of a rotationally variant constellation when the WL MMSE receiver is employed. For example, when a linear MMSE equalizer is employed for $K = 4$ in high signal-to-noise ratio, the minimum of the SER is equivalently achieved [28] by both the conventional 4-QAM constellation and the rhombic constellations with the same *perimeter*, i.e., the perimeter of the largest convex polygon consisting of the lines $c_k - c_\ell$ (see [27] for further details). On the other hand, when a WL MMSE equalizer is employed, a rhombic constellation, which is rotationally variant, is not equivalent to the conventional 4-QAM since the achieved MMSE is dependent on β as shown in (2.40).

A suboptimum procedure based on rhombic transformations

In this section, we propose a suboptimum constellation-design procedure for the WL MMSE equalizer. The method is based on the exploitation of a rhombic transformation that operates on a circularly symmetric constellation making it rotationally variant. Such a transformation depends on two parameters and allows one to control the pseudo-correlation β of the obtained constellation; consequently, the optimization procedure is simplified since the SER in (2.48) is a function of only two parameters, instead of K parameters.

Assume that $\mathbf{c} = [c_1 \ c_2 \ \dots \ c_K]^T$ is a unit-power circularly-symmetric complex-valued constellation and define the complex-valued constellation $\tilde{\mathbf{c}} = [\tilde{c}_1 \ \tilde{c}_2 \ \dots \ \tilde{c}_K]^T$ as follows:

$$\begin{bmatrix} \Re\{\tilde{c}_k\} \\ \Im\{\tilde{c}_k\} \end{bmatrix} = \frac{1}{\sqrt{1+\alpha^2}} \begin{bmatrix} (1+\alpha)\cos(\theta/2) & -(1+\alpha)\sin(\theta/2) \\ -(1-\alpha)\sin(\theta/2) & (1-\alpha)\cos(\theta/2) \end{bmatrix} \begin{bmatrix} \Re\{c_k\} \\ \Im\{c_k\} \end{bmatrix} \quad (2.54)$$

or, more compactly⁸,

$$\tilde{c}_k = \underbrace{\frac{1}{\sqrt{1+\alpha^2}}[\cos(\theta/2) + j\alpha\sin(\theta/2)]}_{\triangleq \mu(\alpha,\theta)} c_k + \underbrace{\frac{1}{\sqrt{1+\alpha^2}}[\alpha\cos(\theta/2) - j\sin(\theta/2)]}_{\triangleq \kappa(\alpha,\theta)} c_k^* \quad (2.55)$$

with $-1 \leq \alpha \leq 1$ and $-\frac{\pi}{2} \leq \theta \leq \frac{\pi}{2}$. When $\alpha > 0$ ($\alpha < 0$), \tilde{c}_k is stretched along the in-phase (quadrature) component and it becomes one-dimensional for $\alpha = \pm 1$; when $\theta \neq 0$, a correlation between $\Re\{\tilde{c}_k\}$ and $\Im\{\tilde{c}_k\}$ is introduced and for $\theta = \pm\frac{\pi}{2}$, even if it is two-dimensional, \tilde{c}_k can be reduced to a one-dimensional constellation by a simple rotation. For symmetry, in the following we consider only the positive values of α and θ . It is easily verified that, if x_k is drawn from $\tilde{\mathbf{c}}$, then

$$\mathbb{E}[|x_k|^2] = 1 \quad \beta = 2\mu(\alpha,\theta)\kappa(\alpha,\theta) \quad (2.56)$$

The method proposed here assumes that the information-bearing symbol sequence, say s_k , is drawn from a fixed constellation \mathbf{c} (for example, the optimum constellation provided by [28]), whereas the possibly rotationally variant channel input x_k is obtained by resorting to the zero-memory precoding defined by the rhombic transformation (2.54). Clearly, such a strategy is sub-optimum since it assumes that the channel input can be drawn from only those constellations $\tilde{\mathbf{c}}$ resulting from a rhombic transformation of the chosen \mathbf{c} . However, the main advantages of such a method in comparison with the optimum one are:

⁸The compact expression is introduced for notation simplicity, whereas the matrix form is utilized to understand the physical meaning.

- the huge reduction of the computational complexity of the constellation optimization procedure when $K \gg 1$; in fact, the SER becomes a function of only two variables (α and θ), regardless of the constellation order K ;
- the reduced implementation complexity of the transmitter stage; in fact, the symbol-mapping is implemented by means of the linear transformation (2.54);
- the decrease of the information amount to be transmitted on the feedback channel; in fact, only the values of two parameters (instead of K) have to be sent to the transmitter.

According to such a choice, the constellation optimization is carried out by solving the minimization problem

$$(\alpha^{(opt)}, \theta^{(opt)}) = \arg \min_{\alpha, \theta} P_e(\alpha, \theta) \quad (2.57)$$

with

$$\begin{aligned} P_e(\alpha, \theta) = & \frac{1}{K} \sum_{i=1}^K \sum_{\ell \neq i} \exp \left\{ -\frac{1}{8(1+\alpha^2)} \left[\frac{(1+\alpha)^2}{\psi_R(\alpha, \theta)} (\cos(\theta/2)(c_{i,R} - c_{\ell,R}) \right. \right. \\ & - \sin(\theta/2)(c_{i,I} - c_{\ell,I}))^2 + \frac{(1-\alpha)^2}{\psi_I(\alpha, \theta)} (\sin(\theta/2)(c_{i,R} - c_{\ell,R}) - \cos(\theta/2) \\ & (c_{i,I} - c_{\ell,I}))^2 - \psi_{RI}(\alpha, \theta) \frac{1-\alpha^2}{1+\alpha^2} \left(\frac{1}{2} \sin(\theta) ((c_{i,R} - c_{\ell,R})^2 + (c_{i,I} - c_{\ell,I})^2) \right. \\ & \left. \left. \left. - (c_{i,R} - c_{\ell,R})(c_{i,I} - c_{\ell,I}) \right) \right] \right\} \quad (2.58) \end{aligned}$$

where (2.58) follows from (2.48) and (2.54), and the dependence of the disturbance parameters on β has been replaced by the dependence on α and θ . Since finding the closed-form expression of $\alpha^{(opt)}$ and $\theta^{(opt)}$ is a difficult problem, here we propose to approximate $P_e(\alpha, \theta)$ with a function, say $P_e^{(low)}(\alpha, \theta)$, whose minimization can be carried out by evaluating it only over a very limited set of points. In the sequel, such an approximation is derived for a 4-QAM constellation $c_k = \frac{1}{\sqrt{2}}(\pm 1 \pm j)$, though it can be analogously determined for denser constellations.

First, we approximate the cost function (2.58) by assuming that the components of the residual disturbance are uncorrelated, i.e., $\psi_{RI}(\alpha, \theta) = 0$. By

means of some tedious but simple algebra operations, it can be shown that $P_e(\alpha, \theta)$ is lower bounded by

$$P_e(\alpha, \theta) \geq P_e^{(low)}(\alpha, \theta) \triangleq \exp \left\{ -\frac{1}{4} \|\Sigma(\alpha, \theta)\|_{-\infty} \cdot d_{min}(\alpha, \theta) \right\} \quad (2.59)$$

where

$$\Sigma(\alpha, \theta) \triangleq \begin{bmatrix} \psi_R(\alpha, \theta)^{-1} \\ \psi_I(\alpha, \theta)^{-1} \end{bmatrix} \quad (2.60)$$

$$d_{min}(\alpha, \theta) \triangleq \min_{\ell \in \{0, \pm 1\}} \|\mathbf{d}_\ell(\alpha, \theta)\|_1 \quad (2.61)$$

$$\mathbf{d}_\ell(\alpha, \beta) \triangleq \frac{1}{1 + \alpha^2} \begin{bmatrix} (1 + \alpha)^2 [(\delta_\ell + \delta_{\ell-1}) \cos(\theta/2) - (\delta_\ell + \delta_{\ell+1}) \sin(\theta/2)]^2 \\ (1 - \alpha)^2 [(\delta_\ell + \delta_{\ell-1}) \sin(\theta/2) - (\delta_\ell + \delta_{\ell+1}) \cos(\theta/2)]^2 \end{bmatrix} \quad (2.62)$$

Since the right-hand-side of (2.59) is minimized by large values of $d_{min}(\bar{\alpha}, \theta)$, we propose to approximate the solution of (2.57) with the following one:

$$\begin{cases} (\hat{\alpha}^{(opt)}, \hat{\theta}^{(opt)}) = \arg \min_{(\alpha, \theta) \in \mathcal{X}} P_e^{(low)}(\alpha, \theta) \\ \mathcal{X} \triangleq \{(\alpha, \theta) : 2 \sin(\theta) - \frac{2\alpha}{1+\alpha^2} \cos(\theta) = 1\} \end{cases} \quad (2.63)$$

where \mathcal{X} is the (α, θ) -curve corresponding to the maximum value of $d_{min}(\bar{\alpha}, \theta)$ for a fixed $\alpha = \bar{\alpha}$ (or, equivalently, to the maximum value of $d_{min}(\alpha, \bar{\theta})$ for a fixed $\theta = \bar{\theta}$). Of course, the restriction to \mathcal{X} leads to a significant decrease in the computational complexity. Let us point out that, interestingly, such a restricted optimization procedure accounts for the possible transmission of the conventional 4-PAM: in fact, it can be easily verified that when $(\alpha_{PAM}, \theta_{PAM}) \triangleq (1, \tan^{-1}(\frac{4}{3})) \in \mathcal{X}$, $\tilde{c}_k = \{\pm \frac{1}{\sqrt{5}}, \pm \frac{3}{\sqrt{5}}\}$.

This also suggests an extreme simplification obtained by choosing just between the 4-PAM and 4-QAM constellation (*two-choice* procedure), i.e., one can resort to an architecture that switches between the 4-QAM and the 4-PAM constellations according to the following rule:

$$P_e^{(low)}(\alpha_{PAM}, \theta_{PAM}) \underset{\text{PAM}}{\overset{\text{QAM}}{\geq}} P_e^{(low)}(0, 0) \quad (2.64)$$

Three remarks about the suboptimum procedure (2.63) follow.

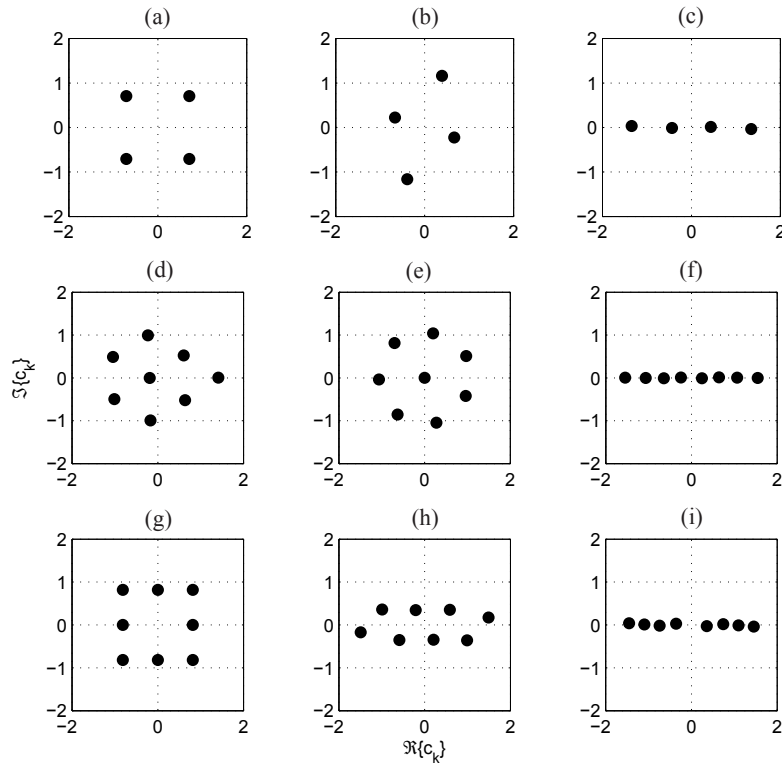


Figure 2.7: Optimum constellations for $K = 4$ and $K = 8$: (a) QPSK, (b) Rhombic QPSK, (c) 4-PAM, (d) Foschini&All 8-QAM, (e) “1-7” 8-QAM, (f) 8-PAM, (g) Rectangular 8-QAM, (h) Non-circular 8-QAM, (i) Non-uniform 8-QAM.

Remark 1: The results carried out here with reference to the 4-QAM constellation can be easily generalized to higher-order constellations. More specifically, the SER-bound approximations (analogous to the one in (2.59)) can be obtained by assuming that the inner summation in (2.58) is restricted to those constellation points closest to the k th one. Moreover, it can be shown that the conventional square K -QAM constellations (with $K = 16, 64, 128$) can be transformed by (2.54) into the conventional uniform K -PAM. Note, however, that such a property is not satisfied by the constellations of any order: for example, as also shown in the next section, when using the rectangular 8-QAM (see Fig. 2.7 (g)) the rhombic transformation allows one to obtain the non uniform 8-PAM reported in Fig. 2.7 (i).

Remark 2: The optimum transmission strategy proposed here requires that the receiver sends on the feedback channel the whole optimum constellation. If the suboptimum procedure is used, the transmitter architecture can be simplified: in fact, a unique symbol mapper for the alphabet \mathbf{c} is needed and the constellation is adapted by adjusting the zero-memory WL filter (2.54). Unfortunately, the main disadvantage in terms of the computational complexity of the receiver remains the adaptation of the decision mechanism for the constellation $\tilde{\mathbf{c}}$.

Remark 3: When the proposed suboptimum strategy is used, the channel input x_k is obtained by performing a zero-memory WL filtering of the information-bearing sequence s_k . For such a reason, it is reasonable to consider an alternative receiver structure that performs the WL MMSE equalization of the received signal in order to estimate $s_{k-\Delta}$, instead of $x_{k-\Delta}$. After some matrix manipulations, it can be verified that such WL MMSE equalizer is the cascade of the WL MMSE equalizer in (2.36)-(2.37) and the WL zero-memory filter performing the inverse⁹ of the transformation (2.54). This allows one to use a unique symbol de-mapper and the standard decision mechanism for the constellation \mathbf{c} . The MMSE achieved by such a structure is:

$$\begin{aligned} \mathbb{E}[|e_s|^2] &\triangleq \mathbb{E}[|s_{k-\Delta} - \mathbf{w}_s^{(opt)H} \mathbf{y}_k - \mathbf{g}_s^{(opt)H} \mathbf{y}_k^*|^2] \\ &= 1 + \frac{1}{|\mu|^2 - |\kappa|^2} [(\sigma_e(\beta)^2 - 1) + 4|\mu|^2|\kappa|^2 - \Re\{\beta^* \mathbb{E}[e(\beta)^2]\}] \end{aligned} \quad (2.65)$$

It can be easily shown that (a) if $\sigma_e(\beta)^2 \rightarrow 0$, then $\mathbb{E}[|e_s|^2] \rightarrow 0$, unless $|\mu|^2 = |\kappa|^2$, and (b) $\mathbb{E}[|e_s|^2] \geq \sigma_e(\beta)^2$ since $|\mu|^2 - |\kappa|^2 \leq 1$. Such results show that the minimum-distance decision based on the WL MMSE estimation of $x_{k-\Delta}$ outperforms the (computationally simpler) minimum-distance decision based on the WL MMSE estimation of $s_{k-\Delta}$.

2.3.4 Numerical results

In this section, we present the results of simulation experiments aimed at assessing the performance improvements achievable by the proposed constellation-optimization procedures. In all the experiments, we assume that: 1) the noise sequence at the output of the channel is zero-mean white Gaussian

⁹Note that (2.54) is not invertible for every value of α and θ , e.g., when a real-valued constellation is adopted ($\alpha = 1$). In such a case, however, an *ad hoc* inverse transformation can be easily defined.

complex-valued circularly symmetric with variance σ_n^2 , i.e., $E[n_k n_{k-\ell}^*] = \sigma_n^2 \delta_{k-\ell} \forall k, \ell$; 2) the decision delay Δ is optimized; 3) the SER has been estimated by stopping the simulation after 100 errors occur.

Fixed channel

In this section, we compare the performances of the constellation design procedures (2.63) and (2.49) in terms of SER. In our simulations, we solve (2.63) by means of an exhaustive search over $\alpha = n \cdot 0.05$ and $\theta = \frac{\pi}{2} \cdot n \cdot 0.05$: note that in our search we consider $(\alpha, \theta) \in \mathcal{X}$, so we consider a finite number of points. On the other hand, we resort to the constrained gradient-based algorithm for solving (2.49). Since the cost function (2.48) exhibits local minima, 1000 starting points have been randomly generated according to a uniform distribution. Due to the amount of time required by the computer simulations to determine the solution of (2.49), we consider, as in [25], the transmission over a two-tap channel $H(z) \triangleq 1 + \rho e^{j\phi} z^{-1}$ affected by an additive circularly symmetric white Gaussian noise with variance σ_n^2 . In our experiments, we have addressed the optimization of the constellation when $K = 4$ and $K = 8$ for different values of ρ , ϕ and N_f .

Let us first plot in Fig. 2.7 some of the optimum constellations obtained during our simulations when solving the optimization problem (2.49) over the considered channel model; moreover, we plot the suboptimum constellation utilized to implement our suboptimum strategy and the 8-PAM constellation obtained by applying to it the rhombic transformation. As in [28], we have found many local optima: some of them were rotated version of the constellations of Fig. 2.7 while others appeared as their rhombic transformation. For $K = 4$ the locally optimum constellation set includes the conventional 4-QAM ($\beta = 0$) and 4-PAM ($\beta = 1$), as well as the 4-QAM subject to a rhombic transformation ($\beta = -0.4 + 0.3j$); note such constellations can be obtained by means of a rhombic transformation of the conventional 4-QAM, which has been utilized to implement our suboptimum strategy when $K = 4$. For $K = 8$, the optimum constellation set includes the non-circular 8-QAM found by Foschini et al. ($\beta = 0.12 - 0.22j$), one of the conventional 8-QAM scheme ($\beta = 0$) called “1-7” 8-QAM [28], the 8-PAM ($\beta = 1$) and the non-circular 8-QAM scheme that we call non-circular 8-QAM. In the following, in order to implement the rhombic-transformation-based constellation-optimization strategy, we resort to the rectangular 8-QAM: we remember that, unlike 4-QAM, such a scheme can not be transformed into the conventional uniform 8-PAM,

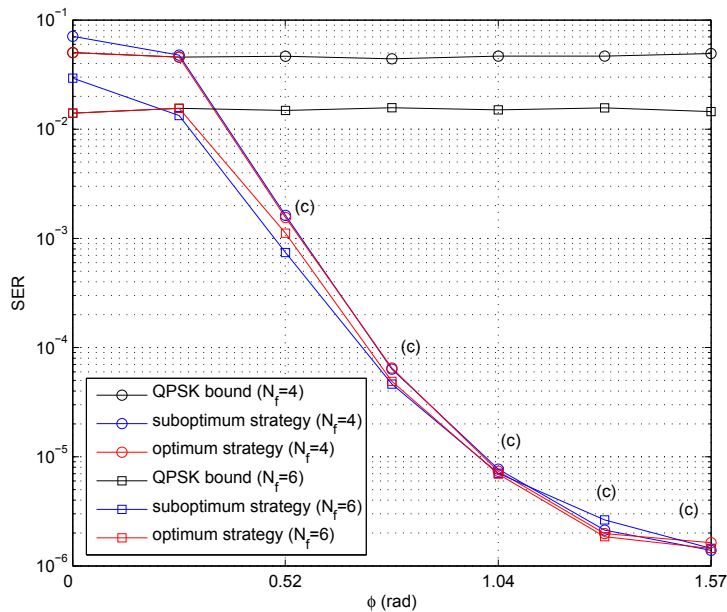


Figure 2.8: Constellation optimization for $K = 4$ over fixed channel ($\rho = 0.9$); for each point, the letter specifies the constellation (of those in Fig. 2.7) typically obtained.

but in the non-optimum non-uniform 8-PAM.¹⁰

In Fig. 2.8, with reference to the case $K = 4$, we have set $\text{SNR} \triangleq \frac{1}{\sigma_n^2} = 15\text{dB}$ and we have plotted the SERs achieved by both the suboptimum strategy (2.63) and the optimum strategy (2.49) versus ϕ , for $\rho = 0.9$ and for different values of N_f ($N_f = 4, 6$); moreover, for each point of Fig. 2.8, the constellation typically obtained by the optimum procedure is specified by the letter used to denote it in Fig. 2.7. The results show that the two strategies have the same performance: more specifically, both strategies switch to the 4-PAM when $\phi > \frac{\pi}{12}$ and outperform the conventional non-adaptive transceiver employing the QPSK modulation jointly with the linear MMSE receiver. Note also that as $\phi \rightarrow \frac{\pi}{2}$, the chosen value of N_f does not affect the performance.

In the next experiments we have addressed the constellation optimization when $K = 8$: more specifically, in Figs. 2.9 and 2.10 we have considered the transmission over $H(z)$ when $\rho = 0.9$ and $\rho = 0.6$, respectively. Fig. 2.9

¹⁰The optimality of uniform PAM over additive white Gaussian noise has been shown in [43].

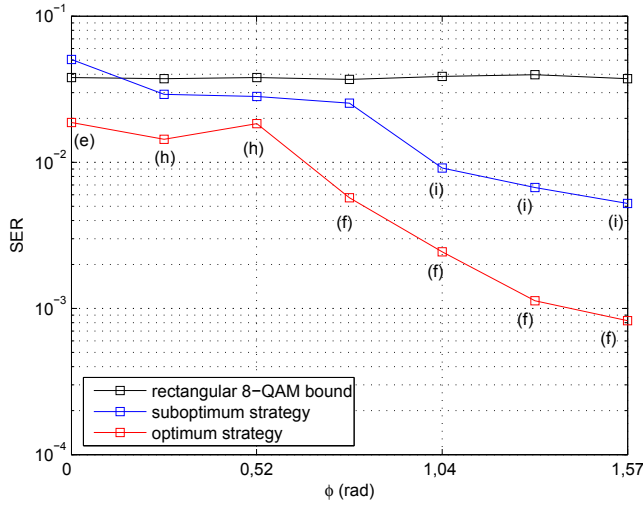


Figure 2.9: Constellation optimization for $K = 8$ over fixed channel ($\rho = 0.9$); for each point, the letter specifies the constellation (of those in Fig. 2.7) typically obtained.

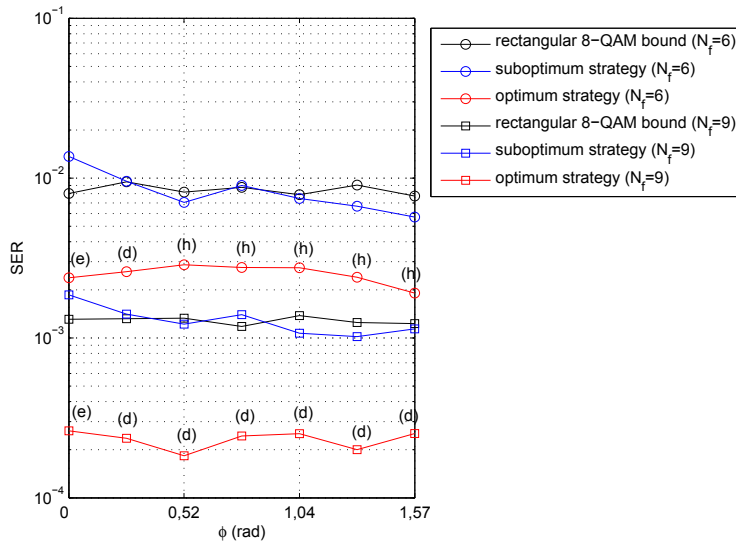


Figure 2.10: Constellation optimization for $K = 8$ over fixed channel ($\rho = 0.6$); for each point, the letter specifies the constellation (of those in Fig. 2.7) typically obtained.

reports the SER achieved by both the suboptimum strategy and the optimum strategy versus ϕ for SNR = 18dB and $N_f = 15$. The optimum strategy provides performance gain over the non-adaptive transceiver employing the conventional rectangular 8-QAM by using the “1-7” 8-QAM and the non-circular 8-QAM for smaller values of ϕ , and, as $\phi > \frac{\pi}{6}$, by using the 8-PAM. In such a case, the performance difference between the suboptimum strategy and the optimum one is important, especially for large values of ϕ , since the suboptimum one employs the non-uniform 8-PAM. Such a result was expected since, when K increases, the optimum strategy can exploit a number of degrees of freedom significantly larger than the suboptimum strategy.

Finally, we observe that, when $K = 4$, an architecture switching between the 4-QAM and the 4-PAM can provide a good trade-off between performance and complexity. Instead, when $K = 8$, the transceiver should switch among the *Foschini&All*, the non-circular 8-QAM and the 8-PAM.

Random channel

In the following simulations, we assume that: *i*) the channel has memory $\nu = 3$ and its taps h_k are randomly generated according to a complex-valued circularly-symmetric zero-mean white Gaussian process with unit variance (i.e., $E[(\Re\{h_k\})^2] = E[(\Im\{h_k\})^2] = \frac{1}{2}$ and $E[\Re\{h_k\}\Im\{h_k\}] = 0$); *ii*) the WL MMSE equalizer has $N_f = 12$ taps; *iii*) the results have been averaged over 500 independent channel realizations. We compare the performances achieved by four architectures: I) the OPTimum-based architecture (OPT-based) that selects α and θ in order to minimize the symbol error rate¹¹ (i.e., $P_e^{(true)}(\alpha, \theta)$, instead of $P_e^{(low)}(\alpha, \theta)$); II) the QAM-based architecture adopting the conventional circularly symmetric 4-QAM constellation; III) the PAM-based architecture utilizing the conventional rotationally variant 4-PAM ($|\beta| = 1$ which corresponds to the maximum WL gain); IV) the *two-choice*-based architecture that switches between the 4-QAM and the 4-PAM constellations according to (2.64). The OPT-based and the *two-choice*-based architectures, unlike the QAM-based and the PAM-based ones, require the existence of a feedback channel between the receiver and the transmitter for constellation adaptation; however, the *two-choice*-based architecture only needs to transmit a binary information on such feedback channel.

¹¹For clarity, we point out that the solution of (2.63) loses about 0.3dB in comparison with the OPT-based one; we consider the OPT-based architecture in order to provide a lower bound to the SER.

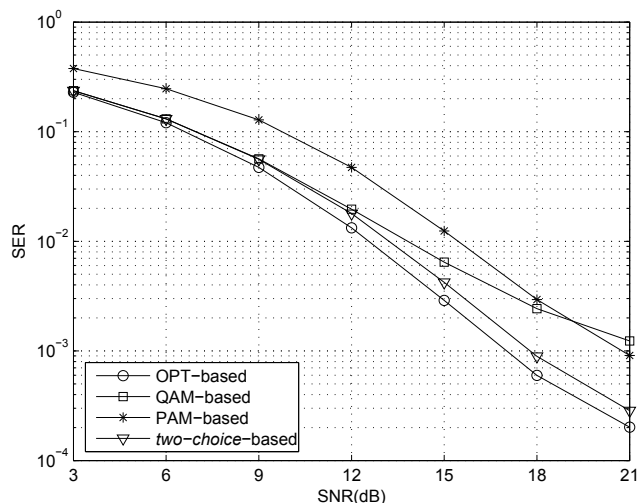


Figure 2.11: SERs of the considered architectures versus SNR.

In Fig. 2.11, the SERs of the considered architectures are plotted versus the SNR (in dB). The OPT-based architecture outperforms all the others and provides an SNR-gain over the non-optimized architectures of almost 3dB for a $\text{SER} = 10^{-3}$. Interestingly, the *two-choice*-based architecture performs well losing only 0.8dB in comparison with the OPT-based one. Let us also note that the PAM-based architecture performs poorly for low SNR, but, as the SNR increases, it outperforms the QAM-based one.

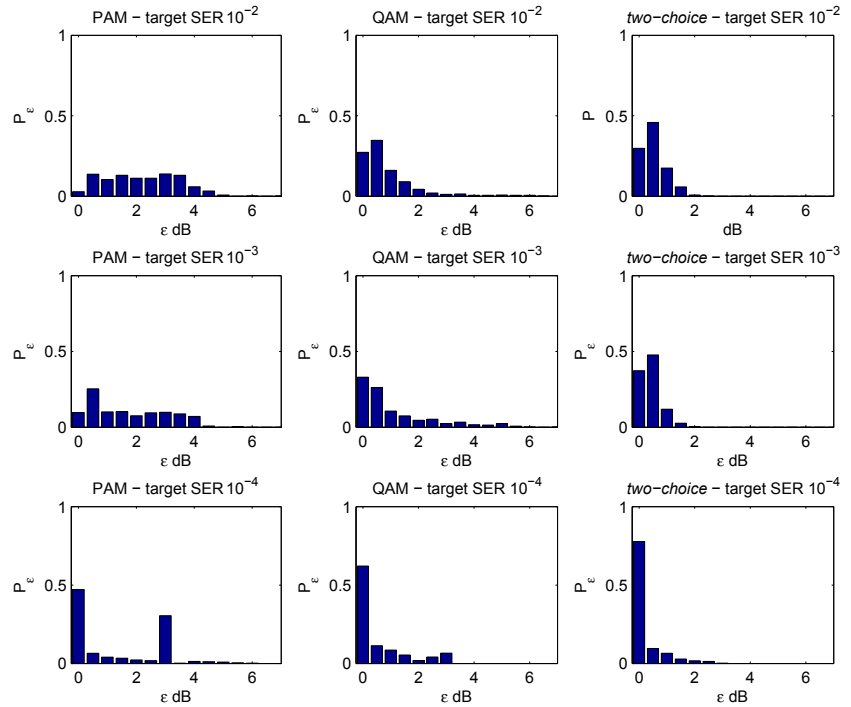
In the next experiment, we compare the considered architectures by evaluating their capability to guarantee the required quality of service (QoS). More specifically, in Table 2.1, we report the percentages of the channels over which the SNR required to achieve the target SER (assumed to be 10^{-2} , 10^{-3} , 10^{-4}) is not larger than 21dB. Moreover, Fig. 2.12 reports the probability, say P_ε , that each architecture loses ε dB in comparison with the OPT-based one for a given target SER under the condition that the SNR is not larger than 21dB.

The results show that:

- The PAM-based architecture is robust with respect to the communication environment since it often achieves the target SER. This is mainly due to the improved capabilities of the WL equalizer when the transmitted and the received signals are rotationally variant. However, it requires a larger SNR in comparison with the OPT-based architecture to compen-

Table 2.1: Percentage of channels over which the target SER is achieved.

Target SER	OPT-based	QAM-based	PAM-based	<i>two-choice</i> -based
10^{-2}	100	97	98	99
10^{-3}	97	83	95	96
10^{-4}	94	63	89	92

**Figure 2.12:** Loss in dB of the PAM-based, QAM-based and *two-choice*-based architectures with respect to the OPT-based one for several target SER.

sate for the reduction of the dimension of the signal space. Note also that such an SNR loss, which is uniformly distributed between 0dB and 4dB when the target SER is 10^{-2} and 10^{-3} , assumes often two specific values (0dB and 3dB) for a target SER equal to 10^{-4} : in practice, the PAM architecture achieves optimum performance on 50% of the channels where the linear equalizer performs unsatisfactorily and the WL processing gain, specific to rotationally variant constellations, compensates for the smaller minimum-distance of the PAM constellation.

- The QAM-based architecture is not robust with respect to the communication environment. When it is able to achieve the target SER, it requires a limited amount of excess SNR over the OPT-based architecture; nevertheless, it is unable to achieve the target SER of 10^{-4} on 37% of the channels. This is due to the circular symmetry of the constellation that does not allow one to improve by means of the WL processing the unsatisfactory performance of the linear equalizer.
- The *two-choice*-based architecture is particularly simple and robust since it combines the advantages of both PAM and QAM constellations.

Conclusion

In our paper [35], we have addressed the problem of the constellation optimization for the WL MMSE equalizer. By modeling the residual disturbance at the output of the WL equalizer as a white Gaussian (possibly rotationally variant) process, we have singled out constellation-design methods which minimize an upper bound of the symbol error rate. The first method exploits all the degrees of freedom ($2K$) associated to the K -order constellation exhibiting, therefore, an unaffordable computational complexity for high order constellation scenarios. To overcome such a problem, a second design method based on a rhombic transformation of a fixed alphabet of order K is proposed. It performs the optimization of only two parameters (instead of $2K$) leading to a huge reduction of the computational complexity in high order K scenario. For low-order constellations the two techniques are practically equivalent in terms of symbol error rate. The results have shown that a WL MMSE transceiver with constellation adaptation is clearly superior to the same equalizer with fixed constellation. Finally, for $K = 4$, it has been shown that the method that switches between a real-valued and a complex-valued constellation exhibits a limited performance loss versus the optimum adaptation scheme, while it achieves a

strong reduction of the computational complexity and it requires to feed back to the transmitter only a binary information.

Chapter 3

Equalization for OFDM-OQAM systems

Orthogonal frequency division multiplexing (OFDM) [44] has become a widely accepted technique for the realization of broadband air-interfaces in high data rate wireless access systems. Indeed, due to its inherent robustness to multipath propagation, OFDM has become the modulation choice for both wireless local area network (WLAN) and terrestrial digital broadcasting (digital audio broadcasting [DAB] and digital video broadcasting [DVB]) standards. Furthermore, multicarrier transmission schemes are generally considered candidates for the future “beyond 3 G” mobile communications.

Current multicarrier systems are based on the conventional cyclic prefix OFDM modulation scheme. In such systems, very simple equalization — one complex coefficient per subcarrier — is made possible by converting the broadband frequency selective channel into a set of parallel flat-fading subchannels. This is achieved using the inverse fast Fourier transform (IFFT) processing and by inserting a time domain guard interval, in the form of a cyclic prefix (CP), to the OFDM symbols at the transmitter. By dimensioning the CP longer than the maximum delay spread of the radio channel, interference from the previous OFDM symbol, referred to as inter-symbol-interference (ISI), will only affect the guard interval. At the receiver, the guard interval is discarded to elegantly avoid ISI prior to transforming the signal back to frequency domain using the fast Fourier transform (FFT).

While enabling a very efficient and simple way to combat multipath effects, the CP is pure redundancy, which decreases the spectral efficiency.

Moreover, there are other drawbacks in using CP-OFDM such as a higher level of out-of-band radiation, since the subcarriers pulse shaping is trivial being the rectangular one; a higher sensibility to narrowband interferers, because the low attenuation of the sidelobes implies an undesired overlap of the subchannels; and a higher sensitivity to frequency offsets due to the transmission channel and to the receiver. As a consequence, there has recently been a growing interest towards alternative multicarrier schemes, which could provide the same robustness without suffering from all these weaknesses. Pulse shaping in multicarrier transmission dates back to the early work of Chang [45] and Saltzberg [46] in the sixties. Since then, various multicarrier concepts based on the Nyquist pulse shaping idea with overlapping symbols and bandlimited subcarrier signals have been developed ([47] and references therein, [48, 49, 50]). One central ingredient in the later developments is the theory of efficiently implementable, modulation-based uniform filter banks. In this context, the filter banks are used in a transmultiplexer configuration.

We refer to the general concept as filter bank based multicarrier (FBMC) modulation. In FBMC, the subcarrier signals cannot be assumed flat-fading unless the number of subcarriers is very high. One approach to deal with the fading frequency selective channel is to use waveforms which are well localized, that is, the pulse energy both in time and frequency domains is well contained to limit the effect on consecutive symbols and neighboring subchannels. In this context, a basic subcarrier equalizer structure of a single complex coefficient per subcarrier is usually considered. Another approach uses finite impulse response (FIR) filters as subcarrier equalizers with cross-connections between the adjacent subchannels to cancel the inter-carrier-interference (ICI) [51, 52, 53, 54, 55]. A third line of studies applies a receiver filter bank structure providing oversampled subcarrier signals and performs persubcarrier equalization using FIR filters ([47] and references therein,[56]).

Among FBMC systems, we have focused on the OFDM with offset quadrature amplitude modulation (OQAM, OFDM-OQAM), where the modulation used for each subcarrier is a staggered offset QAM [57, 58, 59, 60]. Instead of using a rectangular window for shaping the pulses, a finite impulse response (FIR) prototype filter which has longer impulse response than the symbol period, i.e., the number of filter coefficients is higher than the number of subchannels M , is modulated and employed in each subchannel. The design of prototype filter has been based on frequency sampling technique, according to [61]. It is known from filter banks and communications theory [57] that the real and imaginary parts of the inputs of such a system have to be staggered,

resulting in OQAM signals.

The equalization problem in FBMC systems is still an area of active research. From communications theory it is known that the optimal receiver for a frequency selective (band limited) channel with band limited transmit signal and additive white Gaussian noise (AWGN) is composed by a (analog) matched filter (MF), a sampling device (at symbol rate) and a maximum likelihood sequence estimator (MLSE). But the latter is usually impractical in terms of complexity. Two practical sub-optimum solutions with lower computational burden are the linear equalizer and the decision feedback one which work at symbol rate.

We have considered the solution of the decision feedback (DF) multiple-input multiple-output (MIMO) equalizer and of it we have employed the widely linear (WL) version because the input sequence of the OFDM-OQAM system is real. Before this, we have derived the MIMO channel model describing the system, together with the noise correlation matrix. Afterwards, we have generalized the MIMO model to a multiple antenna scenario and on the obtained model we have designed the WL-DF MIMO equalizer, according to the minimum mean square error (MMSE) optimization criterion, which makes use of the conjugate gradient method for solving linear systems; such equalizer exhibits minimum storage requirements and a reduced complexity.

Notation

We will use the following notation in this chapter: the superscripts $*$ and T denote the complex-conjugate operator and the transpose one, respectively; j the imaginary unit; $E[\cdot]$ the statistical expectation; $\|\cdot\|$ and $\text{trace}\{\cdot\}$ the norm and the trace of their arguments; $\langle \cdot \rangle$ the time-average; \mathbf{I}_n the $n \times n$ identity matrix; \otimes the MIMO discrete-time linear convolution operator.

3.1 OFDM-OQAM MIMO model

The OFDM-OQAM discrete-time equivalent system model can be schematized as in Figure 3.1 [57, 61, 62, 47, 63], where the transmitter is usually called the synthesis filter bank (SFB) and the receiver the analysis filter bank (AFB). The filter bank is composed of a transform section which comprises the IFFT (FFT) block, implementing the modulation (demodulation), and some multipliers dependent on the subcarrier index and the time one whose role will be explained later; a polyphase filter section whose coefficients are determined by

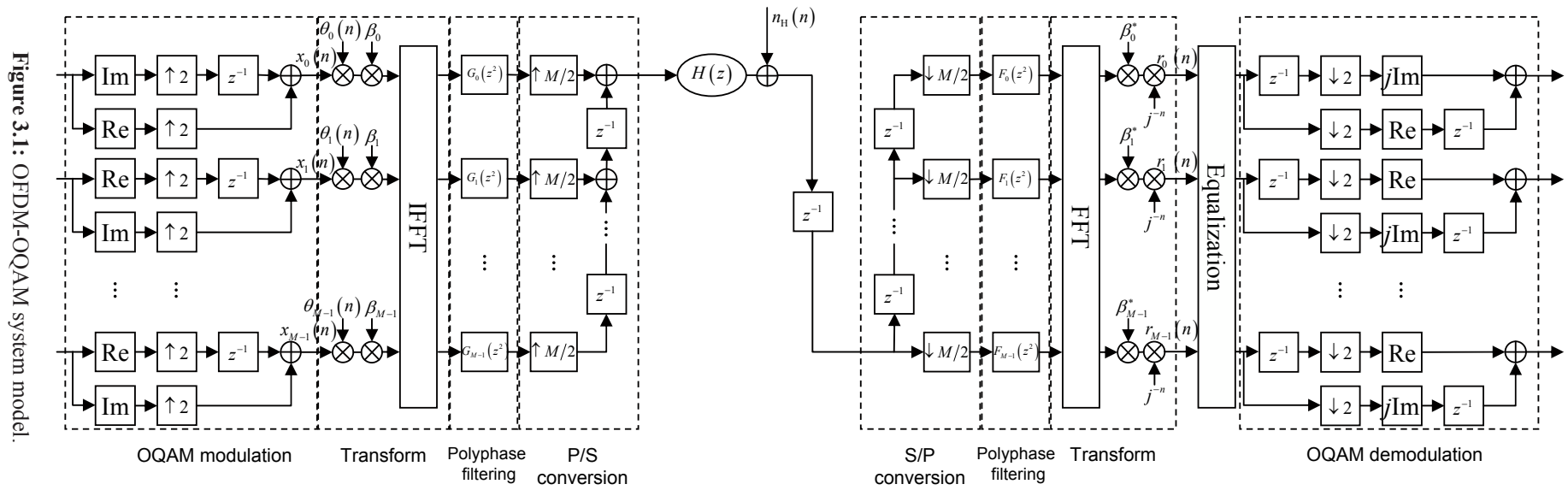


Figure 3.1: OFDM-QOAM system model.

the prototype filter design through the polyphase decomposition; a conversion section both of the sampling rate, by expanders (decimators), and the signal format, by a delay chain and additioners only at the transmitter side; as well as a OQAM staggering section which splits the QAM symbol into its real and imaginary parts to be transmitted alternately in the time: given the time, they are alternating on the subchannels, too. Let us note that the synthesized wide-band signal has a M -times higher sampling rate than the one of the subchannel signals at the SFB input.

We show how the MIMO channel model describing the OFDM-OQAM transceiver has been derived. The effects of the channel noise, $n_H(n)$ (Fig. 3.1), are not dealt with in this section and will be considered separately: this is possible because the MIMO channel output is linearly dependent on the MIMO channel input and the MIMO channel noise. The first transceiver block we have modelled is represented by the cascade of the delay chain at the transmitter side, the communication channel and the delay chain at the receiver side; it is obviously a MIMO linear time invariant (LTI) system with transfer function:

$$\mathbf{C}(z) \triangleq H(z)\mathbf{Z}(z) \quad (3.1)$$

where

$$H(z) \triangleq \sum_{k=0}^{P-1} h(k)z^{-k} \quad (3.2)$$

is the Z -transform of the discrete-time equivalent transmission channel and the $M \times M$ matrix $\mathbf{Z}(z) \triangleq [\mathbf{Z}_0(z) \ \mathbf{Z}_1(z) \ \dots \ \mathbf{Z}_{M-1}(z)]$. The first column $\mathbf{Z}_0(z)$ describes the delay encountered by the first MIMO channel input over all the other MIMO channel outputs and it is equal by definition to $[z^{-M} \ z^{-(M-1)} \ \dots \ z^{-1}]^T$; analogously, $\mathbf{Z}_i(z) \triangleq z^{-i}\mathbf{Z}_0(z)$ for $i = 0, 1, \dots, M-1$, since each MIMO channel subsequent input has one delay more on its path toward the MIMO channel outputs.

The cascade of the M expanders at the transmitter side, the MIMO LTI channel with transfer function $\mathbf{C}(z)$ and the M decimators at the receiver side can be shown to provide the MIMO LTI system with the following transfer function:

$$\mathbf{C}_{\frac{M}{2}}(z) \triangleq \sum_{k=1}^{K_0+3} \mathbf{c}_{\frac{M}{2}}(k)z^{-k} \quad (3.3)$$

with

$$\mathbf{c}_{\frac{M}{2}}(k) \triangleq \text{Toeplitz}(\chi_k, \phi_k) \quad (3.4)$$

where

$$\chi_k \triangleq \left[h\left(\left(k-2\right)\frac{M}{2}\right) h\left(\left(k-2\right)\frac{M}{2}+1\right) \dots h\left(\left(k-2\right)\frac{M}{2}+(M-1)\right) \right]^T \quad (3.5)$$

$$\phi_k \triangleq \left[h\left(\left(k-2\right)\frac{M}{2}\right) h\left(\left(k-2\right)\frac{M}{2}-1\right) \dots h\left(\left(k-2\right)\frac{M}{2}-(M-1)\right) \right] \quad (3.6)$$

K_0 is the superior integer (i.e., the smallest integer larger than or equal to) of $\frac{(P-1)}{\frac{M}{2}}$ and $\text{Toeplitz}(\mathbf{u}, \mathbf{v})$ denotes the Toeplitz matrix with \mathbf{u} as first column and \mathbf{v} as first row. Therefore, apart from the channel noise, $n_H(n)$, the sequence of the three innermost stages in the OFDM-OQAM transceiver scheme in Figure 3.1, the P/S conversion at the transmitter side, the communication channel and the S/P conversion at the receiver side can be described by a MIMO LTI channel with transfer function $\mathbf{C}_{\frac{M}{2}}(z)$.

Proof. See Appendix A. □

It is now simple to derive the MIMO channel impulse response which includes the polyphase filter networks, the IFFT and FFT blocks and the phase coefficients β_k . The length of the M polyphase filters is equal to 2γ , where γ is usually called the overlapping factor in the prototype filter design; the length of the prototype filter — whose M polyphase components are the polyphase filter impulse responses compressed by 2 — is equal to $M\gamma$. Since the polyphase networks act as diagonal MIMO systems both at the transmitter and the receiver side, we can define their transfer functions as:

$$\mathbf{G}(z) \triangleq \text{diag}\left[G_0(z^2) G_1(z^2) \dots G_{M-1}(z^2)\right] = \sum_{\ell=0}^{2\gamma-1} \mathbf{g}(\ell)z^{-\ell} \quad (3.7)$$

$$\mathbf{F}(z) \triangleq \text{diag}\left[F_0(z^2) F_1(z^2) \dots F_{M-1}(z^2)\right] = \sum_{\ell=0}^{2\gamma-1} \mathbf{f}(\ell)z^{-\ell} \quad (3.8)$$

where $G_i(z) \triangleq \sum_{k=0}^{\gamma-1} g_i(k)z^{-k}$ represents the Z-transform of the i th polyphase

component of the prototype filter and $F_i(z) \triangleq \sum_{k=0}^{\gamma-1} f_i(k)z^{-k}$ its adapted filter, for $i = 0, 1, \dots, M-1$. Let it be \mathbf{W}_M the unitary discrete Fourier transform

(DFT) matrix whose (i, k) -entry is equal by definition to $\frac{1}{\sqrt{M}} \exp\left(-jik\frac{2\pi}{M}\right)$ with $(i, k) \in \{0, 1, \dots, M-1\}^2$. The transfer function of the MIMO channel we have considered is:

$$\mathbf{C}_{\text{eq}}(z) \triangleq \sum_{\ell=1}^{K_0+4\gamma+1} \boldsymbol{\beta}_M^H \mathbf{W}_M \mathbf{c}_{\text{PF}}(\ell) \mathbf{W}_M^H \boldsymbol{\beta}_M z^{-\ell} = \sum_{\ell=1}^{K_0+4\gamma+1} \mathbf{c}_{\text{eq}}(\ell) z^{-\ell} \quad (3.9)$$

with

$$\mathbf{c}_{\text{eq}}(n) \triangleq \boldsymbol{\beta}_M^H \mathbf{W}_M \mathbf{c}_{\text{PF}}(n) \mathbf{W}_M^H \boldsymbol{\beta}_M \quad (3.10)$$

$$\mathbf{c}_{\text{PF}}(n) \triangleq \mathbf{g}(n) \otimes \mathbf{c}_{\frac{M}{2}}(n) \otimes \mathbf{f}(n) \quad (3.11)$$

being $\boldsymbol{\beta}_M$ a diagonal matrix with ℓ -entry ($\ell = 0, 1, \dots, M-1$) equal by definition to $\exp\left(-j\ell(M\gamma-1)\frac{\pi}{M}\right)$.

But our modelling hasn't finished yet because there are some additional multipliers (Fig. 3.1): at the transmitter side, $\theta_k(n) \triangleq j^{k+n}$ ($k = 0, 1, \dots, M-1$) switches the input real-valued symbols over the real axis and the imaginary one, alternately; at the receiver side, we have introduced a multiplication stage by j^{-n} in order to preserve the system time-invariance. Therefore, the input-output relationship of the overall MIMO system including the transform, filtering and conversion blocks is:

$$\mathbf{r}(n) = \sum_{\ell=1}^{K_0+4\gamma+1} \mathbf{c}_{\text{eq}}(\ell) j^{-\ell} \mathbf{J}_0 \mathbf{x}(n-\ell) = \mathbf{c}_{\text{eq},\mathbf{J}}(n) \otimes \mathbf{x}(n) \quad (3.12)$$

where $\mathbf{c}_{\text{eq},\mathbf{J}}(n) = \mathbf{c}_{\text{eq}}(n) j^{-n} \mathbf{J}_0$ and \mathbf{J}_0 is a diagonal matrix with k -entry ($k = 0, 1, \dots, M-1$) equal by definition to j^k . The input sequence-vector $\mathbf{x}(n)$, the OQAM modulator output, is composed by iid symbols belonging to the set $\{-1, 1\}$.

Finally, we have obtained that the OQAM demodulator input is related to the OQAM modulator output, which is a real-valued symbol sequence — hence a stationary sequence — by a $M \times M$ MIMO LTI channel with impulse response $\mathbf{c}_{\text{eq},\mathbf{J}}(n)$. We have plotted in Figure 3.2 the energy graph of all the components of the MIMO channel matrix in (3.12) according to the International Telecommunication Union (ITU) Vehicular-A transmission channel model. Let us note that the MIMO channel impulse response exhibits a diagonally dominant structure: it will be exploited for the equalizer design, together with the non-circularity property of the input sequence $\mathbf{x}(n)$.

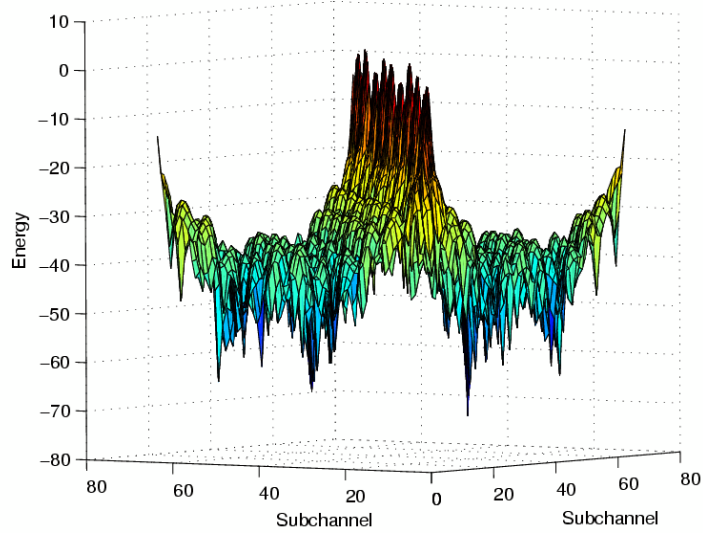


Figure 3.2: Subchannel energy according to the ITU Vehicular-A channel model ($M = 64$).

3.1.1 Noise correlation matrix

Let it be $r_{n_H}(m)$ the correlation function of the noise present at the output of the discrete-time equivalent transmission channel (see Fig. 3.1) and let us assume that the noise is circularly symmetric: $E[n_H(n)n_H(n-m)] = 0$. The noise at the output of the S/P conversion stage is such that

$$n_k(n) \triangleq n_H\left(n\frac{M}{2} - M - k\right) \quad k \in \{0, 1, \dots, M-1\} \quad (3.13)$$

Therefore, its correlation matrix is:

$$\mathbf{R}_{\mathbf{n}_{\text{SP}}}(m)|_{p,q} \triangleq E[n_p(n)n_q^*(n-m)] = r_{n_H}\left(m\frac{M}{2} + p - q\right) \quad (3.14)$$

After the polyphase filtering, it becomes:

$$\mathbf{R}_{\mathbf{n}_{\text{PF}}}(m) \triangleq \mathbf{f}(m) \otimes \mathbf{R}_{\mathbf{n}_{\text{SP}}}(m) \otimes \mathbf{f}(-m)^H \quad (3.15)$$

which can also be written as

$$\mathbf{R}_{\mathbf{n}_{\text{PF}}}(m) \triangleq \sum_{\ell_1=0}^{2\gamma-1} \sum_{\ell_2=0}^{2\gamma-1} \mathbf{f}(\ell_1)\mathbf{R}_{\mathbf{n}_{\text{SP}}}(m + \ell_2 - \ell_1)\mathbf{f}(\ell_2)^H \quad (3.16)$$

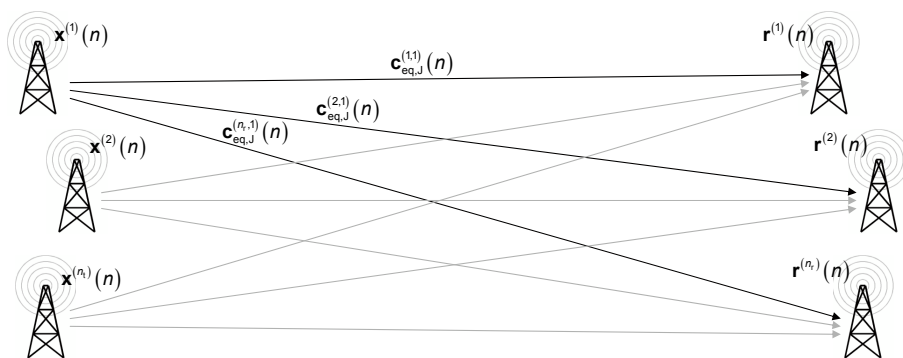


Figure 3.3: Multiple antenna scenario scheme.

After the last stage, the transform block, the noise correlation matrix will be:

$$\mathbf{R}_{\mathbf{n}}(m) \triangleq j^{-m} \boldsymbol{\beta}_M^H \mathbf{W}_M \mathbf{R}_{\mathbf{n}_{\text{PF}}}(m) \mathbf{W}_M^H \boldsymbol{\beta}_M \quad (3.17)$$

Moreover, the noise has remained circularly symmetric: $\mathbb{E}[\mathbf{n}(n) \mathbf{n}^T(n-m)] = \mathbf{0}$.

3.2 Multiple antenna OFDM-OQAM MIMO model

Till now, we have interested ourselves in modelling the OFDM-OQAM transceiver in a single antenna scenario, i.e., a scenario which there are only two antennas in: the former transmitting and the latter receiving; in this section, we will derive the MIMO system model for OFDM-OQAM systems in a multiple antenna scenario. Let us assume to have n_t transmitting antennas and n_r receiving ones and denote with $\mathbf{c}_{\text{eq},j}^{(i,j)}(n)$ the equivalent MIMO channel, analogous to the one in Equation (3.12), between the i th receiving antenna and the j th transmitting one; then, we have used the same notation as the previous sections unless to specify at the superscript the transmitting or receiving antenna index. In Figure 3.3, you can see a illustrative stylized drawing of a multiple antenna scenario, with the right notation.

By a straightforward generalization of the derivation in Section 3.1, we

have got the following input-output relationship:

$$\begin{aligned}
\mathbf{r}(n) &\triangleq \begin{bmatrix} \mathbf{r}^{(1)}(n) \\ \mathbf{r}^{(2)}(n) \\ \vdots \\ \mathbf{r}^{(n_r)}(n) \end{bmatrix} \triangleq \begin{bmatrix} \sum_{j=1}^{n_t} \mathbf{r}^{(1,j)}(n) \\ \sum_{j=1}^{n_t} \mathbf{r}^{(2,j)}(n) \\ \vdots \\ \sum_{j=1}^{n_t} \mathbf{r}^{(n_r,j)}(n) \end{bmatrix} \\
&\triangleq \sum_{\ell=1}^{K_0+4\gamma+1} \underbrace{\begin{bmatrix} \mathbf{c}_{\text{eq},J}^{(1,1)}(\ell) & \mathbf{c}_{\text{eq},J}^{(1,2)}(\ell) & \cdots & \mathbf{c}_{\text{eq},J}^{(1,n_t)}(\ell) \\ \mathbf{c}_{\text{eq},J}^{(2,1)}(\ell) & \mathbf{c}_{\text{eq},J}^{(2,2)}(\ell) & \cdots & \mathbf{c}_{\text{eq},J}^{(2,n_t)}(\ell) \\ \vdots & \vdots & \ddots & \vdots \\ \mathbf{c}_{\text{eq},J}^{(n_r,1)}(\ell) & \mathbf{c}_{\text{eq},J}^{(n_r,2)}(\ell) & \cdots & \mathbf{c}_{\text{eq},J}^{(n_r,n_t)}(\ell) \end{bmatrix}}_{\mathbf{C}_{\text{eq},J}(\ell)} \underbrace{\begin{bmatrix} \mathbf{x}^{(1)}(n-\ell) \\ \mathbf{x}^{(2)}(n-\ell) \\ \vdots \\ \mathbf{x}^{(n_t)}(n-\ell) \end{bmatrix}}_{\mathbf{x}(n-\ell)} \\
&\quad + \underbrace{\begin{bmatrix} \mathbf{n}^{(1)}(n) \\ \mathbf{n}^{(2)}(n) \\ \vdots \\ \mathbf{n}^{(n_r)}(n) \end{bmatrix}}_{\mathbf{n}(n)} \quad (3.18)
\end{aligned}$$

where all the $n_t n_r$ OFDM-OQAM transceivers are assumed to have the same parameters as well as all the $n_t n_r$ transmission channels between each couple of antennas the same length.

Finally, we can express Equation (3.18) more closely in a matrix form, as follows:

$$\mathbf{r}(n) \triangleq \mathbf{C}_{\text{eq},J}(n) \otimes \mathbf{x}(n) + \mathbf{n}(n) \quad (3.19)$$

Therefore, also in a multiple antenna scenario, of course, the discrete-time equivalent MIMO channel describing OFDM-OQAM systems is LTI; the channel matrix, $\mathbf{C}_{\text{eq},J}(n)$, whose size is $M n_r \times M n_t$, exhibits a block diagonally dominant structure.

3.2.1 Ad hoc equalizers

If, for any couple of antennas, the M subchannels of the OFDM-OQAM system are orthogonal, then the matrices $\mathbf{c}_{\text{eq},J}^{(i,j)} \forall i = 1, \dots, n_r$ and $j = 1, \dots, n_t$

(see Equation (3.18)) will be diagonal. This implies that the system model in Equation (3.19) degenerates into M parallel $n_r \times n_t$ MIMO channels and, consequently, the equalization is performed per-subchannel, i.e. the M channels are equalized separately.

But in practice, as the prototype filter is FIR — hence ICI cause — the matrices $\mathbf{c}_{\text{eq},j}^{(i,j)} \forall i = 1, \dots, n_r$ and $j = 1, \dots, n_t$ are diagonally dominant; therefore, the equalization per-subchannel can no longer be the optimum choice because it does not take all the interference terms into account. A solution which exploits the diagonally dominant structure of the matrices $\mathbf{c}_{\text{eq},j}^{(i,j)}$ is such as to perform a *selective* MIMO equalization for each subchannel, i.e., given the subchannel $k \in \{1, \dots, M\}$ to be equalized, to extract from the complete matrix $\mathbf{c}_{\text{eq},j}^{(i,j)}$, given i and j , a submatrix which contains only the most significant interference terms, for instance those related to k_1 adjacent subchannels at the transmitter and k_2 ones at the receiver: this will be the MIMO channel matrix related to the k th subchannel to be equalized. The parameters k_1 and k_2 are the result of a trade-off between performance and complexity.

Therefore, as the MIMO channel impulse response which describes the OFDM-OQAM system, $\mathbf{c}_{\text{eq},j}^{(i,j)}|_{i,j}$, is diagonally dominant, we expect ad hoc equalizers to be able to operate with reduced complexity compared with standard equalizers. More specifically, we have considered the WL-DF MIMO equalizer which has proved to be very useful for the equalization of OFDM-OQAM systems, as we will see in the next section.

3.3 Synthesis of the MMSE WL-DF MIMO equalizer with minimum storage requirements

Decision feedback equalizers draw considerable attention in modern communication scenarios since they greatly outperform the linear equalizers and, at the same time, they keep a limited implementation complexity compared with the maximum likelihood receiver whose computational complexity grows exponentially with the channel memory and the order of the feedforward filter. We have studied the problem of the synthesis of the MMSE WL-DF equalizer for MIMO dispersive channels [7, 64, 65]. Methods present in the literature are mainly based on displacement structure theory (see, for example, [66]) and on fast recursive least squares (RLS) [67, 68]. We have followed the method in [67] in order to show that the synthesis of the feedforward filter is equivalent to a least-square equalization problem. Moreover, we have derived an

algorithm for the equalizer synthesis — especially suitable for the case where the number of taps of the feedforward filter, N_f , is very large — which requires a minimum memory amount and a reduced number of floating point operations per second (flops).

In [67], the authors show that the optimum feedforward filter can also be obtained by solving a least square problem and a fast RLS method is proposed to do it with $O(N^2)$ flops; then, the feedback filter is calculated by convolving the channel impulse response with the optimum feedforward filter by the FFT.

However, the computational complexity of the available methods significantly increases because they exhibit a quadratic dependence on N_f . The average number of flops needed to execute the synthesis and the implementation procedures for each temporal block affects the overall receiver behavior (burden of the receiver processor, energy consumption, etc.).

Unlike the existing algorithms, the proposed approach can be clearly followed and easily implemented since it relies on the basic matrix algebra and no complex matrix theory, such as the displacement structure theory [66] and the fast RLS filtering [67], is needed.

Finally, unlike the method in [66], the assumption of the white additive noise is not introduced; unlike the method in [67], the presence of coloured noise does not introduce any sophistication in the derivation of the procedure and in its implementation, hence, it does not imply a significant increase of the computational complexity.

3.3.1 Problem setting

Let us consider a FIR baseband equivalent noisy MIMO communication channel with n_i jointly wide-sense stationary (WSS) transmitted signals and n_o received signals. The output $\mathbf{r}(k) \in \mathbb{R}^{n_o \times 1}$ of the MIMO channel can be written as

$$\mathbf{r}(k) = \sum_{m=0}^M \mathbf{H}(m)\mathbf{x}(k-m) + \mathbf{n}(k) \quad (3.20)$$

where $\mathbf{x}(k) \in \mathbb{R}^{n_i \times 1}$ is the information-bearing symbol sequence, $\mathbf{n}(k) \in \mathbb{R}^{n_o \times 1}$ is the background noise, $\mathbf{H}(m) \in \mathbb{R}^{n_o \times n_i}$ ($\mathbf{H}(m) = \mathbf{0}$ for $m < 0$ and $m > M$) is the M -order channel matrix — which in our simulations coincides with $\mathbf{C}_{\text{eq},j}(n)$ in Equation (3.18) — whose (i, j) -entry represents the channel impulse response between the j th input and the i th output.

In the following we assume that:

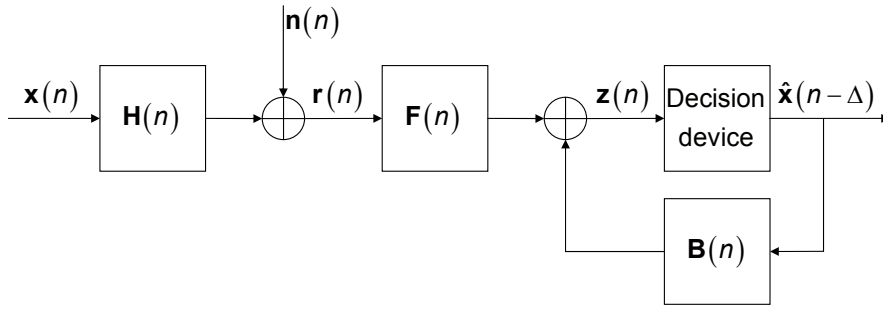


Figure 3.4: DF MIMO equalizer scheme.

- a0. The MIMO channel impulse response is perfectly known at the receiver side: one can have operated in conjunction with blind or training-based identification algorithms.
- a1. The coloured additive noise $\mathbf{n}(k)$ is independent of the input sequence $\mathbf{x}(k)$: actually, it is sufficient that they are uncorrelated, i.e., $\langle \mathbf{E}[\mathbf{x}(k_1)\mathbf{n}^T(k_2)] \rangle = \mathbf{0} \quad \forall k_1, k_2$; moreover, the noise autocorrelation matrix $\mathbf{R}(m) \triangleq \langle \mathbf{E}[\mathbf{n}(k)\mathbf{n}^T(k-m)] \rangle$ is assumed known at the receiver side.
- a2. The power spectral density (PSD) of the input sequence is assumed flat, i.e., $\mathbf{E}[\mathbf{x}(k)\mathbf{x}^T(k-m)] = \mathbf{I}_{n_i}\delta(m)$; such an assumption is common since the scrambling sequence often compensates the effects of a possible channel coding.

According to the DF equalization, at the receiver side, the received signal $\mathbf{r}(k)$ is processed jointly with the equalizer output, i.e., the signal at the output of the decision device, in order to provide an estimate of the transmitted signal $\mathbf{x}(k)$. More specifically, the equalizer is constituted of the following $n_i \times n_o$ feedforward filter $\mathbf{F}(z)$, which processes the channel output, and the $n_i \times n_i$ feedback one $\mathbf{B}(z)$, which processes the output of the decision device:

$$\mathbf{F}(z) \triangleq \sum_{n=0}^N \mathbf{F}(n)z^{-n} \quad \mathbf{B}(z) \triangleq \sum_{m=0}^{N_b} \mathbf{B}(m)z^{-m} \quad (3.21)$$

of order N and N_b , respectively.

In Figure 3.4, you can see the DF MIMO equalizer scheme. In MIMO equalization scenario, the constraint on the feedback filter concerns the matrix-tap $\mathbf{B}(0)$, as we will see later.

With reference to the DF equalization stage, we assume that:

- b0. The order N_b of the feedback filter is such as to optimize the performance of the equalizer. Let us note that feedback-filter implementation requires a smaller computational complexity than feedforward-filter one since its inputs belong to a finite set.
- b1. Filter design assumes that previous decisions are correct: this is a common assumption in filter synthesis.
- b2. In order to account for a possible anticausal feedforward filter, the signal at the equalizer output will be $\mathbf{x}(k - \Delta)$ where Δ is a decision delay which affects the equalizer performance and, hence, needs to be optimized.

According to (3.20) and (3.21), the output $\mathbf{r}_f(k)$ of the feedforward filter can be written as

$$\mathbf{r}_f(k) \triangleq \sum_{\ell=0}^{M+N} \mathbf{G}(\ell)\mathbf{x}(k - \ell) + \sum_{\ell=0}^N \mathbf{F}(\ell)\mathbf{n}(k - \ell) \quad (3.22)$$

where the sequence $\mathbf{G}(\cdot)$ is defined as the MIMO discrete-time convolution of $\mathbf{H}(k)$ and $\mathbf{F}(k)$, i.e.,

$$\mathbf{G}(k) \triangleq \mathbf{H}(k) \otimes \mathbf{F}(k) = \sum_{m=\max(0, k-N)}^{\min(M, k)} \mathbf{H}(m)\mathbf{F}(k-m) \quad k = 0, 1, \dots, M+N \quad (3.23)$$

Assuming that $\Delta \in \{0, 1, \dots, M + N\}$ and by the assumption b1., the equalizer output $\mathbf{z}(k)$ (see Figure 3.4) can be written as

$$\begin{aligned} \mathbf{z}(k) &\triangleq \mathbf{r}_f(k) - \sum_{\ell=0}^{N_b} \mathbf{B}(\ell)\mathbf{x}(k - \Delta - \ell) \\ &= \sum_{\ell=0}^{\Delta-1} \mathbf{G}(\ell)\mathbf{x}(k - \ell) + \sum_{\ell=\Delta}^{M+N} (\mathbf{G}(\ell) - \mathbf{B}(\ell - \Delta))\mathbf{x}(k - \ell) \\ &\quad - \sum_{\ell=M+N-\Delta+1}^{N_b} \mathbf{B}(\ell)\mathbf{x}(k - \Delta - \ell) + \sum_{\ell=0}^N \mathbf{F}(\ell)\mathbf{n}(k - \ell) \end{aligned} \quad (3.24)$$

hence, the error sequence $\mathbf{e}_k \triangleq \mathbf{z}(k) - \mathbf{x}(k - \Delta)$ is given by

$$\begin{aligned}
 \mathbf{e}(k) &= \sum_{\ell=0}^{\Delta-1} \mathbf{G}(\ell)\mathbf{x}(k - \ell) + (\mathbf{G}(\Delta) - \mathbf{B}(0) - \mathbf{I})\mathbf{x}(k - \Delta) \\
 &+ \sum_{\ell=\Delta+1}^{M+N} (\mathbf{G}(\ell) - \mathbf{B}(\ell - \Delta))\mathbf{x}(k - \ell) \\
 &- \sum_{\ell=M+N-\Delta+1}^{N_b} \mathbf{B}(\ell)\mathbf{x}(k - \Delta - \ell) + \sum_{\ell=0}^N \mathbf{F}(\ell)\mathbf{n}(k - \ell)
 \end{aligned} \tag{3.25}$$

By the assumptions a1. and a2.¹, one gets the following MSE:

$$\begin{aligned}
 \text{MSE} &\triangleq \langle \mathbf{E}[\|\mathbf{e}(k)\|^2] \rangle \\
 &= \sum_{\ell=0}^{\Delta-1} \mathbf{E}[\|\mathbf{G}(\ell)\mathbf{x}(k - \ell)\|^2] + \mathbf{E}[\|(\mathbf{G}(\Delta) - \mathbf{B}(0) - \mathbf{I})\mathbf{x}(k - \Delta)\|^2] \\
 &+ \sum_{\ell=\Delta+1}^{M+N} \mathbf{E}[\|(\mathbf{G}(\ell) - \mathbf{B}(\ell - \Delta))\mathbf{x}(k - \ell)\|^2] \\
 &+ \sum_{\ell=M+N-\Delta+1}^{N_b} \mathbf{E}[\|\mathbf{B}(\ell)\mathbf{x}(k - \Delta - \ell)\|^2] \\
 &+ \left\langle \mathbf{E} \left[\left\| \sum_{\ell=0}^N \mathbf{F}(\ell)\mathbf{n}(k - \ell) \right\|^2 \right] \right\rangle
 \end{aligned} \tag{3.26}$$

¹The property $\|\mathbf{x}\|^2 = \text{trace}\{\mathbf{x}\mathbf{x}^T\}$ has been used, too.

which can also be written as

$$\begin{aligned}
\text{MSE} &= \sum_{\ell=0}^{\Delta-1} \text{trace}\{\mathbf{G}(\ell)\mathbf{G}^T(\ell)\} \\
&\quad + \text{trace}\{(\mathbf{G}(\Delta) - \mathbf{B}(0) - \mathbf{I})(\mathbf{G}(\Delta) - \mathbf{B}(0) - \mathbf{I})^T\} \\
&\quad + \sum_{\ell=\Delta+1}^{M+N} \text{trace}\{(\mathbf{G}(\ell) - \mathbf{B}(\ell - \Delta))(\mathbf{G}(\ell) - \mathbf{B}(\ell - \Delta))^T\} \\
&\quad + \sum_{\ell=M+N-\Delta+1}^{N_b} \text{trace}\{\mathbf{B}(\ell)\mathbf{B}^T(\ell)\} \\
&\quad + \sum_{\ell_1=0}^N \sum_{\ell_2=0}^N \text{trace}\{\mathbf{F}(\ell_1)\mathbf{R}(\ell_2 - \ell_1)\mathbf{F}^T(\ell_2)\}
\end{aligned} \tag{3.27}$$

from which it follows that the optimum order of the feedback filter is $N_b = M + N - \Delta$, i.e., $\mathbf{B}(\ell) = \mathbf{0}$ at the optimum for $\ell > M + N - \Delta$; moreover, the optimum feedback filter is

$$\mathbf{B}(\ell - \Delta) = \mathbf{G}(\ell) \quad \ell = \Delta + 1, \Delta + 2, \dots, M + N \tag{3.28}$$

Therefore, unlike the approach in [65], the optimum feedback filter, except for the matrix-tap $\mathbf{B}(0)$, is calculated after the optimum feedforward filter since $\mathbf{G}(k)$ depends on $\mathbf{F}(k)$.

The problem is then reduced to compute the matrix-taps $\{\mathbf{F}(k)\}_{k=0,\dots,N}$ which minimize

$$\begin{aligned}
\text{MSE} &= \sum_{\ell=0}^{\Delta-1} \text{trace}\{\mathbf{G}(\ell)\mathbf{G}^T(\ell)\} + \text{trace}\{(\mathbf{G}(\Delta) - \mathbf{D})(\mathbf{G}(\Delta) - \mathbf{D})^T\} \\
&\quad + \sum_{\ell_1=0}^N \sum_{\ell_2=0}^N \text{trace}\{\mathbf{F}(\ell_1)\mathbf{R}(\ell_2 - \ell_1)\mathbf{F}^T(\ell_2)\} \\
&= \text{trace}\{(\mathbf{G} - \mathbf{B})(\mathbf{G} - \mathbf{B})^T\} + \text{trace}\{\mathbf{F}\mathbf{R}\mathbf{F}^T\}
\end{aligned} \tag{3.29}$$

where $\mathbf{D} \triangleq \mathbf{I} + \mathbf{B}(0)$, $\mathbf{G} \triangleq [\mathbf{G}(\Delta) \ \mathbf{G}(\Delta - 1) \ \dots \ \mathbf{G}(0)]$, $\mathbf{B} \triangleq [\mathbf{D} \ \mathbf{0} \ \dots \ \mathbf{0}]$,

$$\mathbf{F} \triangleq [\mathbf{F}(N) \mathbf{F}(N-1) \dots \mathbf{F}(0)],$$

$$\mathbf{R} \triangleq \begin{bmatrix} \mathbf{R}(0) & \mathbf{R}^T(1) & \dots & \mathbf{R}^T(N) \\ \mathbf{R}(1) & \mathbf{R}(0) & \dots & \mathbf{R}^T(N-1) \\ \vdots & \vdots & \ddots & \vdots \\ \mathbf{R}(N) & \mathbf{R}(N-1) & \dots & \mathbf{R}(0) \end{bmatrix} \quad (3.30)$$

Moreover, by Equation (3.23), it can be shown that $\mathbf{G}^T = \mathbf{H}_e \mathbf{F}^T$ where

$$\mathbf{H}_e \triangleq \begin{bmatrix} \mathbf{H}^T(\Delta - N) & \dots & \dots & \mathbf{H}^T(\Delta) \\ \mathbf{H}^T(\Delta - N - 1) & \dots & \dots & \mathbf{H}^T(\Delta - 1) \\ \vdots & \ddots & \ddots & \vdots \\ \mathbf{H}^T(0) & \dots & \dots & \mathbf{H}^T(N) \\ \mathbf{0} & \dots & \dots & \mathbf{H}^T(N-1) \\ \vdots & \ddots & \ddots & \vdots \\ \mathbf{0} & \dots & \mathbf{H}^T(0) & \mathbf{H}^T(1) \\ \mathbf{0} & \dots & \mathbf{0} & \mathbf{H}^T(0) \end{bmatrix} \quad (3.31)$$

Let us denote with \mathbf{g}_i and \mathbf{f}_i ($i \in \{1, \dots, n_i\}$) the i th column of \mathbf{G}^T and \mathbf{F}^T , respectively:

$$\mathbf{G}^T \triangleq [\mathbf{g}_1 \mathbf{g}_2 \dots \mathbf{g}_{n_i}] \quad \mathbf{F}^T \triangleq [\mathbf{f}_1 \mathbf{f}_2 \dots \mathbf{f}_{n_i}] \quad (3.32)$$

hence, it follows that

$$\mathbf{g}_i = \mathbf{H}_e \mathbf{f}_i \quad (3.33)$$

and the MSE can be written as

$$\begin{aligned} \text{MSE} &= \sum_{i=1}^{n_i} (\|\mathbf{g}_i - \mathbf{b}_i\|^2 + \mathbf{f}_i^T \mathbf{R} \mathbf{f}_i) \\ &= \sum_{i=1}^{n_i} (\|\mathbf{H}_e \mathbf{f}_i - \mathbf{b}_i\|^2 + \mathbf{f}_i^T \mathbf{R} \mathbf{f}_i) \end{aligned} \quad (3.34)$$

where \mathbf{b}_i is defined according to \mathbf{g}_i and \mathbf{f}_i , i.e.,

$$\mathbf{B}^T \triangleq [\mathbf{b}_1 \mathbf{b}_2 \dots \mathbf{b}_{n_i}] \quad (3.35)$$

3.3.2 Scenario 1

Only previous decisions are available at the present time in Scenario 1; it imposes the constraint $\mathbf{B}(0) = \mathbf{0}$. It follows from this that $\mathbf{D} = \mathbf{I}$, hence $\mathbf{b}_i = \mathbf{e}_i$ where \mathbf{e}_i is the vector with all null entries but the i th one which is equal to one. Therefore, by putting equal to zero the gradient of the cost function (3.34), the optimum vector \mathbf{f}_i will satisfy the following normal equation:

$$(\mathbf{H}_e^T \mathbf{H}_e + \mathbf{R})\mathbf{f}_i = \mathbf{H}_e^T \mathbf{e}_i \triangleq \mathbf{h}_i \quad (3.36)$$

where $\mathbf{H}_e^T \triangleq [\mathbf{h}_1 \ \mathbf{h}_2 \ \dots \ \mathbf{h}_{n_i(\Delta+1)}]$. Let us note that the optimization procedure over $\{\mathbf{f}_i\}_{i=1, \dots, n_i}$ can be carried out separately over each \mathbf{f}_i ($i = 1, \dots, n_i$) because the cost function (3.34) is a linear combination whose terms are affected by one \mathbf{f}_i at a time.

Normal Equation (3.36) has a size $n_o N_f$ with $N_f \triangleq N + 1$, but the matrix $\mathbf{A} \triangleq \mathbf{H}_e^T \mathbf{H}_e + \mathbf{R}$ can be stored with much less memory locations than $n_o^2 N_f^2$ ones since it possesses a structure which can be described by the $(\Delta + 1)$ taps of size $n_o \times n_i$ of the channel impulse response $\mathbf{H}(n)$ for $n \in \{0, 1, \dots, \Delta\}$ and by the N_f taps of size $n_o \times n_o$ of the noise autocorrelation matrix $\mathbf{R}(m)$ for $m \in \{0, 1, \dots, N\}$. To conclude, there are n_i linear systems which need to be solved in (3.36) and, in a field programmable gate array (FPGA) implementation, they can be solved with a parallel processing.

3.3.3 Unsorted Scenario 2

Unsorted Scenario 2 is defined as the scenario where the components of $\mathbf{x}(\cdot)$ are not sorted and the order of the decisions coincides with the order of the components in the vector $\mathbf{x}(\cdot)$; when one decides about the i th component of $\mathbf{x}(n)$, the already taken decisions about the first $(i - 1)$ components of $\mathbf{x}(n)$ are fed back for improving the estimation of the i th component of $\mathbf{x}(n)$. Such scenario imposes the condition that $\mathbf{B}(0)$ is strictly lower triangular, i.e., it is lower triangular and null along the diagonal. Therefore, the vector $\mathbf{B}(0)\hat{\mathbf{x}}(n - \Delta)$, where $\hat{\mathbf{x}}(n - \Delta)$ represents the vector with the decisions about $\mathbf{x}(n - \Delta)$ being Δ the decision delay, is subtracted from $\mathbf{r}_f(n)$ (see Equation (3.24)) in order to suppress the effect of the interferences.

Calculating \mathbf{f}_1

By the condition that $\mathbf{B}(0)$ is strictly lower triangular it follows that the first row of $\mathbf{B}(0)$ is null, and therefore the first column of $\mathbf{B}^T(0)$ is null, too. Consequently, the optimum vector \mathbf{f}_1 in unsorted Scenario 2 is the same as the one

in the Scenario 1, i.e., it is the solution of the following normal equation:

$$(\mathbf{H}_e^T \mathbf{H}_e + \mathbf{R})\mathbf{f}_1 = \mathbf{h}_1 \quad (3.37)$$

Calculating \mathbf{f}_i

The constraint over $\mathbf{B}(0)$ imposes that only the first $(i - 1)$ components of the i th row of $\mathbf{B}(0)$ are different from zero; let us denote them with $\lambda_{i,j}$ ($j \in \{1, \dots, i - 1\}$) and let us note that they are free parameters whose values can be chosen for the optimization. Therefore, the i th column of $\mathbf{B}^T(0)$ can be written as $\sum_{j=1}^{i-1} \lambda_{i,j} \mathbf{e}_j^{(s)}$ where the $n_i \times 1$ vector $\mathbf{e}_j^{(s)}$ is the “small” version of \mathbf{e}_j , i.e., \mathbf{e}_j is obtained from $\mathbf{e}_j^{(s)}$ by zero padding. Consequently, the i th column $\mathbf{b}_i^{(s)}$, defined according to $\mathbf{e}_j^{(s)}$, of $\mathbf{D}^T \triangleq \mathbf{I} + \mathbf{B}^T(0)$ can be written as $\mathbf{b}_i^{(s)} = \mathbf{e}_i^{(s)} + \sum_{j=1}^{i-1} \lambda_{i,j} \mathbf{e}_j^{(s)}$; hence, $\mathbf{b}_i = \mathbf{e}_i + \sum_{j=1}^{i-1} \lambda_{i,j} \mathbf{e}_j$. The term in Equation (3.34) dependent on \mathbf{f}_i to be optimized is the following:

$$\|\mathbf{H}_e \mathbf{f}_i - \mathbf{b}_i\|^2 + \mathbf{f}_i^T \mathbf{R} \mathbf{f}_i = \left\| \mathbf{H}_e \mathbf{f}_i - \mathbf{e}_i - \sum_{j=1}^{i-1} \lambda_{i,j} \mathbf{e}_j \right\|^2 + \mathbf{f}_i^T \mathbf{R} \mathbf{f}_i \quad (3.38)$$

The coefficients $\{\lambda_{i,j}\}_{j=1, \dots, i-1}$ can be chosen in order to minimize the norm without affecting the second term, in particular, $\lambda_{i,j}$, which multiplies \mathbf{e}_j , can be exploited to minimize the j th component of the vector within the norm $\|\cdot\|^2$. Since the vector \mathbf{e}_i has its first $(i - 1)$ components null, the first $(i - 1)$ components of $\mathbf{H}_e \mathbf{f}_i$ can be deleted by the coefficients $\lambda_{i,j}$ for $j = 1, \dots, i - 1$. Consequently, the optimization problem

$$\min_{\substack{\lambda_{i,1}, \dots, \lambda_{i,i-1} \\ \mathbf{f}_i}} \left\| \mathbf{H}_e \mathbf{f}_i - \mathbf{e}_i - \sum_{j=1}^{i-1} \lambda_{i,j} \mathbf{e}_j \right\|^2 + \mathbf{f}_i^T \mathbf{R} \mathbf{f}_i \quad (3.39)$$

can be rewritten as

$$\left\{ \begin{array}{l} \min_{\mathbf{f}_i} \|\mathbf{H}_e^{(i-1)} \mathbf{f}_i - \mathbf{e}_i^{(i-1)}\|^2 + \mathbf{f}_i^T \mathbf{R} \mathbf{f}_i \\ \lambda_{i,j} = \mathbf{h}_j^T \mathbf{f}_i \quad j = 1, \dots, i-1 \\ \mathbf{H}_e \triangleq \begin{bmatrix} \mathbf{h}_1^T \\ \vdots \\ \mathbf{h}_{i-1}^T \\ \mathbf{H}_e^{(i-1)} \end{bmatrix} \\ \mathbf{e}_i \triangleq \begin{bmatrix} 0 \\ \vdots \\ 0 \\ \mathbf{e}_i^{(i-1)} \end{bmatrix} \end{array} \right. \quad (3.40)$$

where we have noted that \mathbf{h}_j^T is the j th row of \mathbf{H}_e for $j = 1, \dots, i-1$; we have also denoted with $\mathbf{H}_e^{(i-1)}$ the remaining rows of \mathbf{H}_e and with $\mathbf{e}_i^{(i-1)}$ the vector \mathbf{e}_i without the last $(i-1)$ rows or, equivalently, the vector \mathbf{e}_i without the first $(i-1)$ rows.

Consequently, the optimization problem becomes:

$$\left\{ \begin{array}{l} \left(\mathbf{H}_e^{(i-1)T} \mathbf{H}_e^{(i-1)} + \mathbf{R} \right) \mathbf{f}_i = \mathbf{H}_e^{(i-1)T} \mathbf{e}_i^{(i-1)} = \mathbf{h}_i \\ \lambda_{i,j} = \mathbf{h}_j^T \mathbf{f}_i \quad j = 1, \dots, i-1 \end{array} \right. \quad (3.41)$$

To conclude, while in Scenario 1 the optimum vector \mathbf{f}_i is obtained by solving the following system:

$$\left(\mathbf{R} + \sum_{j=1}^{n_i(\Delta+1)} \mathbf{h}_j \mathbf{h}_j^T \right) \mathbf{f}_i = \mathbf{h}_i \quad (3.42)$$

in unsorted Scenario 2 it is obtained by solving the following one:

$$\left(\mathbf{R} + \sum_{j=i}^{n_i(\Delta+1)} \mathbf{h}_j \mathbf{h}_j^T \right) \mathbf{f}_i = \mathbf{h}_i \quad (3.43)$$

3.3.4 Sorted Scenario 2

In sorted Scenario 2 the columns of $\mathbf{B}(0)$ can be re-ordered arbitrarily; the constraint imposed by the scenario requires that $\mathbf{B}(0)$ after the re-ordering is strictly lower triangular.

Therefore, sorted Scenario 2 is equivalent to unsorted Scenario 2 provided that also the matrices $\mathbf{H}(m)$ and $\mathbf{R}(m)$ are coherently re-ordered. However, a first approach to sorted Scenario 2 can be described as a sequence of three stages:

1. an ordering algorithm is first applied; it takes in input the matrices $\mathbf{H}(m)$ and $\mathbf{R}_x(m)$, autocorrelation matrix of $\mathbf{x}(n)$, as well as the noise autocorrelation matrix $\mathbf{R}(m)$, and it provides as output the new order of the components. Different algorithms can be used at this stage, therefore potentially obtaining a different order. The obtained order can be described by the sequence of values $p(i)$ for $i = 1, \dots, n_i$ with $p(i)$ which assumes all the elements of the set $\{1, \dots, n_i\}$. Equivalently, the ordering can be described by means of the permutation matrix \mathbf{P} whose (i, j) -entry is equal to $\delta(j - p(i))$, i.e., it is such that its i th row is null but for the $(i, p(i))$ -entry which is equal to one. Such a matrix can be used to relate the original vector $\mathbf{x}(n)$ with its re-ordered version $\mathbf{x}^{(o)}(n)$:

$$\mathbf{x}^{(o)}(n) = \mathbf{P}\mathbf{x}(n) \quad (3.44)$$

2. Let us denote with $\mathbf{H}^{(o)}(m)$ the matrix defined as the result of the re-ordering of the columns of $\mathbf{H}(m)$ and with $\mathbf{R}_x^{(o)}(m)$ the matrix defined as the result of the re-ordering of both the rows and the columns of $\mathbf{R}_x(m)$. It can be shown that the new matrices $\mathbf{H}^{(o)}(m)$ and $\mathbf{R}_x^{(o)}(m)$ are related to $\mathbf{H}(m)$ and $\mathbf{R}_x(m)$ as follows:

$$\mathbf{H}^{(o)}(m) = \mathbf{H}(m)\mathbf{P}^T \quad \mathbf{R}_x^{(o)}(m) = \mathbf{P}\mathbf{R}_x(m)\mathbf{P}^T \quad (3.45)$$

where $\mathbf{R}_x^{(o)}(m)$ is also the autocorrelation matrix of the re-ordered version $\mathbf{x}^{(o)}(n)$ of the vector $\mathbf{x}(n)$.

Therefore, this stage of the procedure consists in determining the new matrices $\mathbf{H}^{(o)}(m)$ and $\mathbf{R}_x^{(o)}(m)$. Moreover, if the transmitted symbols are assumed uncorrelated both temporally and spatially, i.e., $\mathbf{R}_x(m) = \mathbf{I}$, then $\mathbf{R}_x^{(o)}(m) = \mathbf{I}$, too.²

3. Let us apply unsorted Scenario 2 to the sorted channel $\mathbf{H}^{(o)}(m)$ with input autocorrelation matrix $\mathbf{R}_x^{(o)}(m)$ in order to obtain an estimation of the ordered channel input $\mathbf{x}^{(o)}(n)$.

²This result can be shown thanks to the fact that \mathbf{P} is orthogonal, i.e., $\mathbf{P}^{-1} = \mathbf{P}^T$.

The channel model (see Equation (3.20)), after the re-ordering, can be written as

$$\begin{aligned} \mathbf{r}(k) &= \sum_{m=0}^M \mathbf{H}(m) \mathbf{P}^T \mathbf{P} \mathbf{x}(k-m) + \mathbf{n}(k) \\ &= \sum_{m=0}^M \mathbf{H}^{(o)}(m) \mathbf{x}^{(o)}(k-m) + \mathbf{n}(k) \end{aligned} \quad (3.46)$$

where Equations (3.44) and (3.45) have been used together with the orthogonality property of \mathbf{P} . Let us note that the noise $\mathbf{n}(k)$ and, consequently, its autocorrelation matrix $\mathbf{R}(k)$ remain unchanged.

Applying an equalization method to the original channel (3.20) or to its sorted counterpart (3.46) usually provides the same performance; in other terms, the performance obtained at stage 3 is usually independent of the permutation matrix \mathbf{P} obtained at stage 1. In such cases, consequently, the simplest method consists in setting $\mathbf{P} = \mathbf{I}$ at stage 1, so, the first two stages are skipped and only the third stage is performed, without any performance loss. However, for some equalization algorithms, the order of the components of the input vector $\mathbf{x}(n)$ determined at stage 1, affects the performance, as it happens for the DF equalizer in Scenario 2; therefore, if one used the simplest method setting $\mathbf{P} = \mathbf{I}$ at stage 1, one would get a performance loss at stage 3, while one could improve the performance of the equalizer if one chose the most suitable ordering at stage 1.

It can be shown that the only method for achieving the optimum performance at stage 3 requires to exhaustively evaluate the equalizer performance for each of the $n_i!$ different permutation matrices. Since the optimum method is NP-hard and the simplest method ($\mathbf{P} = \mathbf{I}$) can provide a poor performance, a suboptimum method is usually employed at stage 1. Moreover, after that the first output of the ordering algorithm $p(1)$ is available, stage 3 can be started using the known part of $\mathbf{H}^{(o)}(m)$; then, the method at stage 1 is continued providing the second output $p(2)$ and stage 3 is continued, too, and so on. Let us note that, when $p(1)$ is known, the first row of \mathbf{P} is available, and therefore, the first column of \mathbf{P}^T is available, too; consequently, according to (3.45), the first column of $\mathbf{H}^{(o)}(m)$ is available. In some cases, such a ping-pong procedure between stages 1 and 3 exhibits a computational complexity not so larger than the one of the algorithm at stage 3 when, using $\mathbf{P} = \mathbf{I}$, the first two stages are bypassed; however, it provides significant performance advantages. We intro-

duce such ping-pong procedure with reference to the DF equalizer in sorted Scenario 2 which is dependent on the permutation matrix \mathbf{P} .

The DF equalizer in sorted Scenario 2 is represented as follows:

$$\begin{aligned}
 \mathbf{z}(k) &\triangleq \mathbf{P}^T \mathbf{z}^{(o)}(k) \\
 &= \sum_{\ell=0}^N \mathbf{P}^T \mathbf{F}^{(o)}(\ell) \mathbf{r}(k-\ell) - \sum_{\ell=0}^{N_b} \mathbf{P}^T \mathbf{B}^{(o)}(\ell) \hat{\mathbf{x}}^{(o)}(k-\Delta-\ell) \\
 &= \sum_{\ell=0}^N \mathbf{F}(\ell) \mathbf{r}(k-\ell) - \sum_{\ell=0}^{N_b} \mathbf{P}^T \mathbf{B}^{(o)}(\ell) \mathbf{P} \hat{\mathbf{x}}(k-\Delta-\ell) \\
 &= \sum_{\ell=0}^N \mathbf{F}(\ell) \mathbf{r}(k-\ell) - \sum_{\ell=0}^{N_b} \mathbf{B}(\ell) \hat{\mathbf{x}}(k-\Delta-\ell)
 \end{aligned} \tag{3.47}$$

where $\mathbf{F}(\ell) \triangleq \mathbf{P}^T \mathbf{F}^{(o)}(\ell)$, $\mathbf{B}(\ell) \triangleq \mathbf{P}^T \mathbf{B}^{(o)}(\ell) \mathbf{P}$ and Equations (3.20) and (3.44) together with the orthogonality of \mathbf{P} have been used. Let us remember that the constraint imposed by the scenario is that $\mathbf{B}^{(o)}(0)$ is strictly lower-triangular.

Let us note that $\mathbf{B}^{(o)}(\ell) = \mathbf{P} \mathbf{B}(\ell) \mathbf{P}^T$, therefore, using the result in (3.45), it is obtained from $\mathbf{B}(\ell)$ by re-ordering its rows and columns; analogously, $\mathbf{B}(\ell)$ is obtained from $\mathbf{B}^{(o)}(\ell)$ by imposing the reverse order on both the rows and the columns. Consequently, the first row of $\mathbf{B}^{(o)}(0)$, which is null since $\mathbf{B}^{(o)}(0)$ is constrained to be strictly lower-triangular, becomes the $p(1)$ th row of $\mathbf{B}(0)$ after the re-ordering of the rows and remains unchanged by the re-ordering of the columns because it is null. Therefore, the $p(1)$ th row of $\mathbf{B}(0)$ is null. Moreover, the second row of $\mathbf{B}^{(o)}(0)$, which is nonnull only in its first component, becomes the $p(2)$ th row of $\mathbf{B}(0)$ after the re-ordering of the rows and becomes different from zero only in its $p(1)$ th component after the re-ordering of the columns.

In order to calculate the i th component of $\mathbf{z}(k)$, we need the i th row of $\mathbf{F}(\ell)$, or, equivalently, the i th column \mathbf{f}_i of \mathbf{F}^T in (3.32). Since $\mathbf{F}^{(o)}(\ell) = \mathbf{P} \mathbf{F}(\ell)$, the matrix $\mathbf{F}^{(o)}(\ell)$ is obtained by re-ordering the rows of $\mathbf{F}(\ell)$. Consequently, in order to calculate the $p(1)$ th component of $\mathbf{z}(k)$, we need the $p(1)$ th row of $\mathbf{F}(\ell)$ (i.e., the $p(1)$ th column $\mathbf{f}_{p(1)}$ of \mathbf{F}^T in (3.32)) or, equivalently, the first row of $\mathbf{F}^{(o)}(\ell)$; moreover, only $\mathbf{f}_{p(1)}$ is needed because the $p(1)$ th component of the second term in (3.47) is null being null the $p(1)$ th row of $\mathbf{B}(0)$, as previously shown. After having calculated the $p(1)$ th component of $\mathbf{z}(k)$ and, therefore, the $p(1)$ th component of $\hat{\mathbf{x}}(k-\Delta)$, in order to calculate the $p(2)$ th

component of $\mathbf{z}(k)$, we need the $p(2)$ th row of $\mathbf{F}(\ell)$ (i.e., the $p(2)$ th column $\mathbf{f}_{p(2)}$ of \mathbf{F}^T in (3.32)) or, equivalently, the second row of $\mathbf{F}^{(o)}(\ell)$; moreover, only the $p(1)$ th component of $\hat{\mathbf{x}}(k - \Delta)$ is needed since only the $p(1)$ th component of the $p(2)$ th row of $\mathbf{B}(0)$ is different from zero. The same line of reasoning can be followed for each of $\mathbf{f}_{p(i)}$ with $i = 1, \dots, n_i$.

Calculating $\mathbf{f}_{p(1)}$

Applying the DF equalizer in unsorted Scenario 2 to the sorted channel, we get that the optimum vector $\mathbf{f}_1^{(o)} \triangleq \mathbf{f}_{p(1)}$ is the solution of the following system:

$$(\mathbf{H}_e^{(o)T} \mathbf{H}_e^{(o)} + \mathbf{R})\mathbf{f}_1^{(o)} = \mathbf{h}_1^{(o)} \quad (3.48)$$

where $\mathbf{H}_e^{(o)}$ is related to $\mathbf{H}^{(o)}(m)$ according to \mathbf{H}_e to $\mathbf{H}(m)$ (see Equation (3.31)). The re-ordering of the columns of $\mathbf{H}(m)$ is equivalent to the re-ordering of the rows of $\mathbf{H}^T(m)$ and, therefore, is equivalent to the re-ordering of the rows of \mathbf{H}_e . From this it follows that blocks of n_i rows of \mathbf{H}_e are sorted according to the re-ordering algorithm dictated by \mathbf{P} , i.e.,

$$\mathbf{h}_{j+i}^{(o)} = \mathbf{h}_{j+p(i)} \quad i = 1, 2, \dots, n_i \quad j = kn_i \quad k = 0, 1, \dots, \Delta \quad (3.49)$$

where $\mathbf{h}_{j+i}^{(o)}$ is the $(j+i)$ th row of $\mathbf{H}_e^{(o)}$. From this one gets that $\mathbf{H}_e^{(o)T} \mathbf{H}_e^{(o)} = \mathbf{H}_e^T \mathbf{H}_e$ and, consequently, the relation (3.48) becomes

$$(\mathbf{H}_e^T \mathbf{H}_e + \mathbf{R})\mathbf{f}_1^{(o)} = \mathbf{h}_1^{(o)} \quad (3.50)$$

The choice of $p(1)$ has to take into account the quality of the estimation of the $p(1)$ th component of $\mathbf{x}(k)$; suboptimum ordering algorithms, where the first decision is taken on the component of $\mathbf{x}(k)$ which can be better estimated (better in the sense of the MSE or of the probability of error), are usually derived. The advantage of using the MSE to set $p(1)$ lies in the smaller computational complexity of the procedure which determines the value of $p(1)$ in comparison with alternative procedures. Therefore, optimizing the MSE, the following algorithm can be derived:

$$p(1) = \arg \min_{i \in \{1, 2, \dots, n_i\}} \min_{\mathbf{f}} \|\mathbf{H}_e \mathbf{f} - \mathbf{e}_i\|^2 + \mathbf{f}^T \mathbf{R} \mathbf{f} \quad (3.51)$$

Three approaches can be followed for determining the value of $p(1)$:

1. defining a simple ordering algorithm and treating the three stages separately; in such case, the complexity increase with respect to unsorted Scenario 2 is maintained reduced by the simplicity of the ordering algorithm. Unless the ordering algorithm uses specific statistical characteristics of the channel matrix to be equalized, the disadvantage of such approach lies in the limited performance improvement with respect to unsorted Scenario 2.
2. Using an algorithm which is able to determine (or, more generally, to estimate) the error residue for each value of i with a complexity much smaller than the one required to solve a single linear system and, consequently, choosing a value of i which guarantees significant performance improvements in comparison with unsorted Scenario 2 with a marginal increase of the computational complexity.

An important example of such approach is the so-called BLAST algorithm: it determines the input ordering with a ping-pong procedure based on its ability to exactly calculate (or, more precisely, to calculate within the machine precision) the MSE of n_i linear systems and to exactly solve a single linear system with a complexity practically equivalent to that required to exactly solve a single linear system.

3. Solving n_i times the system in Equation (3.50) for each possible value of $p(1)$ and evaluate the best choice for $p(1)$ in terms of its consequence on the error probability of the decision about $\mathbf{x}_{p(1)}(k)$.

Let us note that deciding about $\mathbf{x}_{p(1)}(k)$ is more difficult than deciding about $\mathbf{x}_{p(i)}(k)$ for $i > 1$ since such decision cannot make use of no component of $\hat{\mathbf{x}}(k)$; therefore, the probability of error in the decision about $\mathbf{x}_{p(1)}(k)$ has a high chance to be the largest probability of error among those on the components of the vector $\mathbf{x}(k)$; consequently, it is one of the most important parameters in evaluating the quality of the DF equalizer in sorted Scenario 2, in fact, many synthetical performance parameters are significantly influenced by it.

Calculating $\mathbf{f}_{p(i)}$

The constraint on $\mathbf{B}^{(0)}(0)$ imposes that only the first $(i - 1)$ components of its i th row are different from zero; let us denote them with $\lambda_{i,j}^{(0)}$ ($j \in \{1, \dots, i - 1\}$). With the same line of reasoning followed for calculating \mathbf{f}_i in unsorted Scenario 2, we get the same optimization problem (see Equation (3.41)) unless

\mathbf{H}_e and \mathbf{f}_i are replaced by their ordered versions. Therefore, in sorted Scenario 2, the optimum vector $\mathbf{f}_i^{(o)}$ is obtained by solving the following system:

$$\left(\mathbf{R} + \sum_{j=i}^{n_i(\Delta+1)} \mathbf{h}_j^{(o)} \mathbf{h}_j^{(o)T} \right) \mathbf{f}_i^{(o)} = \mathbf{h}_i^{(o)} \quad (3.52)$$

which, using Equation (3.49), can be rewritten as

$$\left(\mathbf{R} + \sum_{j=1, j \neq p(1), \dots, j \neq p(i-1)}^{n_i(\Delta+1)} \mathbf{h}_j \mathbf{h}_j^T \right) \mathbf{f}_i^{(o)} = \mathbf{h}_{p(i)} \quad (3.53)$$

Finally, the BLAST algorithm can be described as follows:

$$\begin{cases} p(i) = \arg \min_{j \in \{1, \dots, n_i\} - \{p(1), \dots, p(i-1)\}} \min_{\mathbf{f}} \|\mathbf{H}_e^{(i-1,p)} \mathbf{f} - \mathbf{e}_j\|^2 + \mathbf{f}^T \mathbf{R} \mathbf{f} \\ \left(\mathbf{R} + \sum_{j=1, j \neq p(1), \dots, j \neq p(i-1)}^{n_i(\Delta+1)} \mathbf{h}_j \mathbf{h}_j^T \right) \mathbf{f}_i^{(o)} = \mathbf{h}_{p(i)} \\ \lambda_{i,j}^{(o)} = \mathbf{h}_j^{(o)T} \mathbf{f}_i^{(o)} \end{cases} \quad (3.54)$$

where $\mathbf{H}_e^{(i-1,p)}$ represents the matrix \mathbf{H}_e with the j th row made null for any $j \in \{p(1), p(2), \dots, p(i-1)\}$.

The BLAST algorithm is able to determine the MMSEs of $(n_i - (i - 1))$ linear systems (and consequently to determine $p(i)$) and to solve a single linear system in (3.54) with a complexity practically equivalent to that required to solve the single linear system. This is based on the fact that the data matrix

$\mathbf{R} + \sum_{j=1, j \neq p(1), \dots, j \neq p(i-1)}^{n_i(\Delta+1)} \mathbf{h}_j \mathbf{h}_j^T$ depends on $\{p(1), p(2), \dots, p(i-1)\}$, which are known, but not on $p(i)$ (unknown). Only its right-hand side depends on the unknown value of $p(i)$.

3.3.5 Scenario 3

Finally, we specialize the general method to Scenario 3, defined as the scenario where, for the decision about the i th component of $\mathbf{x}(k)$, one disposes of the decisions about all the other components of $\mathbf{x}(k)$ as they come from a previous detection stage.

Calculating \mathbf{f}_i

The constraint imposed by the scenario on $\mathbf{B}(0)$ is that it is null on the diagonal. Consequently, $\mathbf{D} \triangleq \mathbf{I} + \mathbf{B}(0)$ is monic, i.e., it is unit on the diagonal. Therefore, the i th row of $\mathbf{B}(0)$ with $i = 1, \dots, n_i$ can be described as $[\lambda_{i,1} \dots \lambda_{i,i-1} 0 \lambda_{i,i+1} \dots \lambda_{i,n_i}]$ and, accordingly, the i th column of $\mathbf{B}^T(0)$ follows

$$\lambda_{i,1}\mathbf{e}_1^{(s)} + \dots + \lambda_{i,i-1}\mathbf{e}_{i-1}^{(s)} + \lambda_{i,i+1}\mathbf{e}_{i+1}^{(s)} + \dots + \lambda_{i,n_i}\mathbf{e}_{n_i}^{(s)} = \sum_{j=1, j \neq i}^{n_i} \lambda_{i,j}\mathbf{e}_j^{(s)} \quad (3.55)$$

hence, the i th column of \mathbf{D}^T will be

$$\mathbf{b}_i^{(s)} = \mathbf{e}_i^{(s)} + \sum_{j=1, j \neq i}^{n_i} \lambda_{i,j}\mathbf{e}_j^{(s)} \quad (3.56)$$

as well as the i th column of \mathbf{B}^T

$$\mathbf{b}_i = \mathbf{e}_i + \sum_{j=1, j \neq i}^{n_i} \lambda_{i,j}\mathbf{e}_j \quad (3.57)$$

The optimum vector \mathbf{f}_i in Scenario 3 is obtained by minimizing the i th term in Equation (3.34), i.e.,

$$\|\mathbf{H}_e\mathbf{f}_i - \mathbf{b}_i\|^2 + \mathbf{f}_i^T \mathbf{R}\mathbf{f}_i \quad (3.58)$$

which can be written as

$$\left\| \mathbf{H}_e\mathbf{f}_i - \mathbf{e}_i - \sum_{j=1, j \neq i}^{n_i} \lambda_{i,j}\mathbf{e}_j \right\|^2 + \mathbf{f}_i^T \mathbf{R}\mathbf{f}_i \quad (3.59)$$

With the same line of reasoning followed for calculating \mathbf{f}_i in unsorted Scenario 2, we get the following optimization problem which is like the one in

Equation (3.41):

$$\left\{ \begin{array}{l} \min_{\mathbf{f}_i} \|\mathbf{H}_e^{(i,r)} \mathbf{f}_i - \mathbf{e}\|^2 + \mathbf{f}_i^T \mathbf{R} \mathbf{f}_i \\ \lambda_{i,j} = \mathbf{h}_j^T \mathbf{f}_i \quad j = 1, \dots, i-1, i+1, \dots, n_i \\ \mathbf{H}_e \triangleq \begin{bmatrix} \mathbf{h}_1^T \\ \vdots \\ \mathbf{h}_{n_i}^T \\ \mathbf{H}_e^{(r)} \end{bmatrix} \\ \mathbf{H}_e^{(i,r)} \triangleq \begin{bmatrix} \mathbf{h}_i^T \\ \mathbf{H}_e^{(r)} \end{bmatrix} \\ \mathbf{e} \triangleq \begin{bmatrix} 1 \\ \mathbf{0}_{n_i \Delta} \end{bmatrix} \end{array} \right. \quad (3.60)$$

where we have separated the first n_i rows of \mathbf{H}_e from the remaining ones, denoted with $\mathbf{H}_e^{(r)}$, to which we have added \mathbf{h}_i^T to form $\mathbf{H}_e^{(i,r)}$; we have also denoted with $\mathbf{0}_{n_i \Delta}$ the $n_i \Delta \times 1$ vector with all null entries, to which we have added the first entry equal to 1 to form \mathbf{e} . Therefore, in this scenario, the optimum vector \mathbf{f}_i is obtained by solving the following system:

$$\left(\mathbf{R} + \mathbf{h}_i \mathbf{h}_i^T + \sum_{j=n_i+1}^{n_i(\Delta+1)} \mathbf{h}_j \mathbf{h}_j^T \right) \mathbf{f}_i = \mathbf{h}_i \quad (3.61)$$

3.3.6 The conjugate gradient method for solving the linear system

The conjugate gradient method [69] is the preferite choice among the efficient iterative procedures for solving the linear system $\mathbf{A} \mathbf{f} = \mathbf{b}$. The algorithm is initialized setting $\mathbf{r} = \mathbf{b}$ and $k = 0$; each iteration step is described by the

following procedure:

```

    k ← k + 1
    if k = 1 then
        p ← r
    else
        γ ← rTr
        β ←  $\frac{\gamma}{\gamma_{old}}$ 
        γold ← γ
        p ← r + βp
    endif
    v = Ap
    α ←  $\frac{\gamma}{\mathbf{p}^T \mathbf{v}}$ 
    f ← f + αp
    r ← r - αv
    
```

Let us note that the most complex operation is provided by the calculation $\mathbf{v} = \mathbf{A}\mathbf{p}$; since the data matrix, $\mathbf{R} + \mathbf{H}_e^T \mathbf{H}_e$, exhibits a special structure, we will show how the computational complexity of the conjugate gradient algorithm, dominated by the calculation $\mathbf{v} = \mathbf{A}\mathbf{p}$, can be made smaller than the one required for a general $n_t \times n_t$ data matrix, which is given by $n_t(2n_t - 1) \simeq 2n_t^2$ flops where $n_t \triangleq n_o N_f$. The number of flops required to construct the data matrix, $\mathbf{R} + \mathbf{H}_e^T \mathbf{H}_e$, from $\mathbf{H}(m)$ and $\mathbf{R}(m)$ is equal to $(2n_i \Delta - 1)n_o^2 N_f^2 \simeq 2n_i n_o^2 \Delta N_f^2$. Therefore, the overall number of flops required to solve the linear system with the conjugate gradient method is practically equal to

$$2n_o^2 N_f^2 N_s + 2n_i n_o^2 \Delta N_f^2 = 2n_o^2 N_f^2 (N_s + n_i \Delta) \quad (3.62)$$

where N_s represents the number of steps required for the algorithm convergence. Moreover, since in Scenario 1 it is necessary to solve n_i linear systems with the same data matrix — which will have to be constructed only once — the complexity becomes

$$2n_i n_o^2 N_f^2 N_s + 2n_i n_o^2 \Delta N_f^2 = 2n_i n_o^2 N_f^2 (N_s + \Delta) \quad (3.63)$$

It is possible to calculate the complexity of the operation $\mathbf{v} = \mathbf{A}\mathbf{p}$ when $\mathbf{v} = \mathbf{R}\mathbf{p} + \mathbf{H}_e^T \mathbf{g}$ where $\mathbf{g} = \mathbf{H}_e \mathbf{p}$. Then, the number of flops at each step of the algorithm is equal to $n_t(2n_t - 1) \simeq 2n_t^2$ for calculating $\mathbf{R}\mathbf{p}$, $n_i(\Delta + 1)(2n_t - 1) \simeq 2n_t n_i \Delta$ for calculating $\mathbf{H}_e \mathbf{p}$, and $n_t(2n_i(\Delta + 1) - 1) \simeq 2n_t n_i \Delta$ for

calculating $\mathbf{H}_e^T \mathbf{g}$; moreover, n_t^2 flops are required for the addition. Therefore, at each step the number of flops follows

$$2n_t^2 + 2n_t n_i \Delta + 2n_t n_i \Delta + n_t^2 = n_t(3n_t + 4n_i \Delta) \quad (3.64)$$

The overall number of flops required to solve a single linear system is practically equal to

$$N_s n_t (3n_t + 4n_i \Delta) \quad (3.65)$$

and the one required to solve the n_i linear systems in Scenario 1 is equal to

$$n_i N_s n_t (3n_t + 4n_i \Delta) \simeq N_s n_i n_o N_f^2 (3n_o + 4n_i) \quad (3.66)$$

where the approximation $\Delta \simeq N_f$ has been used. The comparison between Equations (3.63) and (3.66) is given by

$$2n_i n_o^2 N_f^2 (N_s + \Delta) < N_s n_i n_o N_f^2 (3n_o + 4n_i) \quad (3.67)$$

hence,

$$2n_o(N_s + \Delta) < N_s(3n_o + 4n_i) \quad (3.68)$$

Exemplifying: if we assume $n_o \simeq n_i$, the result of the comparison will become

$$2(N_s + \Delta) < 7N_s \quad \Leftrightarrow \quad N_s > \frac{2}{5} \Delta \quad (3.69)$$

if we assume $n_o \simeq 2n_i$, the result of the comparison will become

$$2(N_s + \Delta) < 5N_s \quad \Leftrightarrow \quad N_s > \frac{2}{3} \Delta \quad (3.70)$$

To conclude, in Scenario 1, the construction at step 0 of the one data matrix, $\mathbf{R} + \mathbf{H}_e^T \mathbf{H}_e$, is useful for the reduction of the computational complexity when $N_s > \alpha \Delta$ where α depends on the ratio $\frac{n_o}{n_i}$ and increases with it.

3.3.7 Specializing the iterative solution method to the given system of equations

Since in the k th iteration step $\mathbf{A}\mathbf{p}^{(k)} = \mathbf{R}\mathbf{p}^{(k)} + \mathbf{H}_e^T \mathbf{g}^{(k)}$ with $\mathbf{g}^{(k)} \triangleq \mathbf{H}_e \mathbf{p}^{(k)}$, three matrix multiplications can replace the direct calculation of $\mathbf{A}\mathbf{p}^{(k)}$: $\mathbf{R}\mathbf{p}^{(k)}$, $\mathbf{g}^{(k)} \triangleq \mathbf{H}_e \mathbf{p}^{(k)}$ and $\mathbf{H}_e^T \mathbf{g}^{(k)}$. Using such an approach, the storage requirements are strongly reduced as the number of entries which describe the matrix \mathbf{R} is equal to $n_o^2 N_f$; the one of the matrix \mathbf{H}_e is equal to $n_o n_i (\Delta + 1)$, having to store the matrices $\mathbf{H}(n)$ for $n = 0, 1, \dots, \Delta$. Therefore, unless $n_i \gg n_o$, the memory required is roughly reduced from $n_o^2 N_f^2$ to $n_o^2 N_f$, showing an advantage when a long feedforward filter is employed.

Calculating $\mathbf{Rp}^{(k)}$

Let us first define two vectors $\mathbf{x} \triangleq [x(0) \ x(1) \ \dots \ x(n_o N_f - 1)]^T$ and

$$\mathbf{y} \triangleq \begin{bmatrix} [y_1(n_o N_f - 1) \ \dots \ y_{n_o}(n_o N_f - 1)]^T \\ [y_1(n_o(N_f + 1) - 1) \ \dots \ y_{n_o}(n_o(N_f + 1) - 1)]^T \\ \vdots \\ [y_1(n_o(2N_f - 1) - 1) \ \dots \ y_{n_o}(n_o(2N_f - 1) - 1)]^T \end{bmatrix} \quad (3.71)$$

such that $\mathbf{y} = \mathbf{R}\mathbf{x}$. Equivalently, the following relation holds:

$$y_i(n) = \bar{r}_i(n) \otimes x(n) \quad i = 1, \dots, n_o \quad (3.72)$$

where

$$\bar{r}_i(n) \triangleq r_i(N_t - 1 - n) \quad n = 0, \dots, N_t - 1 \quad (3.73)$$

with $N_t \triangleq n_o(2N_f - 1)$ and

$$r_i(n) \triangleq \mathbf{R}(N_f - 1)|_{i,n+1} \quad n = 0, \dots, n_o - 1 \quad (3.74)$$

with $\mathbf{R}(N_f - 1)|_{i,n}$ denoting the (i, n) -entry of $\mathbf{R}(N_f - 1)$;

$$r_i(n + n_o) \triangleq \mathbf{R}(N_f - 2)|_{i,n+1} \quad n = 0, \dots, n_o - 1 \quad (3.75)$$

$$r_i(n + jn_o) \triangleq \mathbf{R}(N_f - 1 - j)|_{i,n+1} \quad j \in \{0, 1, \dots, N_f - 1\} \quad (3.76)$$

moreover,

$$r_i(n + (N_f - 1)n_o) \triangleq \mathbf{R}(0)^T|_{i,n+1} \quad (3.77)$$

$$r_i(n + (N_f - 1)n_o + n_o) \triangleq \mathbf{R}(1)^T|_{i,n+1} \quad (3.78)$$

$$r_i(n + (N_f - 1)n_o + jn_o) \triangleq \mathbf{R}(j)^T|_{i,n+1} \quad (3.79)$$

Let us observe that the length of the sequence $x(n)$ is $L_x = n_o N_f$ and the one of the sequence $y_i(n)$ is $L_y = n_o(2N_f - 1)$; moreover, the desired values of the convolution are those between $M_a = n_o N_f - 1$ and $M_b = n_o(2N_f - 1) - 1$. Therefore, the minimum number of DFT-points which can be used is $N_{\text{FFT}} \geq \max(M_b + 1, L_x + L_y - M_a - 1) = \max(n_o(2N_f - 1), n_o(2N_f - 1)) = n_o(2N_f - 1)$.

Finally, the number of flops needed to the calculation $\mathbf{Rp}^{(k)}$ is given by the one required for two FFTs over $n_o(2N_f - 1)$ points plus $n_o(2N_f - 1)$

multiplications in the frequency domain; all this has to be calculated for n_o times. Therefore, the complexity of the operation $\mathbf{R}\mathbf{p}^{(k)}$ follows

$$n_o [n_o(2N_f - 1) + 2n_o(2N_f - 1) \log_2(n_o(2N_f - 1))] \simeq 2n_o^2 N_f [1 + 2 \log_2(2n_o N_f)] \quad (3.80)$$

where we have neglected n_o with respect to $n_o N_f$; let us note that the complexity is practically linear with $N_f \log_2(N_f)$.

Calculating $\mathbf{H}_e \mathbf{p}^{(k)}$

Analogously to the previous section, let us first define the vectors $\mathbf{x} \triangleq [x(0) \ x(1) \ \dots \ x(n_o N_f - 1)]^T$ and

$$\mathbf{y} \triangleq \begin{bmatrix} [y_1(n_o N_f - 1) \ \dots \ y_{n_i}(n_o N_f - 1)]^T \\ [y_1(n_o(N_f + 1) - 1) \ \dots \ y_{n_i}(n_o(N_f + 1) - 1)]^T \\ \vdots \\ [y_1(n_o(N_f + \Delta) - 1) \ \dots \ y_{n_i}(n_o(N_f + \Delta) - 1)]^T \end{bmatrix} \quad (3.81)$$

such that $\mathbf{y} = \mathbf{H}_e \mathbf{x}$. Equivalently, the following relation holds:

$$y_i(n) = \bar{r}_i(n) \otimes x(n) \quad i = 1, \dots, n_i \quad (3.82)$$

where

$$\bar{r}_i(n) \triangleq r_i(N_t - 1 - n) \quad n = 0, \dots, N_t - 1 \quad (3.83)$$

with $N_t \triangleq (\Delta + 1)n_o$ and

$$r_i(n) \triangleq \mathbf{H}^T(0)|_{i,n+1} \quad n = 0, \dots, n_o - 1 \quad (3.84)$$

with $\mathbf{H}^T(0)|_{i,n}$ denoting the (i, n) -entry of $\mathbf{H}^T(0)$;

$$r_i(n + n_o) \triangleq \mathbf{H}^T(1)|_{i,n+1} \quad n = 0, \dots, n_o - 1 \quad (3.85)$$

$$r_i(n + j n_o) \triangleq \mathbf{H}^T(j)|_{i,n+1} \quad j \in \{0, 1, \dots, \Delta\} \quad (3.86)$$

Let us observe that the length of the sequence $x(n)$ is $L_x = n_o N_f$ and the one of the sequence $y_i(n)$ is $L_y = n_o(N_f + \Delta)$; moreover, the desired values of the convolution are those between $M_a = n_o N_f - 1$ and $M_b = n_o(N_f + \Delta) - 1$. Therefore, the minimum number of DFT-points which can be used is $N_{\text{FFT}} \geq$

$\max(M_b + 1, L_x + L_y - M_a - 1) = \max(n_o(N_f + \Delta), n_o(N_f + \Delta)) = n_o(N_f + \Delta)$.

Finally, the number of flops needed to the calculation $\mathbf{H}_e \mathbf{p}^{(k)}$ is given by the one required for two FFTs over $n_o(N_f + \Delta)$ points plus $n_o(N_f + \Delta)$ multiplications in the frequency domain; all this has to be calculated for n_i times. Therefore, the complexity of the operation $\mathbf{H}_e \mathbf{p}^{(k)}$ follows

$$n_i [n_o(N_f + \Delta) + 2n_o(N_f + \Delta) \log_2(n_o(N_f + \Delta))] \simeq n_i n_o 2N_f [1 + 2 \log_2(2n_o N_f)] \quad (3.87)$$

where we have approximated Δ with N_f ; let us note that the complexity is practically linear with $N_f \log_2(N_f)$.

Calculating $\mathbf{H}_e^T \mathbf{g}^{(k)}$

Analogously to the previous section, let us first define the vectors $\mathbf{x} \triangleq [x(0) \ x(1) \ \dots \ x(n_i(\Delta + 1) - 1)]^T$ and

$$\mathbf{y} \triangleq \begin{bmatrix} [y_1(n_i(\Delta - N + 1) - 1) \ \dots \ y_{n_o}(n_i(\Delta - N + 1) - 1)]^T \\ [y_1(n_i(\Delta - N + 2) - 1) \ \dots \ y_{n_o}(n_i(\Delta - N + 2) - 1)]^T \\ \vdots \\ [y_1(n_i(\Delta + 1) - 1) \ \dots \ y_{n_o}(n_i(\Delta + 1) - 1)]^T \end{bmatrix} \quad (3.88)$$

such that $\mathbf{y} = \mathbf{H}_e^T \mathbf{x}$. Equivalently, the following relation holds:

$$y_i(n) = r_i(n) \otimes x(n) \quad i = 1, \dots, n_o \quad (3.89)$$

where

$$r_i(n) \triangleq \mathbf{H}(0)|_{i, n_i - n} \quad n = 0, \dots, n_i - 1 \quad (3.90)$$

with $\mathbf{H}(0)|_{i, n}$ denoting the (i, n) -entry of $\mathbf{H}(0)$;

$$r_i(n + n_i) \triangleq \mathbf{H}(1)|_{i, n_i - n} \quad n = 0, \dots, n_i - 1 \quad (3.91)$$

$$r_i(n + jn_i) \triangleq \mathbf{H}(j)|_{i, n_i - n} \quad j \in \{0, 1, \dots, \Delta\} \quad (3.92)$$

With passages like the ones of the previous section, we have found out that the minimum number of DFT-points which can be used is $N_{\text{FFT}} \geq (n_i(N_f + \Delta))$ and the complexity of the operation will be $n_i n_o 2N_f [1 + 2 \log_2(2n_i N_f)]$ where, as in the previous section, we have approximated Δ with N_f ; let us note that the complexity is practically linear with $N_f \log_2(N_f)$.

3.3.8 Implementation complexity and numerical results

Let C_m be the number of real-valued multiplications required by the considered equalizer; it can be written as³

$$C_m = 2n_f N_f \quad (3.93)$$

where n_f is the overall number of feedforward filters composing the equalizer (let us remind that the filters are widely linear, so they process both the signal itself and its complex conjugate version, or, equivalently, the real part of the signal and the imaginary one). It is equal to M for the per-subcarrier equalizer, to M^2 for the complete equalizer and to $(2k_1 + 1)M$ for the proposed ad hoc equalizer (see Section 3.2.1). Analogous considerations can be done for the feedback filters; however, they perform only additions whose overall number increases linearly with the number of the feedback filters and with the one of their taps N_b . It is useful to note that the per-subcarrier equalizer performs well only if the diagonal dominance of the equivalent MIMO channel is significant: this implies the need of a large value of M .

The number of multiplications required by the equalizer for each equalized symbol is equal to $C_{ma} = \frac{C_m}{M}$; if $n_f = M$, i.e., in presence of the per-subcarrier equalizer, then $C_{ma} = 2N_f \triangleq C_s$; in presence of the complete equalizer, hence, for $n_f = M^2$, one will have that $C_{ma} = MC_s$ and, finally, in presence of the ad hoc equalizer, $C_{ma} = (2k_1 + 1)C_s$ being $n_f = (2k_1 + 1)M$.

It is useful to note that the number of taps needed for the feedforward filter of the equalizer is proportional to the length of the discrete-time MIMO channel. Let us denote with k_f such proportionality factor, i.e., $k_f: N_f = k_f(K_0 + 4\gamma + 1)$ where $K_0 \triangleq \left\lceil \frac{P-1}{\frac{M}{2}} \right\rceil$ and P can be written as $\frac{\Delta\tau B}{1+\beta}$ where $\Delta\tau$ is the delay spread of the channel, B its bandwidth, β the roll-off factor in the conversion from the discrete-time to the continuous-time. Therefore, for a difference of 1 km between the longest and the shortest path, we obtain an upper bound to $\Delta\tau$ of 4 μ s and, for a bandwidth of 20 MHz, a value of P about 64, too: consequently, $N_f \propto \frac{2 \cdot 64}{M} + 4\gamma + 1$. All things considered, a large value of M would allow the equalizer to operate per-subcarrier by a feedforward filter which has almost its minimum length ($\simeq 4\gamma + 1$): this minimizes the computational complexity of the equalizer.

More specifically, with a very large number of subcarriers (e.g., 1024), it is possible to operate using a diagonal WL-DF equalizer. This provides the maximum reduction of the equalizer complexity; however, such a simplification

³The feedforward filters have been implemented in direct form.

is obtained thanks to the use of a large number of subcarriers, which creates important problems to the system, e.g., it increases the delay of the equalizer and we may determine a symbol period, which is proportional to M , too long with respect to the horizon of stationarity of the communication channel.

We have first considered a discrete-time equivalent transmission channel with 10 taps and unit energy. We have used the equalizer in Scenario 1 and the following other parameters: $M = 4$, $\text{SNR} = 20$ dB, $N_f = 15$, $\Delta = N_f - 1$, $N_b = 12$. To obtain acceptable performance we have needed a single WL feedforward filter for each subcarrier and a feedback filter which accounts for the adjacent subcarriers. Let us note that in such a condition the per-subcarrier WL-DF equalizer performs poorly. When we move to 8 subcarriers, we note that the WL feedforward filter has to account for a single adjacent subcarrier and the feedback filter has to account for two adjacent subcarriers. We have also verified that, in presence of an estimation noise on channel response coefficients, we can correctly equalize the channel provided that the standard deviation of the estimation noise is equal to the average value of the modules of the channel coefficients. Moreover, we have verified that the propagation of the error introduces important performance degradations. Therefore, the system needs to work with correct previous decisions in order to provide acceptable performance, i.e., the probability of error must be maintained sufficiently low in each transmitted packet, which is formed also by a known preamble representing the training symbols.

This means that the computational complexity can be maintained limited even with a limited number of subcarriers; but this does not mean that the computational complexity of the equalizer can be made practically equivalent to its smaller value, C_s , which is attained thanks to the use of a large number of subcarriers, but that the factor $(2k_1 + 1)$ which describes its increase with respect to C_s can be marginal. If it is really marginal, however, it will depend on the general conditions, e.g., on how long the discrete-time equivalent MIMO channel is, i.e., how large the bandwidth is and how long the delay spread is, how fast it is time-variant, how efficient the techniques for managing a large number of subcarriers are, and so on. We have dealt with in the simulation experiments an equalizer which is able to combat the interferences present when the number of the subcarriers is not so large to allow per-subcarrier equalization. We have proposed important modifications to the classical WL-DF scheme in order to reduce the computational complexity both in the design stage of the WL-DF equalizer and in the implementation stage by using a simplified structure for the overall MIMO equalizer which contains only a minimal number of

feedforward and feedback WL single-input single-output (SISO) filters.

In the following, we report some numerical results which support our evaluations. In Figure 3.5, the probability of error is represented versus the signal-to-noise ratio with the number of iteration steps of the conjugate gradient algorithm, N_s , increasing from 1 to 15 till the algorithm converges. More precisely, this result is obtained by exactly calculating the probabilities of error of one component of the channel input at each iteration step and then averaging them over 50 different channels of unit energy and length 10; each channel tap is described by a complex Gaussian random variable normalized according to the unit-energy constraint. Moreover, we have set: $M = 4$, $\gamma = 4$, $N_f = 30$, $\Delta = 29$, $N_b = 12$, $k_1 = 0$, $k_2 = 1$ in Scenario 1. In Figure 3.6, it is represented the probability of error versus the iteration steps with reference to the four input symbols of a specific channel. We have set $\text{SNR} = 25$ dB, besides all the other parameters as in the previous figure. In Figure 3.7, the same quantities as Figure 3.6 are represented but, with respect to it, the channel is changed among the 50 channels used for Figure 3.5. All the parameters coincide with those of Figure 3.6. Let us note how there can be a strong difference in the convergence speed among the components of the feedforward filter related to the various subcarriers. In Figure 3.8, the same quantities as Figures 3.6 and 3.7, with the same parameters, are represented, but now they are averaged over the 4 input symbols and over the 50 different channels used for Figure 3.5. Finally, in Figure 3.9, it is represented the the symbol error probability in two different scenarios, i.e., in presence of the per-subcarrier equalizer and the ad hoc one (with $k_1 = 0$ and $k_2 = 1$ as in the other figures). We have set: $N_f = 15$, $\Delta = 14$, besides all the other parameters as in the previous figures. This result confirms our evaluations about the estimation noise on channel response coefficients and about the propagation of the error. In the same conditions as Figure 3.9 and for $\text{SNR} = 25$ dB, we have found out, for different choices of k_1 and k_2 , the values of the error probability which are reported in Table 3.1.

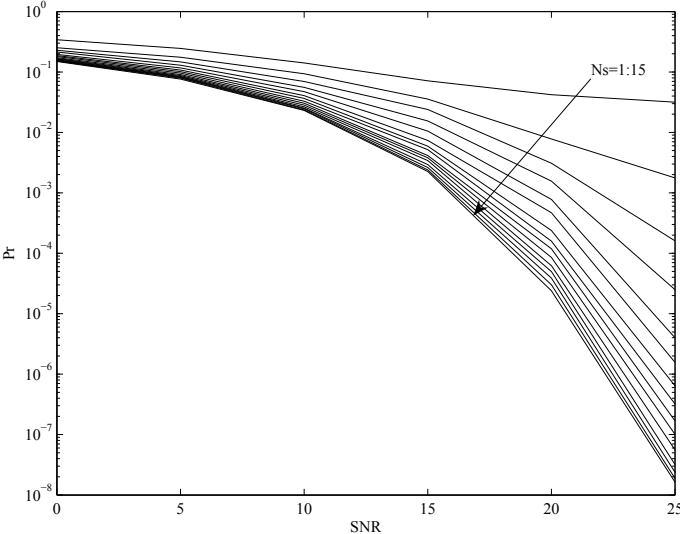


Figure 3.5: Error probability versus SNR with the number of iterations varying.

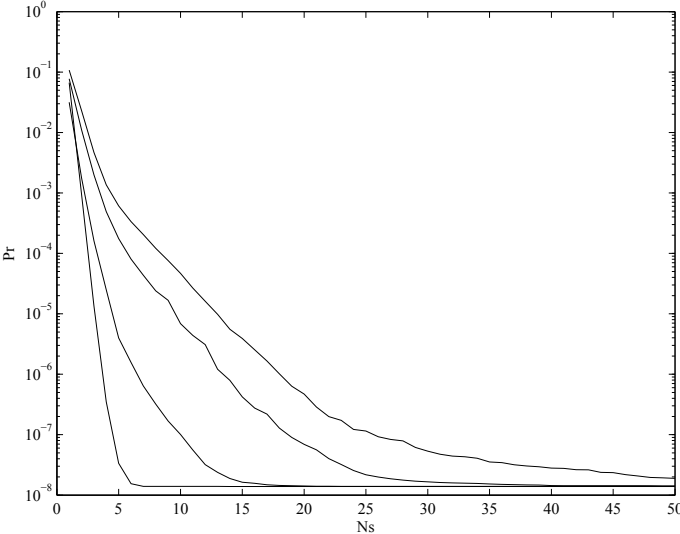


Figure 3.6: Error probability versus the number of iterations for each input symbol to a specific channel.

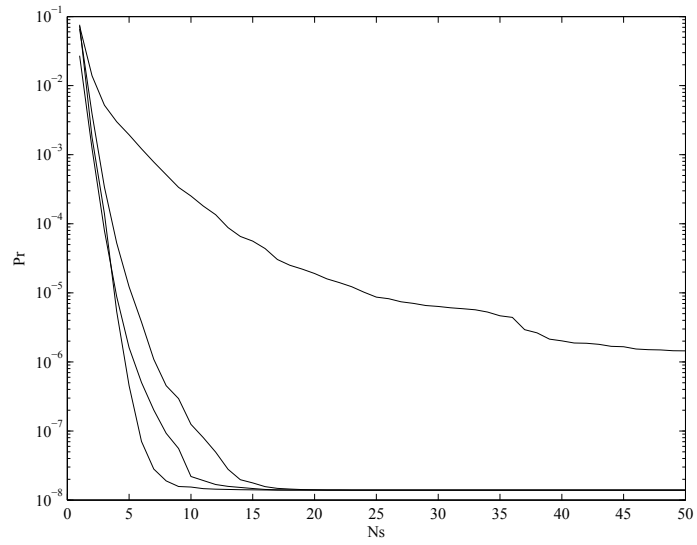


Figure 3.7: Error probability versus the number of iterations for each input symbol to another specific channel.

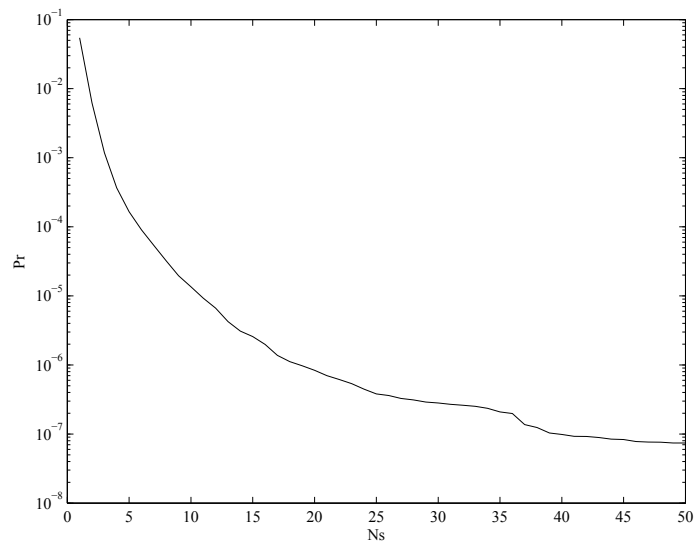


Figure 3.8: Error probability versus the number of iterations averaged over the input symbols and the channels.

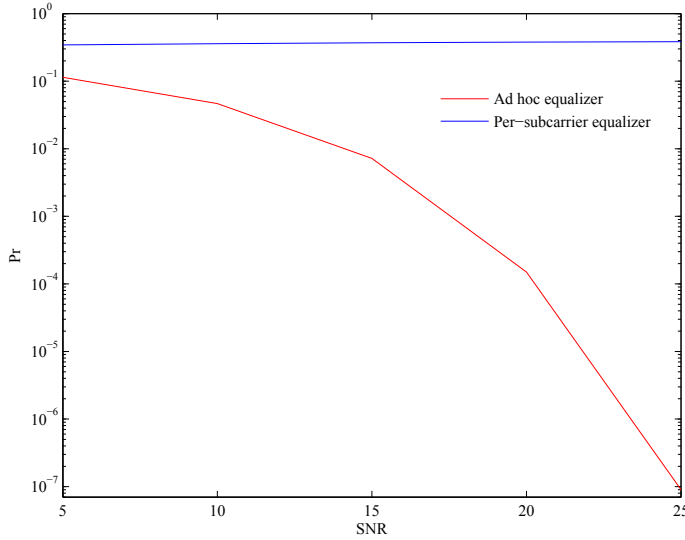


Figure 3.9: Symbol error probability in two different scenarios: per-subcarrier equalization and ad hoc one.

Table 3.1: Error probability for some different choices of k_1 and k_2 .

(k_1, k_2)	Pr
(0, 1)	0.0239
(0, 2)	0.0239
(0, 3)	0.0239
(0, 0)	0.3847
(1, 0)	0.4003
(1, 1)	$\approx 10^{-8}$

Conclusion

In this thesis, the main subject has been the equalization, with a particular reference to OFDM-OQAM systems.

In Chapter 1, we have introduced the MIMO system model, which has been widely employed throughout the thesis as a starting point to design the equalization techniques.

We have first focused on WL filtering which, generalizing the linear one, allows one to get performance improvements in presence of *rotationally variant* signals. In Chapter 2, in fact, there are two results deriving by the employment of the WL filtering: the former concerns the transmitter and the receiver IQ imbalance compensation by the WL MMSE equalizer; the latter deals with the problem of the constellation optimization in presence of the WL MMSE equalizer: a scheme which performs a WL transformation of the transmitted signals dependent on the state of channel has been proposed, in order to optimize the receiver performance in terms of SER.

In Chapter 3, we have considered OFDM-OQAM systems, modelling them as a MIMO channel, both in a single antenna and multiple antenna scenario. We have observed the diagonally dominant structure of the channel impulse response which has allowed us to conceive some ad hoc structures for the equalizer, i.e., structures where, according to the size of the interference terms, only some adjacent subcarriers to that to be equalized are selected for the MIMO equalization. More specifically, we have employed the MMSE WL-DF MIMO equalizer, proposing a synthesis algorithm with minimum storage requirements. Such equalizer provides a good trade-off between performance and complexity.

Appendix A

A.1 Proof of Lemma 3.3

Let us remind of $\mathbf{C}(z) \triangleq H(z)\mathbf{Z}(z)$ where $\mathbf{Z}(z)$ is a Toeplitz $M \times M$ matrix, i.e. a matrix in which each descending diagonal from left to right is constant; $H(z) \triangleq \sum_{k=0}^{P-1} h(k)z^{-k}$ and we assume $h(k) = 0$ for $k \notin \{0, 1, \dots, P-1\}$.

Let us develop the passages:

$$\begin{aligned}
 \mathbf{C}(z) &\triangleq h(0) \begin{bmatrix} z^{-M} & z^{-(M+1)} & \dots & z^{-(2M-1)} \\ z^{-(M-1)} & \ddots & \ddots & \vdots \\ \vdots & \ddots & \ddots & z^{-(M+1)} \\ z^{-1} & \dots & z^{-(M-1)} & z^{-M} \end{bmatrix} \\
 &+ h(1) \begin{bmatrix} z^{-M} & z^{-(M+1)} & \dots & z^{-(2M-1)} \\ z^{-(M-1)} & \ddots & \ddots & \vdots \\ \vdots & \ddots & \ddots & z^{-(M+1)} \\ z^{-1} & \dots & z^{-(M-1)} & z^{-M} \end{bmatrix} z^{-1} + \dots \\
 &+ h(P-1) \begin{bmatrix} z^{-M} & z^{-(M+1)} & \dots & z^{-(2M-1)} \\ z^{-(M-1)} & \ddots & \ddots & \vdots \\ \vdots & \ddots & \ddots & z^{-(M+1)} \\ z^{-1} & \dots & z^{-(M-1)} & z^{-M} \end{bmatrix} z^{-(P-1)}
 \end{aligned} \tag{A.1}$$

If we place M expanders by $\frac{M}{2}$ before the channel $\mathbf{C}(z)$ and M decimators by $\frac{M}{2}$ after it, such channel will be characterized by the following transfer

function:¹

$$\begin{aligned}
 \mathbf{C}_{\frac{M}{2}}(z) \triangleq & h(0) \begin{bmatrix} z^{-2} & \mathbf{0} & z^{-3} & \mathbf{0} \\ \mathbf{0} & \ddots & \ddots & \vdots \\ z^{-1} & \ddots & \ddots & \vdots \\ \mathbf{0} & \dots & \dots & \vdots \end{bmatrix} \\
 & + h(1) \begin{bmatrix} 0 & \mathbf{0} & z^{-3} & \mathbf{0} & z^{-4} \\ z^{-2} & \ddots & \ddots & \ddots & \vdots \\ \mathbf{0} & \ddots & \ddots & \ddots & \vdots \\ z^{-1} & \ddots & \ddots & \ddots & \vdots \\ \mathbf{0} & \dots & \dots & \dots & \vdots \end{bmatrix} + \dots \\
 & + h\left(\frac{M}{2} - 1\right) \begin{bmatrix} 0 & z^{-3} & \mathbf{0} & z^{-4} & \mathbf{0} \\ \mathbf{0} & \ddots & \ddots & \ddots & \vdots \\ z^{-2} & \ddots & \ddots & \ddots & \vdots \\ \mathbf{0} & \ddots & \ddots & \ddots & \vdots \\ z^{-1} & \dots & \dots & \dots & \vdots \end{bmatrix} + \dots
 \end{aligned} \tag{A.2}$$

Let us note that, while the time index (k) increases, each descending diagonal from left to right shifts towards left and on the extreme right a new component appears.

¹The matrices are all Toeplitz ones.

Equation (A.2) can also be written as

$$\begin{aligned}
 \mathbf{C}_{\frac{M}{2}}(z) \triangleq & \begin{bmatrix} \mathbf{0} & 0 & 0 & \mathbf{0} & 0 \\ h(0) & \ddots & \ddots & \ddots & \vdots \\ h(1) & \ddots & \ddots & \ddots & \vdots \\ \vdots & \ddots & \ddots & \ddots & \vdots \\ h\left(\frac{M}{2}-1\right) & \dots & \dots & \dots & \vdots \end{bmatrix} z^{-1} \\
 + & \begin{bmatrix} h(0) & 0 & \mathbf{0} & 0 \\ h(1) & \ddots & \ddots & \vdots \\ \vdots & \ddots & \ddots & \vdots \\ h(M-1) & \dots & \dots & \vdots \end{bmatrix} z^{-2} \\
 + & \begin{bmatrix} h\left(\frac{M}{2}\right) & h\left(\frac{M}{2}-1\right) & \dots & h(0) & \mathbf{0} & 0 \\ h\left(\frac{M}{2}+1\right) & \ddots & \ddots & \ddots & \ddots & \vdots \\ \vdots & \ddots & \ddots & \ddots & \ddots & \vdots \\ h(M+1) & \ddots & \ddots & \ddots & \ddots & \vdots \\ \vdots & \ddots & \ddots & \ddots & \ddots & \vdots \\ h\left(3\frac{M}{2}-1\right) & \dots & \dots & \dots & \dots & \vdots \end{bmatrix} z^{-3} \\
 + & \begin{bmatrix} h(M) & h(M-1) & \dots & h(1) \\ h(M+1) & \ddots & \ddots & \vdots \\ \vdots & \ddots & \ddots & \vdots \\ h(2M-1) & \dots & \dots & \vdots \end{bmatrix} z^{-4} + \dots
 \end{aligned} \tag{A.3}$$

Therefore, we obtain

$$\mathbf{C}_{\frac{M}{2}}(z) \triangleq \sum_{k=1}^{K_0+3} \mathbf{c}_{\frac{M}{2}}(k) z^{-k} \tag{A.4}$$

with

$$\mathbf{c}_{\frac{M}{2}}(k) \triangleq \text{Toeplitz}(\chi_k, \phi_k) \tag{A.5}$$

where

$$\chi_k \triangleq \left[h\left(\left(k-2\right)\frac{M}{2}\right) h\left(\left(k-2\right)\frac{M}{2}+1\right) \dots h\left(\left(k-2\right)\frac{M}{2}+(M-1)\right) \right]^T \quad (\text{A.6})$$

$$\phi_k \triangleq \left[h\left(\left(k-2\right)\frac{M}{2}\right) h\left(\left(k-2\right)\frac{M}{2}-1\right) \dots h\left(\left(k-2\right)\frac{M}{2}-(M-1)\right) \right] \quad (\text{A.7})$$

$K_0 \triangleq \left\lceil \frac{P-1}{\frac{M}{2}} \right\rceil$ and $\text{Toeplitz}(\mathbf{u}, \mathbf{v})$ denotes the Toeplitz matrix with \mathbf{u} as first column and \mathbf{v} as first row.

The values k can assume have been calculated by the following equations:

$$\left(k-2\right)\frac{M}{2}-(M-1) \leq P-1 \quad (\text{A.8})$$

$$\left(k-2\right)\frac{M}{2}+(M-1) \geq 0 \quad (\text{A.9})$$

from which one gets that $1 \leq k \leq K_0 + 3$.

Bibliography

- [1] F. Sterle. *The exploitation of widely linear filtering in MIMO communication systems*. PhD thesis, Università degli Studi di Napoli Federico II Facoltà di Ingegneria, 2005.
- [2] G.J. Foschini. Layered space-time architecture for wireless communication in a fading environment when using multi-elements antennas. *Bell Labs Tech. Journal*, 1(2):41–59, August 1996.
- [3] W.C. Jakes. *Microwave mobile communications*. Wiley, 1974.
- [4] G.L. Stuber, J.R. Barry, S.W. McLaughlin, Y.(G.) Li, M.A. Ingram, and T.G. Pratt. Broadband MIMO-OFDM wireless communications. *Proceedings of IEEE*, 92(2):271–294, February 2004.
- [5] D. Mattera, L. Paura, and F. Sterle. Widely linear MMSE equaliser for MIMO linear time-dispersive channel. *Electronics Letters*, 39(20):1481–1482, October 2003.
- [6] S. Verdù. *Multiuser detection*. Cambridge University Press, 1998.
- [7] D. Mattera, L. Paura, and F. Sterle. Widely linear decision-feedback equalizer for time-dispersive linear MIMO channels. *IEEE Trans. Signal Processing*, 53(7):2525–2536, July 2005.
- [8] A. Scaglione, S. Barbarossa, and G.B. Giannakis. Filterbank transceivers optimizing information rate in block transmissions over dispersive channels. *IEEE Trans. on Information Theory*, 45(3):1019–1032, April 1999.
- [9] H. Sampath, P. Stoica, and A. Paulraj. Generalized linear precoder and decoder design for MIMO channels using the weighted MMSE criterion. *IEEE Trans. Communications*, 49(12):2198–2207, December 2001.

-
- [10] P. Stoica, Y. Jang, and J. Li. On MIMO channel capacity: an intuitive discussion. *IEEE Signal Processing Magazine*, 22(3):83–84, May 2005.
- [11] Y. Jang, J. Li, and W. Hager. Uniform channel decomposition for MIMO communications. *IEEE Trans. Signal Processing*, 53(11):4283–4294, November 2005.
- [12] Y. Jiang, J. Li, and W.W. Hager. Joint transceiver design for MIMO communications using geometric mean decomposition. *IEEE Trans. Signal Processing*, 53(10):3791–3803, October 2005.
- [13] F. Sterle. Widely linear MMSE transceivers for MIMO channels. *IEEE Trans. Signal Processing*, 55(8):4258–4270, August 2007.
- [14] P.J. Schreier and L.L. Scharf. Second-order analysis of improper complex random vectors and processes. *IEEE Trans. Signal Processing*, 51(3):714–725, March 2003.
- [15] F.D. Neeser and J.L. Massey. Proper complex random processes with applications to information theory. *IEEE Trans. Inform. Theory*, 39(4):1293–1302, July 1993.
- [16] B. Picinbono and P. Chevalier. Widely linear estimation with complex data. *IEEE Trans. Signal Processing*, 43(8):2030–2033, August 1995.
- [17] B. Picinbono. On circularity. *IEEE Trans. Signal Processing*, 42(12):3473–3482, December 1994.
- [18] B. Picinbono. Second-order complex random vectors and normal distributions. *IEEE Trans. Signal Processing*, 44(10):2637–2640, October 1996.
- [19] B. Picinbono and P. Bondon. Second-order statistics of complex signals. *IEEE Trans. Signal Processing*, 45(2):411–420, February 1997.
- [20] B. Razavi. Design considerations for direct-conversion receivers. *IEEE Trans. Circuits Syst. II*, 44(6):428–435, June 1997.
- [21] A. Tarighat and A.H. Sayed. Joint compensation of transmitter and receiver impairments in OFDM systems. *IEEE Trans. Wireless Communications*, 6(1):240–247, January 2007.

- [22] M. Lipardi, D. Mattera, and F. Sterle. MMSE equalization in presence of transmitter and receiver IQ imbalance. In *International Waveform Diversity and Design Conference*, pages 165–168, June 2007.
- [23] A. Tarighat, R. Bagheri, and A.H. Sayed. Compensation schemes and performance analysis of IQ imbalances in OFDM receivers. *IEEE Trans. Signal Processing*, 53(8):3257–3268, August 2005.
- [24] D. Mattera, L. Paura, and F. Sterle. MMSE WL equalizer in presence of receiver IQ imbalance. *IEEE Trans. Signal Processing*, 56(4):1735–1740, April 2008.
- [25] W.H. Gerstacker, R. Schober, and A. Lampe. Receivers with widely linear processing for frequency-selective channels. *IEEE Trans. Communications*, 51(9):1512–1523, September 2003.
- [26] J. Tubbax, B. Come, L. Van der Perre, S. Donnay, M. Engels, H. De Man, and M. Moonen. Compensation of IQ imbalance and phase noise in OFDM systems. *IEEE Trans. Wireless Communications*, 4(3):872–877, May 2005.
- [27] R. Lucky and J. Hancock. On the optimum performance of N-ary systems having two degrees of freedom. *IRE Trans. Commun. Systems*, 10(2):185–192, January 1962.
- [28] G. Foschini, R. Gitlin, and S. Weinstein. Optimization of two-dimensional signal constellations in the presence of gaussian noise. *IEEE Trans. Communications*, 22(1):28–38, January 1974.
- [29] D.P. Palomar and S. Barbarossa. Designing MIMO communication systems: constellation choice and linear transceiver design. *IEEE Trans. Signal Processing*, 53(10):3804–3818, October 2005.
- [30] P. Chevalier and F. Picon. New insights into optimal widely linear array receivers for the demodulation of BPSK, MSK, and GMSK signals corrupted by noncircular interferences - Application to SAIC. *IEEE Trans. Signal Processing*, 54(3):870–883, March 2006.
- [31] D.P. Palomar, J.M. Cioffi, and M.A. Lagunas. Joint Tx-Rx beamforming design for multicarrier MIMO channels: a unified framework for convex optimization. *IEEE Trans. Signal Processing*, 51(9):2381–2401, September 2003.

- [32] Fang Xu, T.N. Davidson, Jian-Kang Zhang, and K.M. Wong. Design of block transceivers with decision feedback detection. *IEEE Trans. Signal Processing*, 54(3):965–978, March 2006.
- [33] A. Scaglione, P. Stoica, S. Barbarossa, G.B. Giannakis, and H. Sampath. Optimal designs for space-time linear precoders and decoders. *IEEE Trans. Signal Processing*, 59(5):1051–1064, May 2002.
- [34] Y.P. Lin and S.M. Phoong. Optimal ISI-free DMT transceivers for distorted channels with colored noise. *IEEE Trans. Signal Processing*, 49(11):2702–2712, November 2001.
- [35] M. Lipardi, D. Mattera, and F. Sterle. Constellation design in widely linear transceivers. submitted for the publication on EURASIP Journal on Advances in Signal Processing, October 2009.
- [36] W.H. Gerstaecker, R. Schober, and A. Lampe. Equalization with widely linear filtering. *IEEE International Symposium on Information Theory, Proceedings.*, page 265, June 2001.
- [37] A. Mirbagheri, K.N. Plataniotis, and S. Pasupathy. An enhanced widely linear CDMA receiver with OQPSK modulation. *IEEE Trans. Communications*, 54(2):261–272, February 2006.
- [38] A. Parihar, L. Lampe, R. Schober, and C. Leung. Equalization for DS-UWB systems — Part II: 4BOK modulation. *IEEE Trans. Communications*, 55(8):1525–1535, August 2007.
- [39] G. Gelli, L. Paura, and A.R.P. Ragozini. Blind widely linear multiuser detection. *IEEE Commun. Lett.*, 4(6):187–189, June 2000.
- [40] A. Parihar, L. Lampe, R. Schober, and C. Leung. Equalization for DS-UWB systems — Part I: BPSK modulation. *IEEE Trans. Communications*, 55(6):1164–1173, June 2007.
- [41] A. Lampe and M. Breiling. Asymptotic analysis of widely linear MMSE multiuser detection-complex vs real modulation. *IEEE Information Theory Workshop, Proceedings.*, pages 55–57, September 2001.
- [42] J.B. Anderson. *Digital transmission engineering*. IEEE Press, second edition, 2005.

- [43] A.M. Makowski. On the optimality of uniform pulse amplitude modulation. *IEEE Trans. on Information Theory*, 52(12):5546–5549, December 2006.
- [44] R. van Nee and R. Prasad. *OFDM for wireless multimedia communications*. Artech House, Boston, Mass, USA, 2000.
- [45] R.W. Chang. Synthesis of band-limited orthogonal signals for multichannel data transmission. *Bell System Technical Journal*, 45:1775–1796, 1966.
- [46] B.R. Saltzberg. Performance of an efficient parallel data transmission system. *IEEE Trans. Communications*, 15(6):805–811, 1967.
- [47] T. Ihalainen, T.H. Stitz, M. Rinne, and M. Renfors. Channel equalization in filter bank based multicarrier modulation for wireless communications. *EURASIP Journal on Advances in Signal Processing*, 2007:1–18, August 2006.
- [48] N. Benvenuto, S. Tomasin, and L. Tomba. Receiver architectures for FMT broadband wireless systems. *IEEE VTS 53rd Vehicular Technology Conference*, 1:643–647, May 2001.
- [49] Amin Ben Salem, Mohamed Siala, and Hatem Boujemaa. Performance comparison of OFDM and OFDM/OQAM systems operating in highly time and frequency dispersive radio-mobile channels. *12th IEEE International Conference on Electronics, Circuits and Systems*, pages 1–4, December 2005.
- [50] N. Benvenuto, S. Tomasin, and L. Tomba. Equalization methods in OFDM and FMT systems for broadband wireless communications. *IEEE Trans. Communications*, 50(9):1413–1418, September 2002.
- [51] S.D. Sandberg and M.A. Tzannes. Overlapped discrete multitone modulation for high speed copper wire communications. *IEEE Journal on Selected Areas in Communications*, 13(9):1571–1585, 1995.
- [52] L. Vandendorpe, L. Cuvelier, F. Deryck, J. Louveaux, and O. van de Wiel. Fractionally spaced linear and decision-feedback detectors for transmultiplexers. *IEEE Trans. Signal Processing*, 46(4):996–1011, April 1998.

- [53] D.S. Waldhauser, L.G. Baltar, and J.A. Nossek. MMSE subcarrier equalization for filter bank based multicarrier systems. *IEEE 9th Workshop on Signal Processing Advances in Wireless Communications*, pages 525–529, July 2008.
- [54] L.G. Baltar, D.S. Waldhauser, and J.A. Nossek. MMSE subchannel decision feedback equalization for filter bank based multicarrier systems. *IEEE International Symposium on Circuits and Systems*, pages 2802–2805, May 2009.
- [55] L.G. Baltar, D.S. Waldhauser, and J.A. Nossek. Adaptive decision feedback equalization for filter bank based multicarrier systems. *IEEE International Symposium on Circuits and Systems*, pages 2794–2797, May 2009.
- [56] T. Ihalainen, T.H. Stitz, and M. Renfors. Efficient per-carrier channel equalizer for filter bank based multicarrier systems. *IEEE International Symposium on Circuits and Systems*, pages 3175–3178, May 2005.
- [57] P. Siohan, C. Siclet, and N. Lacaille. Analysis and design of OFDM/OQAM systems based on filterbank theory. *IEEE Trans. Signal Processing*, 50(5):1170–1183, May 2002.
- [58] Helmut Bolcskei, Pierre Duhamelb, and Rima Hleissb. Design of pulse shaping OFDM/OQAM systems for high data-rate transmission over wireless channels. *IEEE International Conference on Communications*, 1:559–564, June 1999.
- [59] M. Bellanger. Filter banks and OFDM-OQAM for high throughput wireless LAN. *3rd International Symposium on Communications, Control and Signal Processing*, pages 758–761, March 2008.
- [60] A. Skrzypczak, P. Siohan, N. Chotkan, and M. Djoko-Kouam. OFDM/OQAM: an appropriate modulation scheme for an optimal use of the spectrum. *3rd International Symposium on Communications, Control and Signal Processing*, pages 405–410, March 2008.
- [61] M.G. Bellanger. Specification and design of a prototype filter for filter bank based multicarrier transmission. *IEEE International Acoustics, Speech, and Signal Processing, Proceedings.*, 4:2417–2420, May 2001.

- [62] P.P. Vaidyanathan. *Digital transmission engineering*. Prentice Hall, Englewood Cliffs, New Jersey, USA, 1993.
- [63] Lorenzo Vangelista and Nicola Laurenti. Efficient implementations and alternative architectures for OFDM-OQAM systems. *IEEE Trans. Communications*, 49(4):664–675, April 2001.
- [64] L. Vandendorpe, J. Louveaux, B. Maison, and A. Chevreuil. About the asymptotic performance of MMSE MIMO DFE for filter-bank based multicarrier transmission. *IEEE Trans. Communications*, 47(10):1472–1475, October 1999.
- [65] N. Al-Dhahir and A.H. Sayed. The finite-length multi-input multi-output MMSE DFE. *IEEE Trans. Signal Processing*, 48(10):2921–2936, October 2000.
- [66] N. Al-Dhahir and J.M. Cioffi. MMSE decision-feedback equalizers: finite-length results. *IEEE Trans. Inform. Theory*, 41(4):961–975, July 1995.
- [67] R. Merched and N.R. Yousef. Fast techniques for computing finite-length MIMO MMSE decision feedback equalizers. *IEEE Trans. Signal Processing*, 54(2):701–711, February 2006.
- [68] R. Merched. Fast computation of constrained decision feedback equalizers. *IEEE Trans. Signal Processing*, 55(6):2446–2457, June 2007.
- [69] G.H. Golub and C.F. Van Loan. *Matrix computations*. The Johns Hopkins University Press, Baltimore, Maryland, USA, 2nd edition, 1989.
- [70] I.E. Telatar. Capacity of multi-antenna gaussian channels. *Europ. Trans. Telecomm.*, 10:585–595, Nov./Dec. 1999.
- [71] G. Garbo, S. Mangione, and V. Maniscalco. Wireless OFDM-OQAM with a small number of subcarriers. *IEEE Wireless Communications and Networking Conference*, pages 187–192, 2008.
- [72] John G. Proakis. *Digital communications*. McGraw-Hill, New York, NY, fourth edition, 2001.
- [73] Sergio Benedetto and Ezio Biglieri. *Principles of Digital transmission*. Kluwer Academic, 1999.

